Gersonde, R., Hodell, D.A., Blum, P., et al., 1999
Proceedings of the Ocean Drilling Program, Initial Reports Volume 177

9. Site 1094[1]

Shipboard Scientific Party[2]

BACKGROUND AND OBJECTIVES

Site 1094 (proposed site TSO-7C) was the highest latitude site drilled during Leg 177 and represents the southernmost anchor of sites drilled along a north-south transect across the Antarctic Circumpolar Current (ACC) (Fig. **F1,** p. 35, in the "Leg Summary" chapter). The site is located in the center of the ice-free Antarctic Zone bounded to the north by the Polar Front (PF) and to the south by the Weddell Gyre/ACC boundary, which coincides approximately with the present average winter sea-ice edge. The site is presently north of the winter sea-ice edge, but the presence of sea-ice diagnostic diatoms indicates that Site 1094 was covered by sea ice during the last Ice Age. The water depth of 2807 m places the site within the core of Circumpolar Deep Water (CDW) (Fig. **F2,** p. 36, in the "Leg Summary" chapter).

Site 1094 is located in a small sedimentary basin north/northeast of Bouvet Island. A multichannel seismic line (AWI 94080) shows a thick package of acoustically stratified sediment with basement estimated at ~1100 meters below seafloor (mbsf) on the basis of interval velocities (Figs. **F1, F2;** Table **T1**). The site is close to the Bouvet Fracture Zone, and the basement age cannot be determined precisely from magnetic anomalies in the area (Fig. **F6,** p. 40, in the "Leg Summary" chapter). If the results of Cande and Kent (1992) are extrapolated to the area of Site 1094, basement age would be late Miocene.

Parasound echosounder profiles near Site 1094 indicate the presence of high-amplitude reflectors at ~66 and 105 mbsf (Fig. **F3**), which are associated with porcellanite in nearby piston cores (PS2089-1, 2) collected to the east of Site 1094 (Fig. **F4**). The porcellanite is found in sediments belonging to marine isotope Stage (MIS) 11, suggesting a very young formation age (~400 ka; Bohrmann et al., 1994). On the basis of the porcellanite reflector at 66 mbsf (Fig. **F3**), we deduced an average sedimentation rate of 170 m/m.y. The presence of porcellan-

F1. Track lines and shotpoints for the site surveys of Site 1094, **p. 18.**

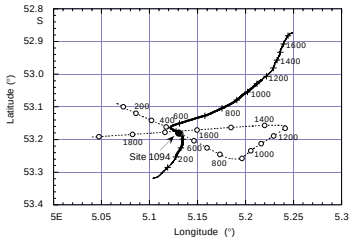

F2. Seismic line showing the location and penetration depth of Site 1094, **p. 19.**

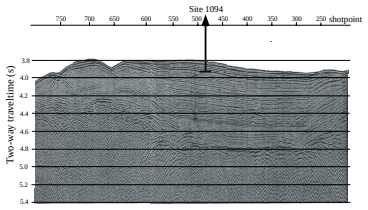

T1. Velocities used for stacking of multichannel seismic data, **p. 49.**

F3. Analog Parasound profiles collected near Site 1094, **p. 20.**

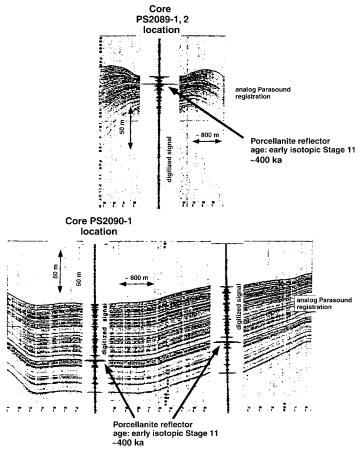

[1]**Examples of how to reference the whole or part of this volume.**
[2]**Shipboard Scientific Party addresses.**

Ms 177IR-109

ites at Site 1094 will permit geochemical studies of low-temperature silica diagenesis by studying sediments and interstitial waters. The porcellanite beds in the sediment cores are only a few centimeters thick and, thus, were not expected to impede penetration of the advanced hydraulic piston corer (APC).

Sediment cores (PS2089-1, 2, PS2090-1, and TTN057-13-PC4) collected in the vicinity of Site 1094 with a piston corer are composed of diatom ooze and diatom mud, but foraminifers are sufficiently abundant to permit the development of stable isotopic stratigraphies. Variations in magnetic susceptibility and natural gamma radiation (NGR) show strong contrasts between high values in glacial sediments and low values in interglacial sediments, which is useful for identifying glacial–interglacial cycles downhole.

The purpose of Site 1094 was to obtain a high-resolution record of biosiliceous sediments south of the present-day position of the PF. Site 1094 (53°S) represents the southernmost anchor of high-resolution sites across the ACC, including Sites 1089 (41°S), 1091 (47°S), and 1093 (50°S) (Fig. **F15,** p. 49, in the "Leg Summary" chapter). The paleoclimatic record from this site will be used to study rapid climate change on suborbital time scales and will be correlated to similar high-resolution climate records from other marine cores, as well as to climatic signals from Antarctic and Greenland ice cores. Specific objectives include the reconstruction of (1) surface-water parameters (sea-surface temperatures, water chemistry) south of the present Polar Front Zone; (2) sea-ice distribution in the Southern Ocean during Pleistocene glacial–interglacial cycles; (3) paleoproductivity changes (e.g., biogenic opal, organic carbon export rates) in relation to surface-water mass changes and sea-ice distribution; (4) deep-water circulation, including changes in the physical and chemical properties of CDW; and (5) early low-temperature silica diagenesis.

F4. Bathymetric map of the area surrounding Site 1094, **p. 21.**

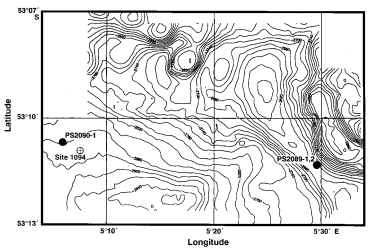

OPERATIONS

The voyage to Site 1094 north of Bouvet Island began with the wind gusting to 38 kt and seas and swell nearly at right angles to the ship's track. Rolling heavily, the vessel made only about 6 kt on her southerly course for the remainder of the evening. At 2330 hr, it was necessary to slow the shafts and to alter course because of excessive vessel motion.

At 0030 hr on 20 January, the drilling crew reported that the forward retaining pin and the two safety slings of the lower guide horn (LGH) in the moonpool had broken and that the port half of the LGH was swinging free about its hinges on the aft pin. The ship was slowed to ~2 kt in heavy weather while attempts were made to restrain the LGH. These attempts were unsuccessful, and speed was increased to 5 kt in the direction of the drill site, which was still ~150 nmi away. At 0315 hr, the aft pin failed just above the water line and allowed the upper part of the unrestrained section of the LGH to move forward and outboard until it came to rest against the wall of the moonpool. The port LGH section (of undetermined length, later determined to be complete) remained attached to the starboard half at a lower corner by a section of the aft retaining pin. The displaced portion was securely wedged across the moonpool and remained in place as the ship proceeded at full speed toward the drill site in rapidly improving weather.

Visual inspection indicated that the center of the moonpool was unobstructed and that drilling operations were feasible to the extent allowed by the 20-ft reduction of the port LGH. Operations thus contin-

ued according to plan, and a positioning beacon was launched at 2000 hr on 20 January.

Hole 1094A

While the vessel was stabilizing its position over the beacon, a stand of drill pipe was picked up and run through the moonpool to confirm that the center well was unobstructed. The signal from the positioning beacon was weak and considered unreliable, so a backup beacon was launched at 2050 hr while the bottom-hole assembly (BHA) was being assembled.

Weather and swell conditions improved dramatically to nearly flat calm as spud time approached, allaying concerns about stricter operating limits on vessel motion that were expected from the Ocean Drilling Program (ODP) engineers. The pipe trip was slowed somewhat because stands of drill pipe had shifted on the piperack during the rough weather and had to be repositioned for handling by the automatic racker.

At 0408 hr on 21 January, Hole 1094A was spudded with an APC core from 2814 meters below rig floor (mbrf). The initial 4.6-m core set the seafloor depth at 2818.9 mbrf. Temperature readings were taken with the APC temperature (APCT) tool for Cores 1H (for bottom-water temperature), 4H, 6H, 8H, 10H, 12H, 14H, and 16H. The majority of cores were oriented azimuthally as the one remaining operational instrument permitted. Coring results were affected adversely by the accumulation of ice-rafted debris (IRD) in the hole and by persistent core-liner failures (nearly 100% of the liners failed in some manner).

Core 18H indicated incomplete stroke and produced no recovery. A 3-m interval was drilled in case the refusal was a result of a thin, hard stratum. Core 19H also had incomplete stroke but recovered 8 m of core, which apparently was a stack of two sections resulting from two successive stabs with the corer. As APC refusal apparently had been reached, a Davis-Villinger temperature probe (DVTP) run was made to complete the temperature gradient profile.

One additional attempt was made to obtain an APC core before abandoning the hole. Several attempts to actuate the corer were unsuccessful and the APC was recovered with the shearpins intact. Coring in Hole 1094A was discontinued at the request of the scientific party and the drill string was withdrawn from the hole.

Hole 1094B

The rig was offset 10 m, and Hole 1094B was spudded with a seafloor APC core at 0015 hr on 22 January. Core recovery provided close agreement with the seafloor depth of Hole 1094A.

The anticipated guidelines for coring with a damaged LGH were received while Hole 1094B was being cored. Roll and pitch limits were reduced, as expected, and the use of knobby drilling joints was mandated for all drilling/coring operations. The knobbies were put into service beginning with Core 4H.

Cores 1H and 2H gave essentially full recovery, but recovery was poor for Cores 3H and 4H. All four cores gave pressure indications of incomplete stroke. Because of the good results in Hole 1094A, the presence of IRD in the hole was blamed for the unsatisfactory performance in Hole 1094B. To make the best use of remaining operating time, the decision

was made to pull clear of the seafloor, offset 10 m to the opposite side of Hole 1094A, and start over.

Hole 1094C

A third successful mudline core was collected with Core 1H, shot at 0443 hr from 2818 mbrf. All three seafloor depths agreed within 1 m. Problems with APC performance again were experienced as eight cores were attempted and six of them gave pressure indications of incomplete stroke. The two cores that indicated full stroke had no recovery. After Core 8H, which recovered 1.3 m of sediment, the drill struck hard material after reaming 7.2 m toward the next core point. No measurable penetration was made after 20 min of rotation. Again the coring problems were attributed to IRD in the sediment, with the final hard streak interpreted as a boulder. Coring attempts were abandoned, and the bit was raised above the seafloor.

Hole 1094D

The ship was offset about 20 m to the northwest of the coordinates of the earlier holes. The hole was drilled to 19.1 m below inferred seafloor depth before the APC was deployed. Continuous APC cores 1H through 13H were taken to 142.6 mbsf before it was necessary to replace the knobby joints with standard drill pipe. When the bit reached total depth (TD) following the 2-hr short trip, about 1.5 m of fill was found in the hole. A mud flush was pumped concurrently with Core 14H, following the trip.

At the time Core 16H was being recovered from 171.1 mbsf (0215 hr on January 23), a partial load shedding to the ship's dynamic positioning (DP) system occurred, presumably the result of an unexpected drift-off (2% yellow alarm) in relatively calm seas and moderately windy weather (30–40 kt gusts). Within 3 min, position was recovered to 1%. The load shed led to the decision by the operations manager to terminate the scientific drilling operations of Leg 177. Coring at Site 1094 was therefore terminated about 1.5 days ahead of schedule. Weather conditions at the time of termination did not exceed the restricting limits (4° pitch or roll) set for safe operation with the damaged LGH. As per load-shed incident report by the DP operator, maximum pitch since 0000 hr occurred at 0050 hr and was 3.8°, whereas roll was 1.7°. Wind and sea state moderated slightly within a few hours of the incident, which could have potentially permitted resumption of coring operations.

When the drill string had cleared the seafloor, weather and motion conditions were essentially unchanged, and it was deemed safe to run the coring line back down the pipe so that it could be sprayed with protective coating while being retrieved. The drill string was tripped during improving weather conditions, and the BHA was broken down and stored for transit. The bit arrived on deck at 1145 hr on 23 January.

An extensive effort then was made to secure the broken LGH-half in the moonpool before the transit to Punta Arenas. A retaining frame consisting of two 17-ft I-beams in an open cross configuration was fabricated on the rig. The frame, complete with padeyes and heavy slings, was keelhauled over the side of the vessel (the moonpool doors could not be opened) and suspended from the main traveling block by cable slings through the center well of the moonpool. The block then was raised to engage the bottom of the LGH-half with the frame. After sev-

eral attempts, the frame was determined to be supporting the LGH. Efforts to lift and realign the LGH-half were unsuccessful, but a tension of 30 kips on the slings, in addition to the attachment of the lower corner at the locking pin, seemed to stabilize the assembly and prevent motion relative to the moonpool wall and the starboard half of the LGH. That appeared to be the best possible preparation for the long, rough transit ahead, and the rig floor was secured with the driller at his station to monitor the tension on the support frame.

The vessel had remained in full DP mode for the securing operation, and an additional 3 hr was required to recover the positioning beacons, house the hydrophones, raise the thrusters, and do the protective maintenance for transit that normally is done during the final pipe trip. The vessel departed Site 1094 at 1845 hr on 23 January.

Site 1094 to Punta Arenas

The ship had been under way less than 2 hr when the driller reported a loss of tension on the damaged LGH. The ship was slowed, and investigation revealed that the forward locking pin had failed and that the port LGH-half was moving unrestrained in the moonpool, supported only by the cross frame at its base. The surge produced by moderate swells was causing too much movement of the massive (22-ton) structure for it to be restrained. With forward motion of the ship, the movement became so violent that serious damage to the moonpool appeared imminent. For the safety of the vessel, the crew had no choice but to lower the LGH until it fell free. The retaining cross was also released, and the vessel continued at full speed with deteriorating weather conditions.

LITHOSTRATIGRAPHY

Overview

Site 1094 was drilled to a TD of 171 mbsf. Sediments from this site are of Pleistocene age and predominantly consist of olive gray to gray mud-bearing diatom ooze, with minor and varying amounts of foraminifers and nannofossils (Figs. **F5, F6**). Smear-slide analysis (see **"Site 1094 Smear Slides,"** p. 42) shows that diatom abundance varies from 60% to 100%, total biogenic carbonate components (foraminifers + nannofossils) range from 0% to 40%, and mud ranges from 0% to 20% (Fig. **F7**). Total carbonate contents estimated by smear-slide analysis are somewhat higher, by ~0% to 30%, than those determined by coulometry (Fig. **F7**). X-ray diffraction (XRD) results (Table **T2,** also in ASCII format in the **TABLES** directory) indicate that opal ranges from 50 to 95 wt% and siliciclastics range from 5 to 60 wt% (Fig. **F7**).

Biogenic calcareous components (foraminifers + nannofossils) show an increase below 95 mcd, diatom abundance decreases below this point, and mud abundance remains fairly constant throughout. Several carbonate-bearing intervals are present within the sedimentary column (Fig. **F5**). Those with the highest carbonate content are thin, pink- or salmon-colored intervals that contain both foraminifers and nannofossils with a combined abundance of 20% to 30% and a maximum abundance of 45%. Spacing between the carbonate-bearing intervals decreases and the thickness of the intervals increases below 95

F5. Lithologic summary of Site 1094, **p. 22.**

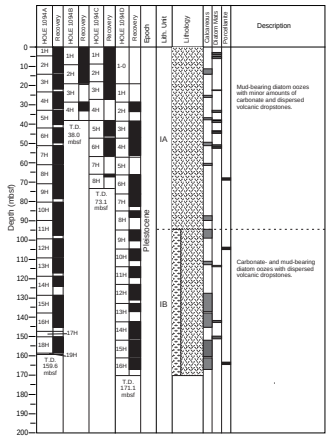

F6. Core correlation diagram for Site 1094, **p. 23.**

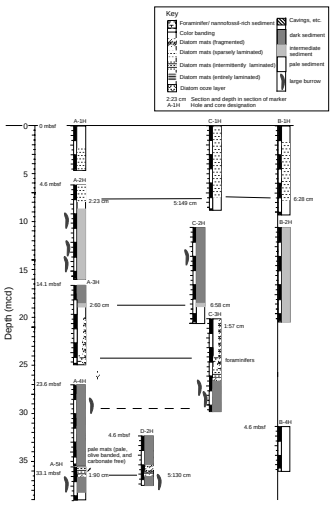

F7. Comparison of carbonate, opal, and siliciclastic contents, **p. 27.**

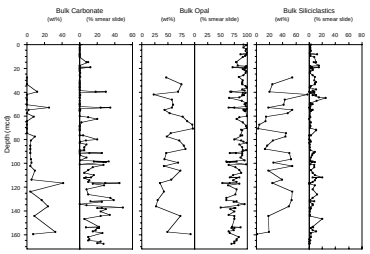

T2. X-ray diffraction data for Site 1094, **p. 50.**

mbsf. This increase in carbonate below 95 mbsf marks the boundary between two lithostratigraphic subunits.

Dispersed sand- to gravel-sized volcanic material is a minor but ubiquitous component throughout the section, particularly in dark-colored, mud-rich intervals. Although diatoms are the dominant component at this site, pure laminated diatom oozes, which were abundant at Sites 1093 and 1091 situated further north in the circum-Antarctic opal belt, are less common at this site (Fig. F5). Several intervals of fragmented diatom-rich laminae are observed, possibly remnants of a laminated diatom ooze subjected to bioturbation. Fragments of porcellanite were recovered, indicating porcellanite layers at 68, 104, and 164 mbsf (Table T3). At 142 mbsf in Hole 1094A, a porcellanite concretion was found that displays concentric "growth" rings (Fig. F8). XRD analyses reveal an opal-CT composition of the porcellanite concretions (Fig. F9).

T3. Occurrences of porcellanite at Site 1094, p. 51.

F8. Porcellanite concretion (interval 177-1094A-16H-3, 130–150 cm), p. 28.

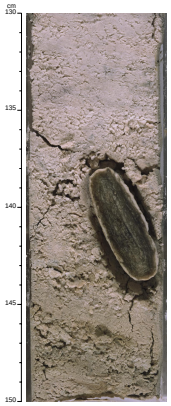

F9. X-ray diffractogram of opal-CT (interval 177-1094D-16H-2, 110–111 cm), p. 29.

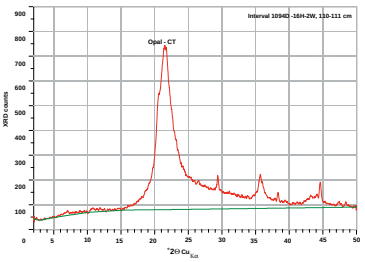

F10. Ash layer in interval 177-1094A-8H-4, 65–90 cm, p. 30.

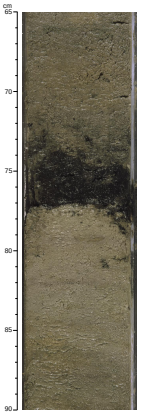

Description of Lithostratigraphic Unit

The lithostratigraphic characteristics of the sediments are defined primarily on the basis of visual core descriptions and sediment smear-slide analyses. Additional information is obtained from diffuse spectral reflectance measurements, XRD analyses for opal abundance, and calcium carbonate contents measured by coulometry. One lithostratigraphic unit that comprises two subunits was defined.

Unit I

Subunit IA

Intervals: 177-1094A-1H through 11H (0–98.0 mbsf; 0–100.83 meters composite depth [mcd]); 177-1094B-1H through 4H (0–33.2 mbsf; 0.52–36.05 mcd); 177-1094C-1H through 8H (0–67.2 mbsf; 0.28–69.52 mcd); 177-1094D-2H through 8H (28.6–93.2 mbsf; 32.25–96.55 mcd). Note: in Hole 1094D, the interval 0–28.6 mbsf was drilled ("washed") without coring.
Age: Holocene to Pleistocene

The upper 95 mbsf of sediment in Hole 1094A consists primarily of olive gray diatom ooze containing significant amounts of mud and minor amounts of carbonate. In the upper ~6 mbsf, the diatom ooze is quite soupy as a result of very high water content (see "Physical Properties," p. 14). Thin, pink- or salmon-colored intervals of carbonate-bearing to calcareous diatom ooze are present throughout Subunit IA. These intervals contain both nannofossils and foraminifers, with nannofossils showing higher relative abundances.

A 3-cm-thick vitric volcanic ash layer at 66.9 mbsf in Hole 1094A exhibits no size grading and is not scoured at its base (Fig. F10). Rare occurrences of concentrated volcanic glass were also observed as burrow fills. Dispersed sand to gravel-sized volcanic material is present throughout the subunit. Its coarse grain size suggests ice rafting by icebergs and/or sea ice as a likely mode of transport to the site. The volcanic origin and the apparent lack of coarse-grained crystalline rock fragments suggest a nearby volcanic island (Bouvet) or the Scotia Arc as the primary source area rather than the Antarctic continent.

A porcellanite layer at 68 mbsf in Hole 1094A (Fig. F11) indicates low-temperature silica diagenesis (Bohrmann et al., 1994). As a result of the fragmented nature of the recovered porcellanite and disturbance

during core splitting, the position and thickness of this layer is difficult to ascertain. Features unique to Subunit IA are large Echiurid-type burrows similar to those reported from ODP Site 846 in the eastern equatorial Pacific. Several of the large burrows (some >40 cm in length) are found in all four holes, but most extensively in Hole 1094A (8–45 mbsf) (Fig. **F12;** Table **T4**). Though not abundant or extensive, laminated diatom ooze composed predominantly of *Thalassiothrix* sp. is present throughout the upper portion of the subunit and, except for isolated fragments of laminated diatom ooze, is absent in the lower portion of the subunit below ~52 mbsf.

Subunit IB

Intervals: 177-1094A-11H through 18H (98.0–157.6 mbsf; 100.83–160.11 mcd); 177-1094D-9H through 16H (93.2–171.1 mbsf; 96.55–169.75 mcd)
Age: Pleistocene

Below 95 mbsf in Hole 1094A, the sediments are predominantly gray carbonate-bearing diatom ooze. Both nannofossils and foraminifers show higher abundances in Subunit IB relative to Subunit IA. The increase in total biogenic carbonate content, however, is primarily a result of an increase in the abundance of foraminifers (from typically ≤10% in Subunit IA to typically 10%–25% in Subunit IB), whereas nannofossil abundance shows only a minor increase. In addition to the general downhole increase in foraminifer abundance throughout this subunit, the thin, pink- or salmon-colored carbonate-rich intervals seen in Subunit IA are present throughout Subunit IB with greater frequency and increasing thickness. In Hole 1094A, a second and third porcellanite interval are present at 104 and 142 mbsf, respectively. Intact, laminated diatom ooze is present only rarely within Subunit IB, and even fragmented laminated diatom ooze is sparse. As in Subunit IA, small volcanic dropstones are observed throughout.

Interpretation

The alternation of diatom ooze and carbonate-rich intervals may reflect lithologic changes corresponding to glacial–interglacial cycles. In general, darker diatom oozes include cold-water diatom assemblages (see **"Biostratigraphy,"** p. 8) and contain more abundant sand- to gravel-sized dropstones, thus supporting the hypothesis that these sediments accumulated during glacial intervals. The lighter, carbonate-rich layers lack or contain only a few coarse-grained dropstones, suggesting deposition during interglacial intervals. This variable pattern of dropstone occurrence is seen in both Subunit IA and the lower, relatively carbonate-rich Subunit IB.

CHRONOSTRATIGRAPHY

Composite Depths

Multisensor track (MST) and color reflectance data (650–750 nm) collected from Holes 1094A–1094D were used to determine depth offsets in the composite section. Gamma-ray attenuation (GRA) bulk density and magnetic susceptibility data were collected at 2- to 4-cm intervals

F11. Fragmented porcellanite layer (interval 177-1094A-8H-5, 22–68 cm), **p. 31.**

F12. Extremely large Echiurid-type burrow (interval 177-1094A-2H-6, 5–50 cm), **p. 32.**

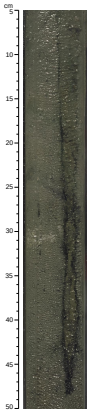

T4. Occurrences of Echiurid-type burrows at Site 1094, **p. 52.**

on cores recovered from Holes 1094A–1094D. Color reflectance data were collected at 4- to 6-cm intervals on cores from Holes 1094A–1094D (see "Physical Properties," p. 14, and "Lithostratigraphy," p. 5, for details about these MST and color reflectance data sets).

The composite data show that the cores from Site 1094 provide a nearly continuous overlap to 121 mcd (base of Core 177-1094D-11H). The data used to construct the composite section and determine core overlaps are presented on a composite depth scale in Figures F13, F14, and F15. The depth offsets that comprise the composite section for Holes 1094A–1094D are given in Table T5 (also in ASCII format in the TABLES directory).

Stretching and compression of sedimentary features in aligned cores indicate distortion of the cored sequence. Because of the distortion within individual cores on depth scales of <9 m, it was not possible to align every feature in the MST and color reflectance records accurately by simply adding a constant to the mbsf core depth. Within-core scale changes will require postcruise processing to align smaller sedimentary features. Only after allowing variable adjustments of peaks within each core can an accurate estimate of core gaps be made.

Following construction of the composite depth section for Site 1094, a single spliced record was assembled for the aligned cores over the upper 121 mcd by using cores from Holes 1094A–1094D. The composite depths were aligned so that tie points between adjacent holes occurred at exactly the same depths in mcd. Intervals having significant disturbance or distortion were avoided whenever possible. The Site 1094 splice (Table T6, also in ASCII format in the TABLES directory) can be used as a sampling guide to recover a single sedimentary sequence between 0 and 121 mcd. Spliced records of magnetic susceptibility, GRA bulk density, and color reflectance are shown in Figure F16.

In the Site 1094 spliced record there is one known core gap between Cores 177-1094A-7H and 8H. The offset of 8H was arbitrarily set to the cumulative offset of Core 7H. Furthermore, the Site 1094 splice contains seven ambiguous tie points. Ambiguities in the splice points result from insufficient overlap between adjacent cores (e.g., <1 m), lack of strong features that can be correlated across the overlapping segments of adjacent cores (e.g., diatom-mat intervals), or disagreement in magnetic susceptibility, GRA bulk density, and/or color reflectance data across the spliced interval. We have identified the ambiguous tie points with an asterisk in Table T6.

Biostratigraphy

Calcareous Nannofossils

Sediments recovered from Site 1094 provide a nearly continuous late to early Pleistocene record. Calcareous nannofossils in this interval are abundant to rare and are characterized by low diversity and by medium to poor preservation. Several barren intervals characterize the Pleistocene record (Table T7, also in ASCII format in the TABLES directory). The biostratigraphic zones of Martini (1971) and Okada and Bukry (1980), as well as some additional events according to Raffi et al. (1993) and Wei (1993) (see "Explanatory Notes" chapter), were recognized. Tables T7, T8, and T9 (all also in ASCII format in the TABLES directory), and Figure F17, summarize the main calcareous nannofossil biostratigraphic results.

F13. Smoothed color reflectance data for Site 1094, p. 33.

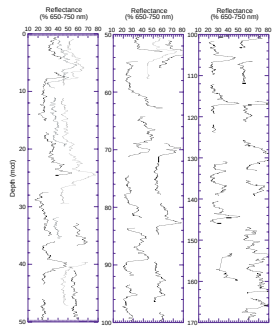

F14. Smoothed magnetic susceptibility data for Site 1094, p. 34.

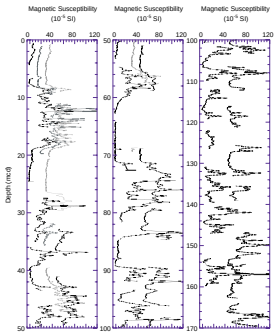

F15. Smoothed GRA bulk density data for Site 1094, p. 35.

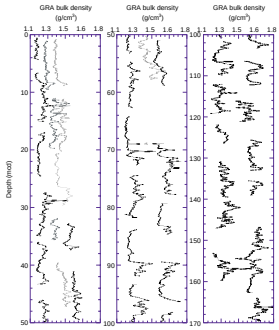

T5. Composite depths for Site 1094, p. 53.

T6. Site 1094 splice tie points, p. 54.

The first occurrence (FO) of *Emiliania huxleyi* is present from 39.97 to 40.31 mcd (base of Zone NN21). The last occurrence (LO) of *Pseudoemiliania lacunosa* is present between 81.09 and 84.71 mcd, defining the base of Zone NN20. The LO of *Reticulofenestra asanoi* is recognized from 106.87 to 114.36 mcd. The reentrance of medium *Gephyrocapsa* (4–5.5 µm) is present between 125.07 and 125.29 mcd. The FO of *R. asanoi* is identified from 130.72 to 133.04 mcd. The LO of large *Gephyrocapsa* (>5.5 µm) is observed between 139.23 and 143.90 mcd, whereas its FO is present between 165.29 and 165.86 mcd. The continuous record of medium *Gephyrocapsa* (4–5.5 µm) from the lower portion of this site allows us to assign an early Pleistocene age to the bottom of the sequence (Table **T7;** Figs. **F17, F18**).

Planktic Foraminifers

The sediment recovered from the four holes drilled at Site 1094 is dominated by foraminifer-bearing diatom ooze. The abundance of planktic foraminifers is generally higher below ~82 mcd. The pattern of increasing abundance with increasing depth is similar to Site 1093. The higher abundance of planktic foraminifers at Site 1094 compared to Site 1093 could possibly be explained by lower sedimentation rates at Site 1094 because of less dilution by biogenic silica. However, the relatively high sedimentation rates at Site 1094, as well as the shallower water depth, are probably additional important factors for the abundance and preservation of planktic foraminifers. Preservation is good to moderate in all studied core-catcher (CC) samples, and even in samples where only rare occurrences of planktic foraminifers were recorded. The dominant species at Site 1094 is, as expected, *Neogloboquadrina pachyderma* (sinistral). In addition to this species, *Globigerina bulloides, Globigerina quinqueloba,* and *Globigerinita glutinata* were recorded in some of the samples. Moreover, single specimens of two species, *Globorotalia inflata* and *Globorotalia puncticuloides,* were recorded in a few of the studied CC samples (Table **T10**, also in ASCII format in the **TABLES** directory). A nearly continuous planktic foraminifer stable isotopic record measured on *Neogloboquadrina pachyderma* (sinistral) will be achievable at Site 1094.

Benthic Foraminifers

Benthic foraminifers at Site 1094 are generally not very abundant and vary considerably in their state of preservation from poor to good. Highly abundant, needle-like remains of the diatom genus *Thalassiothrix* in the >63-µm fraction made it necessary to wet-sieve sediment samples at 150 µm.

Benthic foraminifers are highly variable, typically constituting between 5% and 100% of the total foraminifer fauna from the >150-µm fraction studied. Absolute foraminifer abundances are variable and low, reaching a maximum of 22 specimens/cm³ in Sample 177-1094A-16H-CC, 0–10 cm (147.07 mcd). There is a general trend toward higher abundances below ~120 mcd. Low benthic foraminifer abundance may be explained by relatively high sedimentation rates (see "**Stratigraphic Summary,**" p. 12). No barren intervals are observed, but some of the glacial intervals, characterized by low color reflectance and high magnetic susceptibility (Fig. **F16**), only contain very sparse benthic foraminiferal assemblages that are dominated by low-diversity agglutinated forms such as *Martinotiella* sp. Continuous benthic diatom isotopic

F16. Spliced color reflectance, magnetic susceptibility, and GRA bulk density for Site 1094, **p. 36.**

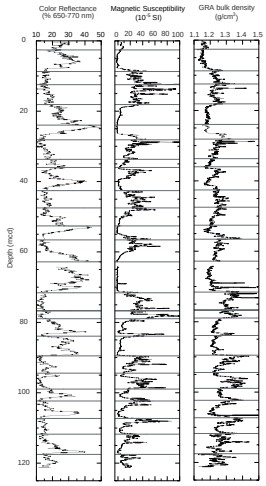

T7. Main calcareous nannofossil species at Site 1094, **p. 55.**

T8. Biostratigraphic age assignments for Site 1094, **p. 58.**

T9. Control points used to calculate sedimentation rates at Site 1094, **p. 60.**

F17. Bio- and magnetostratigraphic correlations and age designations for Site 1094, **p. 37.**

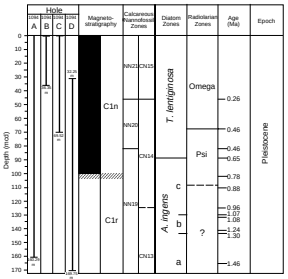

T10. Major planktic foraminifer species at Site 1094, **p. 61.**

records may be difficult to obtain from this site. However, *Cibicidoides wuellerstorfi* appears to be present fairly consistently in 12 out of 17 CC samples from Hole 1094A, suggesting that a benthic stable isotopic record, albeit discontinuous, should be achievable.

Quantitative estimates of relative species abundance were made from Holes 1094A, 1094C, and 1094D, with counts of up to 239 specimens/20-cm³ sample. Species richness is variable, with a maximum of 33 taxa recorded in Sample 177-1094A-14H-CC, 0–10 cm (126.38 mcd). High-diversity, relatively abundant assemblages correspond to interglacial intervals, and low-diversity, low-abundance assemblages correspond to glacial intervals. This pattern is clearly seen in the intervals adjacent to MIS 11, centered at 65 mcd (Table **T11,** also in ASCII format in the **TABLES** directory).

T11. Benthic foraminifers in Hole 1094A, **p. 62.**

The most common benthic taxa recorded at Site 1093 include *C. wuellerstorfi, Eggerella bradyi, Epistominella exigua, Globocassidulina subglobosa, Melonis barleeanum, Melonis pompiliodes, Oridorsalis umbonatus, Pullenia bulloides, Pullenia quinqueloba,* and *Pullenia subcarinata*. The assemblages present are very similar to those recorded at Sites 1091 and 1093. No biostratigraphic subdivision, other than glacial–interglacial cyclicity, can be suggested on the basis of the recovered benthic foraminifer assemblages.

Diatoms

Site 1094 sediments provide a continuous Pleistocene record with a basal age of lower early Pleistocene. For biostratigraphic age assignments we used the late Pliocene–Pleistocene zonation proposed by Gersonde and Bárcena (1998), although this zonation scheme could be applied only partially because of the trace abundance of the marker species *Hemidiscus karstenii*. All diatom stratigraphic information from the four holes cored at Site 1094 was combined and converted to the mcd scale (Tables **T8, T9,** and **T12;** all also in ASCII format in the **TABLES** directory).

T12. Diatom, silicoflagellate, ebridian, Actiniscus, sponge spicule, and phytolith occurrence, Site 1094, **p. 63.**

Diatoms are generally abundant, and preservation is good to moderate. Silicoflagellates, which were also examined during diatom analyses, were encountered in trace to rare abundances in half of the samples. Sponge spicules and Ebridians are sporadic (Table **T12**).

Biostratigraphy

Trace occurrence of the marker species *H. karstenii* precluded the subdivision of the *Thalassiosira lentiginosa* Zone into its three subzones according to the zonation proposed by Gersonde and Bárcena (1998) for the northern area of the Southern Ocean. Because *H. karstenii* is most abundant in warmer waters north of the present PF (see **"Chronostratigraphy,"** p. 9, in the "Site 1093" chapter), this datum could not be used for the identification of MISs 7, 9, and 11. The boundary between the *T. lentiginosa* and the underlying *Actinocyclus ingens* Subzone c, reflecting an age of 0.65 Ma, was observed at 88 mcd (Fig. **F17**). The marker species *Thalassiosira elliptipora,* whose first abundant appearance datum at ~1.07 Ma is used to define the underlying boundary of the *A. ingens* Subzone b (Gersonde and Bárcena, 1998), was not encountered until ~130 mcd. The transition to *A. ingens* Subzone a at ~143 mcd, corresponding to an age of 1.3 Ma, is marked by the last appearance datum of *Fragilariopsis barronii* (Gersonde and Bárcena, 1998). Common occurrences of specimen, which probably document the transition between *F. barronii* and the extant *F. kerguelensis,* make

the definition of *A. ingens* Subzone b difficult. However, ages older than 1.24 Ma derived from calcareous nannofossil biostratigraphy (see above) support the assignment of these sediments to *A. ingens* Subzone a, spanning the time interval between 1.3 and 1.8 Ma (Fig. F18).

F18. Age-depth plot of biostratigraphic and paleomagnetic events at Site 1094, p. 38.

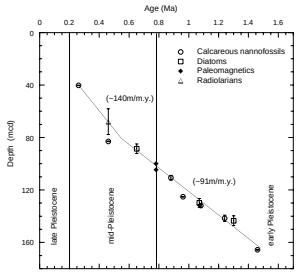

Radiolarians

Radiolarian biostratigraphy at Site 1094 is based on the examination of 22 samples (Table T13, also in ASCII format in the TABLES directory). Radiolarian abundance at Site 1094 varies from abundant to rare, depending on the relative amount of diatoms in the samples, and preservation is excellent throughout the recovered sequence.

The boundary between the Omega and Psi Zones, marked by the LO of *Stylatractus universus* at 0.46 Ma, is placed at 67.83 mcd (Table T9). Except for *Stylatractus universus,* no marker species were found in the lower portion of the recovered sequence. Calcareous nannofossils and diatoms provide datums of 1.46 and 1.3–1.8 Ma below ~160 mcd, respectively (see above), which indicates that samples from the lower portion can be assigned to the Chi Zone. Samples 177-1094A-14H-CC, 0–10 cm (126.38 mcd), and 16H-CC, 0–10 cm (147.07 mcd), contain reworked specimens of *Desmospyris spongiosa, Eucyrtidium carvertense,* and *Helotholus vema,* all of which are characteristic species below the Chi Zone.

The occurrence of *Pterocanium trilobum,* defining the top of the Chi Zone, is generally very rare; this fact has also been noted by previous studies (e.g., Lazarus, 1990). A significant revision may be necessary for the Pliocene–Pleistocene radiolarian biostratigraphy of the Antarctic region to establish reliable datums.

T13. Main components of the radiolarian assemblages at Site 1094, p. 65.

Paleomagnetism

Archive halves of APC cores recovered at Site 1094 were measured using the shipboard pass-through magnetometer. Measurements were made at 5-cm intervals. Sections obviously affected by drilling disturbance were not measured. All core sections from Site 1094 were measured after alternating-field (AF) demagnetization at peak fields of 0 (natural remanent magnetization [NRM]), 5, 10, 15, 20, and 25 mT.

NRM intensities are ~5 × 10^{-2} A/m throughout most of the APC section. After AF demagnetization at peak fields of 25 mT, intensities generally decreased to ~10^{-2} A/m. NRM inclinations are typically downward or shallow as a result of a downward-directed magnetic overprint, possibly a viscous remanent magnetization attributable to the drill string. The drill-string remagnetization was largely removed at peak demagnetization fields in excess of 10 mT. The resulting inclination values (Fig. F19) define a normal polarity zone (Brunhes Chron) overlying a reversed polarity zone (Matuyama Chron). In Hole 1094D, several normal polarity zones are recognized within the Matuyama Chron. Interpretation of these normal polarity intervals should be clarified by shore-based study of discrete samples. The normal polarity interval between 120 and 128 mbsf at Hole 1094D may represent the Jaramillo Subchron. The Brunhes/Matuyama boundary is best identified in the 95.4- to 100.0-mbsf interval at Hole 1094A (Fig. F19; Table T9).

F19. Inclination of the remanent magnetization after AF demagnetization at Holes 1094A and 1094D, p. 39.

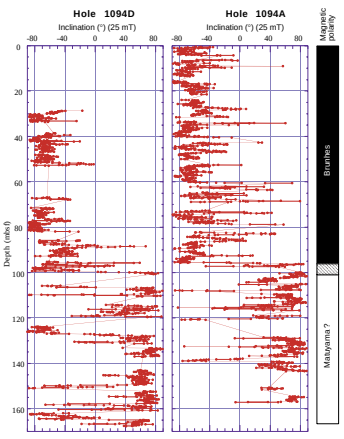

Stratigraphic Summary

At Site 1094, the sedimentary section is nearly continuous to a depth of 121 mcd (base of Core 177-1093D-10H, early Pleistocene), and has a total thickness of ~170 mcd (base of Core 177-1094D-16H) (Figs. F13, F14, F15, F16). Holes 1094A–1094D were cored with the APC to 159.6, 38.0, 73.1, and 171.1 mbsf, respectively. The depth offset of cores below the spliced record is the same as the greatest cumulative offset of the overlying cores.

An expanded and continuous Pleistocene sequence was recovered at Site 1094. The lowermost biostratigraphic datum is the FO of large *Gephyrocapsa* (>5.5 µm) at 165.86 mcd (Sample 177-1094D-16H-2, 87 cm), which suggests an age older than 1.46 Ma.

All biostratigraphic datums, including calcareous nannofossil, diatom, and radiolarian events and available magnetostratigraphic events, yield consistent age assignments throughout the record at Site 1094. The sedimentation rates in the diatom-dominated upper to mid-Pleistocene sequences at Site 1094 average ~140 m/m.y. The transition between the Brunhes and Matuyama Chrons is identified between 98.20 and 101.58 mcd in Hole 1094A. Early Pleistocene sedimentation rates are lower, averaging ~90 m/m.y. This pattern of higher sedimentation rates during the last ~0.45 m.y. is similar to the pattern observed Site 1093.

The extremely expanded upper and mid-Pleistocene sediments provide a unique opportunity for paleoceanographic reconstructions at ultra-high time resolution in a pelagic environment. Sedimentation rates of ~140 m/m.y. throughout this interval will allow sampling at millennial and submillennial time-scale resolution. Such records can be correlated in detail with paleoclimatic records from Greenland and Antarctic ice cores. In addition, they will allow a detailed study of the sea-ice record as reflected in the abundance fluctuations of sea-ice diatoms. Based on the examination of CC samples, it seems likely that a nearly continuous planktic stable isotopic stratigraphy (*N. pachyderma* [sinistral]) and a more or less continuous benthic foraminiferal stable isotopic record can be established for Site 1094.

GEOCHEMISTRY

Volatile Hydrocarbons

As a part of the shipboard safety and pollution program, volatile hydrocarbons (methane, ethane, and propane) were measured in the sediments of Holes 1094A and 1094D using the standard ODP headspace sampling techniques. Headspace methane concentrations were quite low (2 to 5 parts per million by volume [ppmv]) in the sedimentary sequence at Site 1094 (Table T14; Fig. F20). Ethane, propane, and other higher molecular weight hydrocarbons were not observed.

Interstitial Water Chemistry

Shipboard chemical analyses of the interstitial water from Site 1094 followed the procedures for Sites 1088–1093. The results from the standard shipboard analyses of 5-cm whole rounds are presented in Table T15 and Figure F21, and were obtained from 16 interstitial water samples from Hole 1094A (to a depth of 155 mbsf) and two samples from Hole 1094D (from 158 to 166 mbsf). Interstitial water samples were

T14. Concentrations of methane at Site 1094, p. 66.

F20. Concentration of methane vs. depth at Site 1094, p. 40.

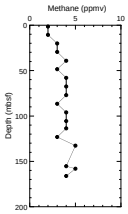

T15. Interstitial water chemistry at Site 1094, p. 67.

F21. Interstitial water chemistry profiles vs. depth at Holes 1094A and 1094D, p. 41.

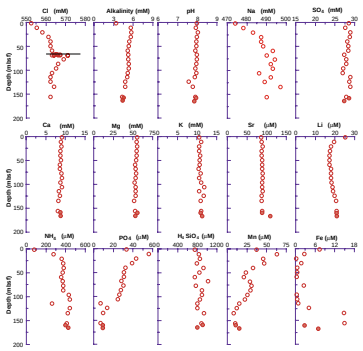

taken from every core throughout the entire section except when recovery was insufficient.

After splitting the cores, two porcellanite (opal-CT) layers were discovered in Hole 1094A at ~68 and ~104 mbsf, and a porcellanite concretion was discovered at 142 mbsf. The same porcellanite intervals were also observed in Hole 1094D, along with an additional layer at ~164 mbsf (see "Lithostratigraphy," p. 5). Five intervals comprising the porcellanites (68 and 104 mbsf in Hole 1094A; 68, 142, and 164 mbsf in Hole 1094D) were sampled at closely spaced intervals near the porcellanites, using two adjacent 10-cm^3 plugs for squeezing ~20 cm^3 of sediment in small-volume titanium squeezers. A very limited number of shipboard analyses were performed on the samples from three of the porcellanite intervals, and these data are presented in Table T16.

T16. Interstitial water chemistry from porcellanite intervals in Holes 1094A and 1094D, p. 69.

The chlorinity profile from Site 1094 is clearly influenced by the diffusional barriers imposed by the porcellanite layer at 68 mbsf and, therefore, provides an interesting comparison with the profiles at Sites 1091 and 1093. If it were not for the porcellanite at 68 mbsf, the trend of the Cl^- profile would probably be nearly identical to these other sites, showing a maximum of ~570 mM at 50–60 mbsf (considered by some as a by-product of the ice-age increase in salinity). However, there is a sharp discontinuity in the Cl^- maximum at Site 1094, indicating that vertical exchange of interstitial water across the porcellanite layer became severely impeded at some time. The conformity to the Cl^- trend established in Sites 1093 and 1091 below the porcellanite layer suggests that the Cl^- maximum was in place before the formation of the diffusional barrier. Therefore, if the maximum is indeed associated with the last ice age, then the porcellanite must be significantly younger than 20 ka. However, it is possible that the porcellanite might be older if the Cl^- maximum at Site 1094 is a remnant of an earlier ice age.

The diffusional barriers do not affect the major cation profiles (Ca, Mg, Sr, and K), which all show virtually no change from seawater values downhole. This lack of variability suggests little or no influence from diagenetic processes (such as carbonate recrystallization, or ash or clay alteration) downhole, at least above 200 mbsf. Dissolved silica increases gradually downhole, but there is some suggestion of reduced concentrations of silica in and around the porcellanite layers. This observation will be quantified more precisely with shore-based laboratory analyses, particularly on the high-resolution samples bracketing the porcellanites.

The sediments at Site 1094 can be classified as suboxic, because there is no evidence for sulfate reduction; sulfate concentrations at the bottom of Hole 1094A are indistinguishable from seawater values. There are some basic similarities between the redox characteristics of Site 1094 and those of the other diatom sites, namely Sites 1091 and 1093; however, there are also significant differences. Dissolved phosphate reaches a maximum in the upper 20 mbsf at Site 1094, just as in the other sites. On the other hand, ammonium and alkalinity also rise sharply to near maximum values in the upper 20 mbsf at Site 1094, unlike Sites 1091 and 1093, where ammonium and alkalinity increase more gradually to maximum values at around 150 mbsf (see "Geochemistry" in the "Site 1091" and "Site 1093" chapters). In addition, the peak in phosphate is significantly greater than can be accounted for by the increases in ammonium and alkalinity. The phosphate profile follows the Mn^{+2} profile almost exactly, suggesting that reactive metal (oxy)hydroxide phases may contribute partially to interstitial water phosphate. Because there are similarities in the phosphate

and Mn^{+2} profiles at Sites 1091 and 1093, metal oxide-bound phosphate may partly explain the shallow phosphate peaks observed at those sites as well. This observation does not negate the possibility that there is a shallow reactive organic fraction and a deeper, more refractory organic fraction in diatomaceous oozes, as discussed in the previous site chapters. It simply implies that some phosphate may be transiently associated with metal oxides before being released to interstitial waters.

Considering Sites 1091, 1093, and 1094 together, the behavior of the redox-sensitive species delineates a consistent pattern in diatom ooze sedimentation. There must be some, as yet unknown, aspect of diatom organic-matter remineralization that not only allows sulfate to remain high (even in the absence of diffusion of sulfate from seawater, as in the case of Site 1094), but also allows the downhole mobility and reduction of reactive metals.

Solid Phase Analysis

The shipboard solid phase analysis at Site 1094 consisted of measurements of inorganic carbon, total carbon, total nitrogen (TN), and total sulfur (TS) throughout the sedimentary sequence of Site 1094 (Table **T17;** Fig. **F22;** see **"Explanatory Notes"** chapter for methods). $CaCO_3$ contents at Site 1094 were generally low, ranging from 0.0 to 41.6 wt%, with an average value of 6.6 wt%. $CaCO_3$ was not detected in the sediments above 30 mbsf in the upper Pleistocene section, but this is likely an artifact of the low-resolution sampling because some carbonate intervals were observed over this interval (see **"Lithostratigraphy,"** p. 5). Below 30 mbsf, $CaCO_3$ shows a generally increasing trend downhole. Relatively high $CaCO_3$ corresponds to intervals of nannofossil- and foraminifer-bearing diatom ooze (see **"Lithostratigraphy,"** p. 5).

Total organic carbon (TOC) contents vary between 0.41 and 1.09 wt%, with an average value of 0.83 wt% in the Pleistocene section. TS concentrations vary between 0.07 and 0.36 wt%. TN contents are quite low (0.02–0.04 wt%) and are probably underestimated because the measurements of these samples were performed under poor analytical conditions (an air leak in the carbon-nitrogen-sulfur analyzer). Although TOC/TN values vary between 15.7 and 67.9, the higher TOC/TN values are likely also overestimated in the sediments of Site 1094 (Fig. **F22**). These lower TN and higher TOC/TN values will likely be modified by detailed shore-based analysis. Pyrolysis analyses were not performed because of the organic-carbon-poor nature of the sediments.

PHYSICAL PROPERTIES

GRA bulk density, magnetic susceptibility, NGR emission, and *P*-wave velocity were measured with the MST on whole-core sections recovered from Site 1094. Color reflectance and resistivity were measured on the working half of all split APC cores using the Oregon State University Split Core Analysis Track (OSU-SCAT) (see **"Explanatory Notes"** chapter). Other physical properties measurements conducted on discrete core samples included moisture, density, and *P*-wave velocity. Measured parameters were initial wet bulk mass (M_b), dry mass (M_d), and dry volume (V_d). Velocity was measured on split-core sections using the *P*-wave velocity sensor 3 (PWS3). Table **T18** and Figure **F23** summarize the physical properties measurements performed at Site 1094.

T17. Analytical results of IC, $CaCO_3$, TC, TOC, TN, TS, and TOC/TN at Site 1094, **p. 70.**

F22. $CaCO_3$, TOC, TN, TS, and TOC/TN vs. depth at Site 1094, **p. 42.**

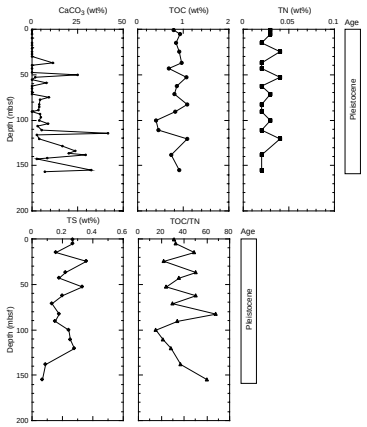

T18. Physical properties measurements conducted at Site 1094, **p. 71.**

F23. Site 1094 *P*-wave velocity, porosity, resistivity, bulk density, reflectance, magnetic susceptibility, and NGR, **p. 43.**

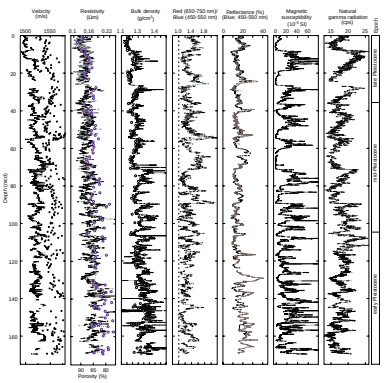

Multisensor Track and Split Core Analysis Track

At previous Leg 177 sites, sedimentary physical properties were controlled largely by changes in the proportion of carbonate vs. siliceous components. At Site 1094, terrigenous material is much more common and has considerably more influence. At previous sites, high GRA and discrete-sample (moisture and density [MAD] method) bulk densities were observed within carbonate layers. GRA and MAD bulk densities generally agree very well (Fig. F24). At Site 1094, greatest densities are generally associated with muddy intervals (as determined from smear slide analysis; see "Lithostratigraphy," p. 5).

F24. Relationship between GRA and MAD bulk density at Site 1094, p. 44.

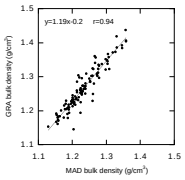

The characteristics of the reflectance spectrum for sediments from Site 1094 are somewhat different from those of the more northerly Leg 177 sites. As with previous sites, high blue reflectance at Site 1094 is caused by an increase in carbonate, but red/blue values do not show the decrease toward 1.0 in carbonate-rich intervals that characterized the previous sites. The reason for this is that the carbonate layers are not as pure at Site 1094 (<40% carbonate; see "Lithostratigraphy," p. 5), and other components, either diatoms and/or mud, impart the carbonate layers with a salmon-pink color that causes red overprinting of the reflectance signal. The red/blue values do, however, show a marked increase when diatoms dominate the sediment. In core photographs, it can be observed that the diatom-rich layers directly underlie the carbonate layers, and this is clearly evident in the lead of high red/blue peak values relative to blue reflectance peak values in Figure F23.

Porosity decreases and bulk density increases downhole because of compaction. The decrease in porosity is closely mirrored by an increase in resistivity. Superimposed on the general trend is a cyclic variability related to alternations between muddy diatom ooze and layers of less muddy foraminifer- and nannofossil-bearing diatom ooze (see "Lithostratigraphy," p. 5). The muddy diatom ooze layers also contain dispersed sand and gravel that indicate ice-rafting (see "Lithostratigraphy," p. 5). In the upper 90 mcd, the cyclicity has a dominant period of ~20 m (Fig. F23). The cyclicity is also clearly evident in the records of magnetic susceptibility, NGR, and spectral reflectance. The shipboard age-depth model (see "Chronostratigraphy," p. 7) indicates that these cycles represent the 100-k.y. climatic cycles of the late Pleistocene.

Above 90 mcd, NGR, GRA bulk density, and reflectance all display a prominent saw-tooth signal, although the relationship is inverted in the reflectance record (Fig. F23). GRA density and NGR show a steady increase with time following the deposition of each diatom-rich layer, which is low in mud content. The steady increase culminates at a maximum value (minimum in reflectance), and then abruptly decreases at the base of the next low-mud interval. Furthermore, there is an abrupt increase and decrease in magnetic susceptibility during the transition into and out of the muddy diatom-rich layers. The saw-tooth pattern of GRA and NGR signals probably represents either a gradual increase in terrigenous influx (probably through ice-rafting) or a gradual decrease in biogenic input. In any case, the abrupt decrease in each signal suggests a rapid termination of the environmental conditions characterized by increased terrigenous components. A similar pattern was observed at Site 1093, where carbonate layers are overlying sediments with high magnetic susceptibility that has been attributed to a greater concentration of IRD (see "Physical Properties," p. 18, in the "Site 1093" chapter).

Below 90 mcd, there is an abrupt decrease in the red/blue values, probably as a result of increased carbonate content compared with the upper section (see "Lithostratigraphy," p. 5). In addition, the period of cyclicity recorded in physical properties decreases to ~5 m, as a result of more frequent alternations between carbonate-bearing intervals and muddy diatom-rich intervals that were deposited at reduced sedimentation rates (see "Lithostratigraphy," p. 5, and "Chronostratigraphy," p. 7).

P-wave Velocity

Figure F23 shows *P*-wave velocities measured with the PWS3 velocimeter and *P*-wave logger (PWL) at Site 1094. PWL velocities are somewhat lower than PWS3 velocities by a mean difference of ~35 m/s. Overall, velocity is inversely correlated with fluctuations in GRA bulk density. PWL velocities range from 1510 to 1525 m/s (median = 1518 m/s) and PWS3 velocities range from 1521 to 1575 m/s (median = 1553 m/s).

Measurements on discrete porcellanite/chert pieces with the PWS3 probe provided velocities between 3000 and 4000 m/s.

Heat Flow

As with the diatom oozes at Sites 1091 and 1093, the total of 65 thermal conductivity measurements gave values within a narrow range (0.61–0.79 W/[m·K]; Table T19, also in ASCII format in the TABLES directory; Fig. F25). The frequency distribution of the measured values resembles a normal distribution and the mean of 0.68 W/(m·K) appears to be characteristic for this lithology. The standard deviation of 0.04 W/(m·K) can be attributed to analytical error, indicating that there is very little variability in the measured material in terms of thermal conductivity.

At Site 1094, seven successful downhole temperature measurements were obtained using the APCT shoe (Adara tool), one in bottom water and six in sediment between 33 and 147 mbsf. One additional measurement was taken at 159 mbsf using the DVTP. As at Site 1093, measurements at Site 1094 were also slightly to severely affected by frictional heat and/or downhole flow of cold water during deployment (Fig. F26). The temperature-time series was evaluated using shipboard processing programs to derive equilibrium temperatures. The relatively large measurement errors of ±0.3° to ±0.5°C were estimated from repeated application of decay models to different intervals of the temperature curve, and consideration of the heating and cooling disturbance during deployment (Fig. F26).

The depth-temperature relationship reveals a consistent, anomalously low temperature gradient of 8.3°± 0.5°C/km (Fig. F27). Using an average thermal conductivity of 0.7 W/(m·K) for the sedimentary section, a very low average heat flow of 6 ± 1 mW/m² is calculated for the drilled interval. This anomalously low heat flow has important implications for the origin of young porcellanites at Site 1094 (see "Lithostratigraphy," p. 5) and supports their formation at low temperature (Bohrmann et al., 1994; Botz and Bohrmann, 1991).

T19. Thermal conductivity measurements at Site 1094, p. 72.

F25. Thermal conductivity measurements at Site 1094, p. 45.

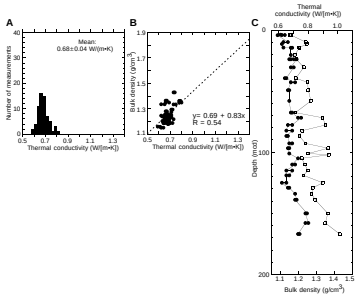

F26. Downhole temperature measurements at Site 1094, p. 46.

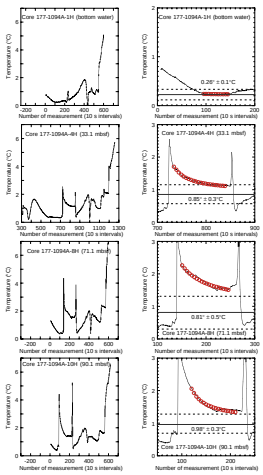

F27. Depth-temperature curve for Site 1094, p. 48.

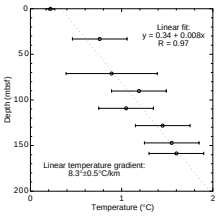

REFERENCES

Bathmann, U., Schulz-Baldes, M., Fahrbach, E., Smetacek, V., and Hubberten, H.-W., 1992. The Expeditions ANTARKTIS IX/1-4 1990/1991. *Rep. Polar Res.,* 100.

Bohrmann, G., Abelmann, A., Gersonde, R., Hubberten, H., and Kuhn, G., 1994. Pure siliceous ooze, a diagenetic environment for early chert formation. *Geology,* 22:207–210.

Botz, R., and Bohrmann, G., 1991. Low temperature opal-CT precipitation in Antarctic deep-sea sediments: evidence from oxygen isotopes. *Earth Planet. Sci. Lett.,* 107:612–617.

Cande, S.C., and Kent, D.V., 1992. A new geomagnetic polarity time scale for the Late Cretaceous and Cenozoic. *J. Geophys. Res.,* 97:13917–13951.

Gersonde, R., and Bárcena, M.A., 1998. Revision of the late Pliocene–Pleistocene diatom biostratigraphy for the northern belt of the Southern Ocean. *Micropaleontology,* 44:1–15.

Lazarus, D., 1990. Middle Miocene to Recent radiolarians from the Weddell Sea, Antarctica, ODP Leg 113. *In* Barker, P.F., Kennett, J.P., et al., *Proc. ODP, Sci. Results,* 113: College Station, TX (Ocean Drilling Program), 709–727.

Martini, E., 1971. Standard Tertiary and Quaternary calcareous nannoplankton zonation. *In* Farinacci, A. (Ed.), *Proc. 2nd Int. Conf. Planktonic Microfossils Roma:* Rome (Ed. Tecnosci.), 2:739–785.

Okada, H., and Bukry, D., 1980. Supplementary modification and introduction of code numbers to the low-latitude coccolith biostratigraphic zonation (Bukry, 1973; 1975). *Mar. Micropaleontol.,* 5:321–325.

Raffi, I., Backman, J., Rio, D., and Shackleton, N.J., 1993. Plio-Pleistocene nannofossil biostratigraphy and calibration to oxygen isotopes stratigraphies from Deep Sea Drilling Project Site 607 and Ocean Drilling Program Site 677. *Paleoceanography,* 8:387–408.

Wei, W., 1993. Calibration of Upper Pliocene-Lower Pleistocene nannofossil events with oxygen isotope stratigraphy. *Paleoceanography,* 8:85–99.

Figure F1. Track lines and shotpoints for the site surveys of Site 1094 conducted during *Polarstern* Cruise ANT-XI/3 (Line AWI-94080; solid line, pluses) and *Thompson* Cruise TTN057 (dashed line, circles). The bold portion of the track line corresponds to the segment of the seismic profile displayed in Fig. **F2,** p. 19.

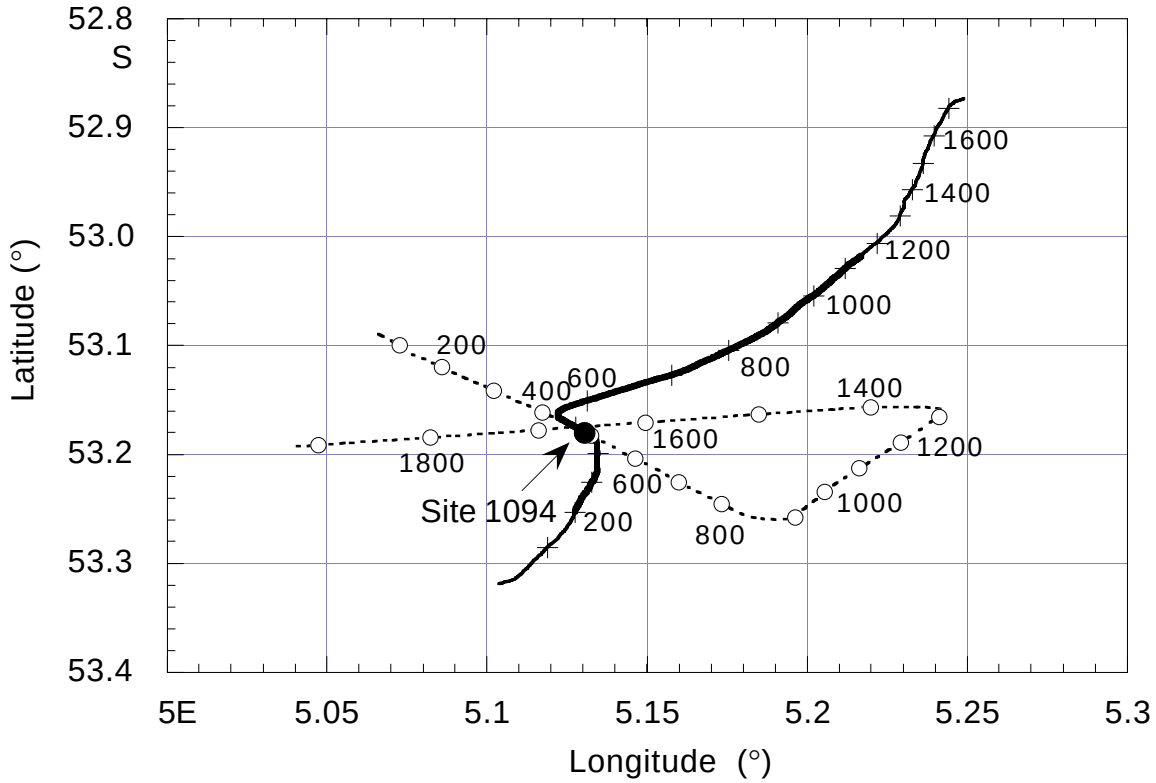

Figure F2. Segment of multichannel seismic Line AWI-94080 collected during site-survey *Polarstern* Cruise ANT-XI/3 showing the location and penetration depth of Site 1094. Depth was assigned according to the preliminary interval velocity estimates presented in Table T1, p. 49.

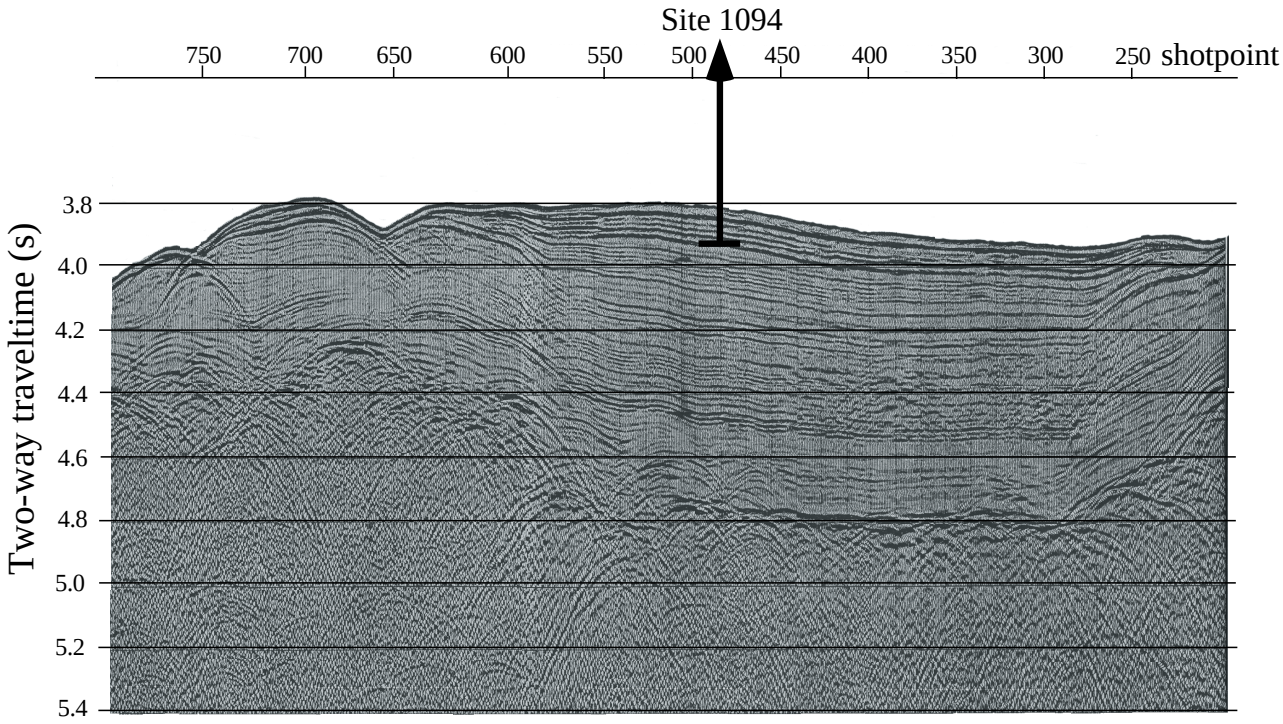

Figure F3. Analog Parasound profiles collected near Site 1094 and digitized signal illustrating high-amplitude reflectors corresponding to porcellanite horizons (Bathmann et al., 1992).

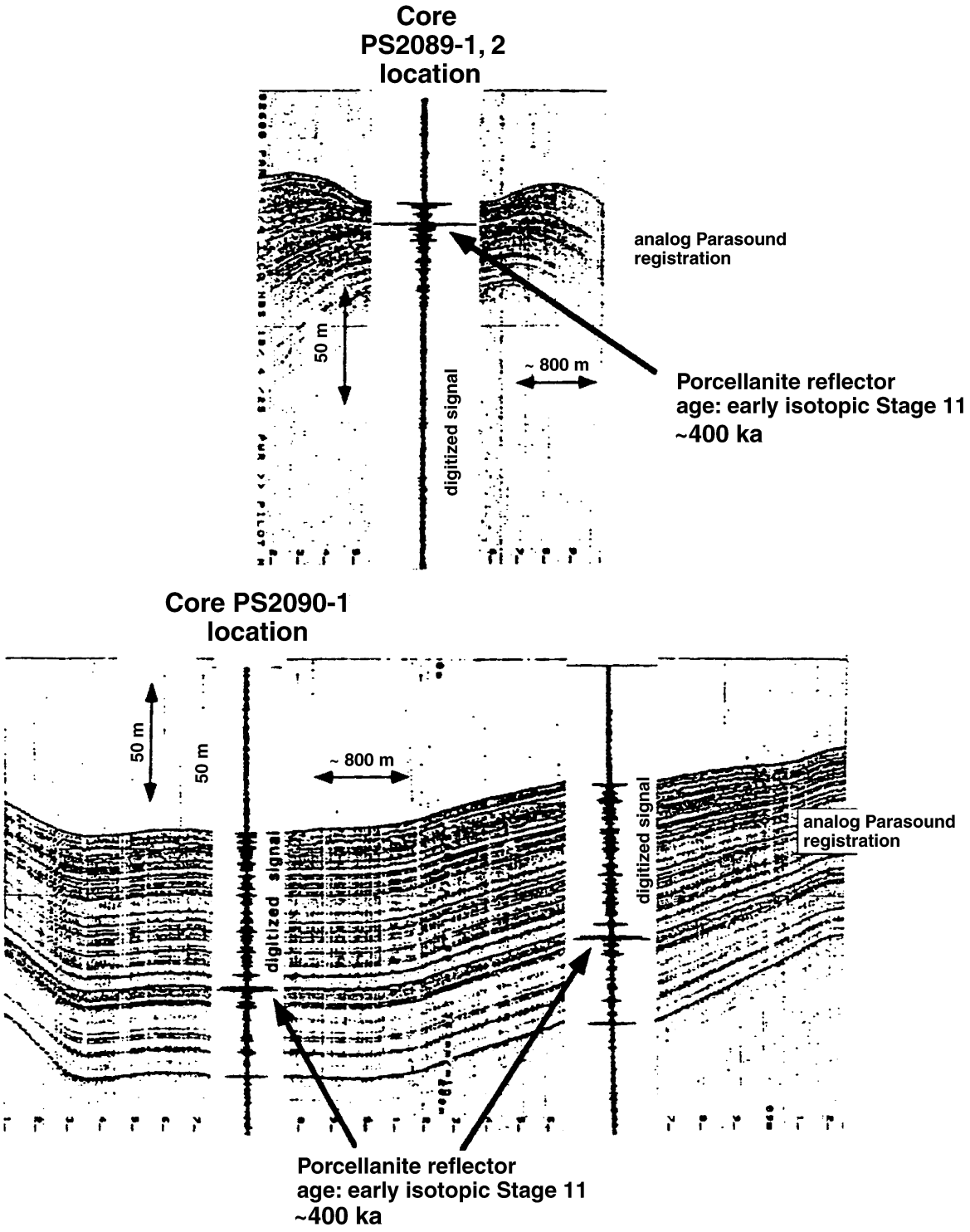

Figure F4. Bathymetric map of the area surrounding Site 1094 showing the location of Site 1094 and piston cores PS2089-1, 2, and PS2090-1.

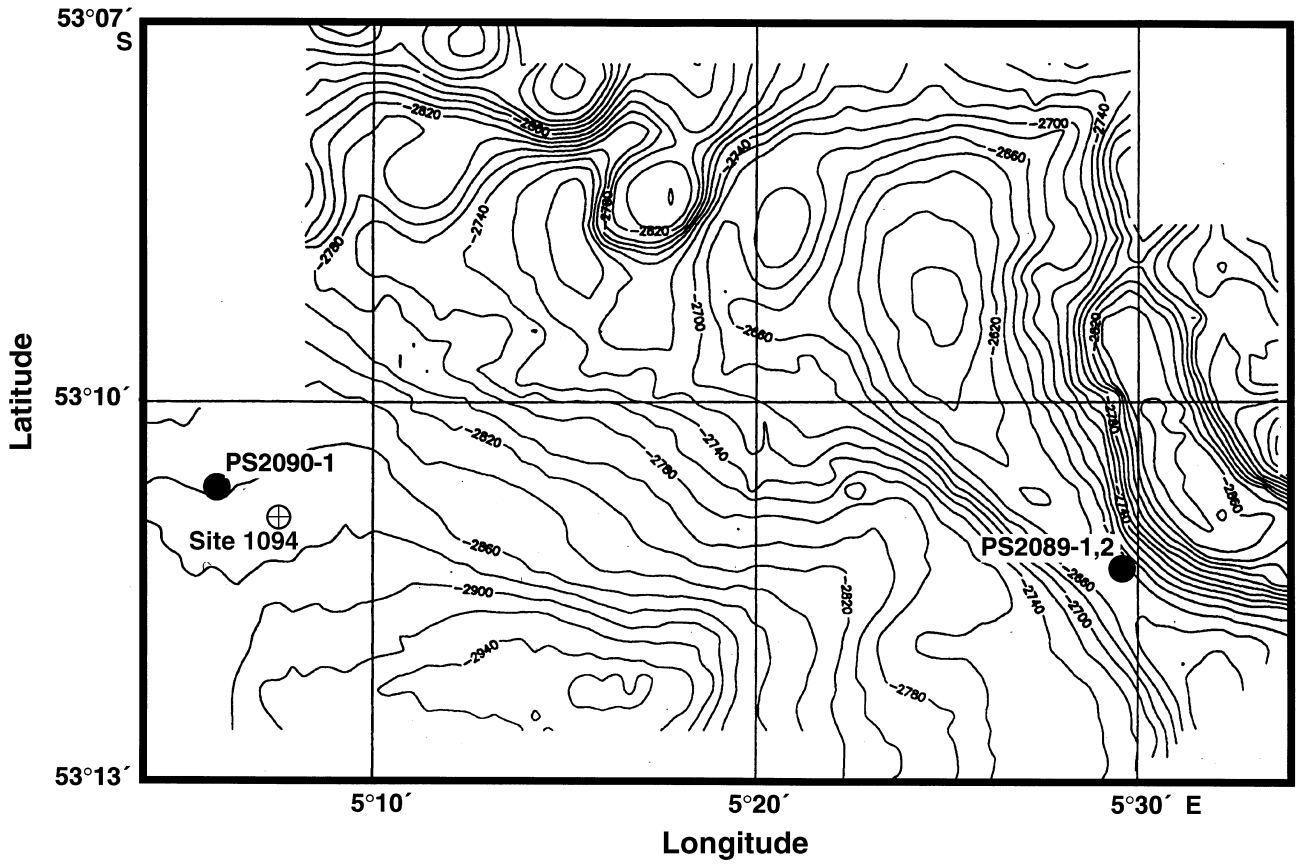

Figure F5. Summary of lithology, core recovery, and occurrence of carbonate-bearing intervals and laminated diatom ooze in the four holes drilled at Site 1094. T.D. = total depth.

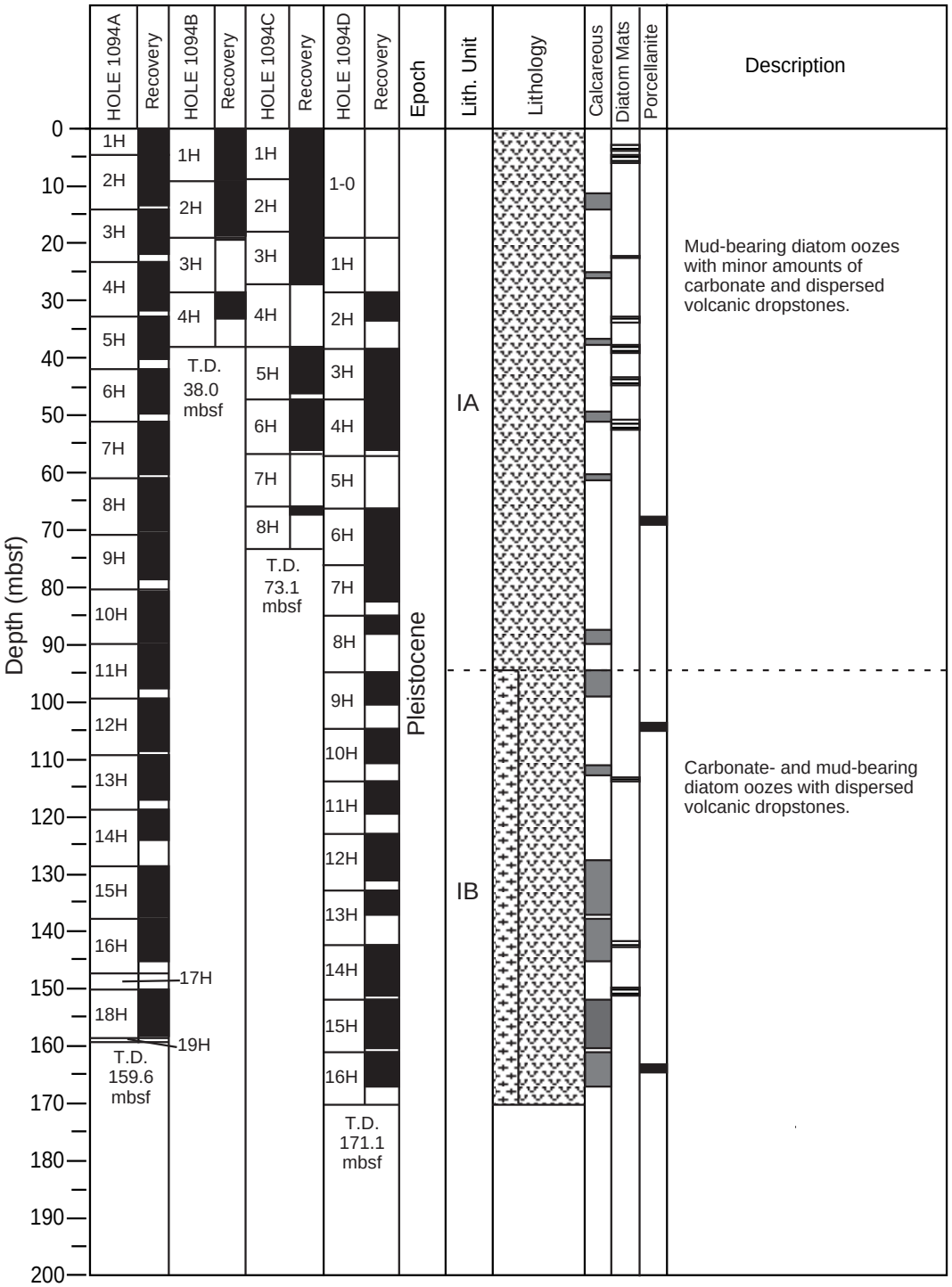

Figure F6. Core correlation diagram for Site 1094. (Continued on next three pages.)

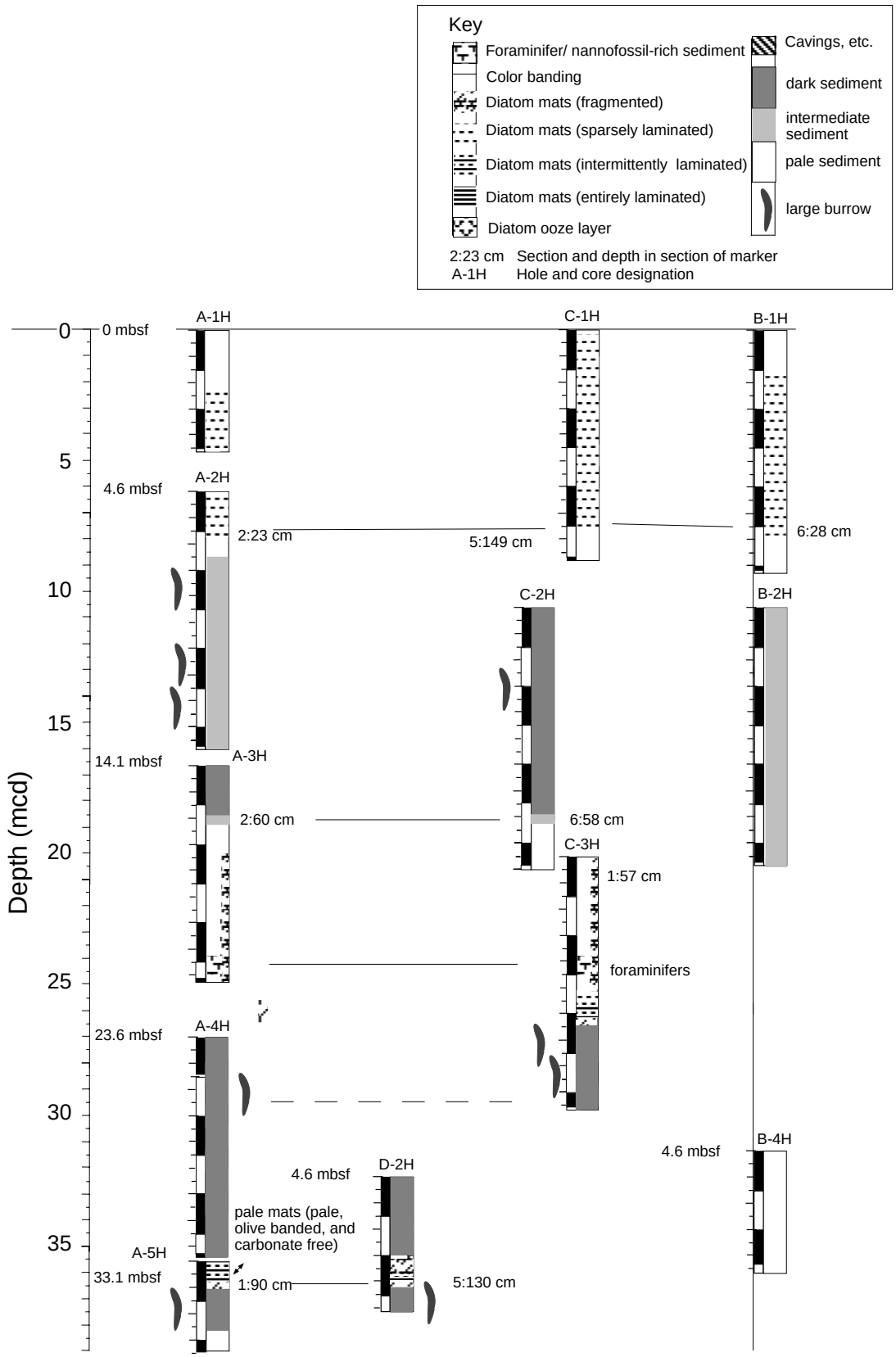

Figure F6 (continued).

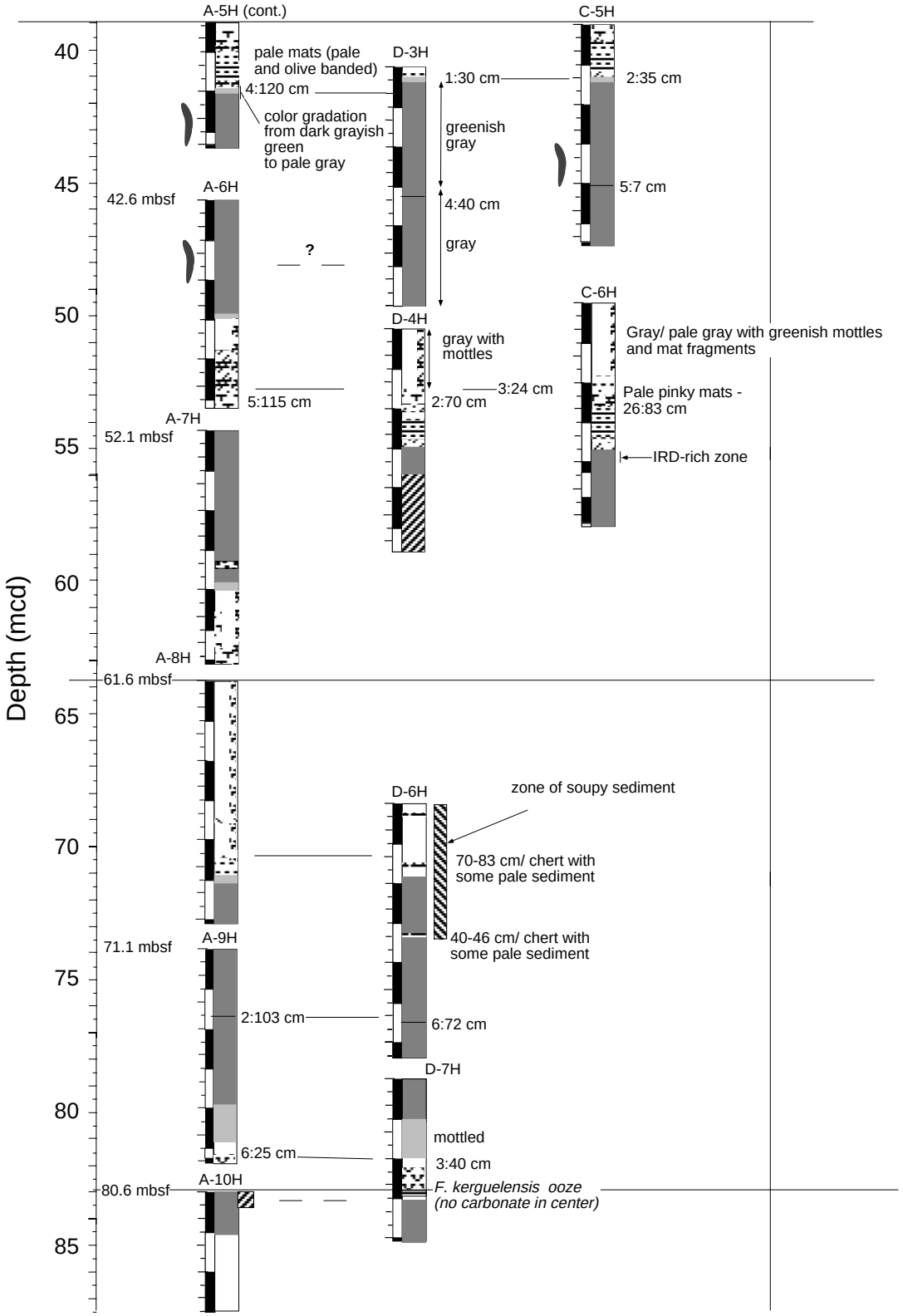

Figure F6 (continued).

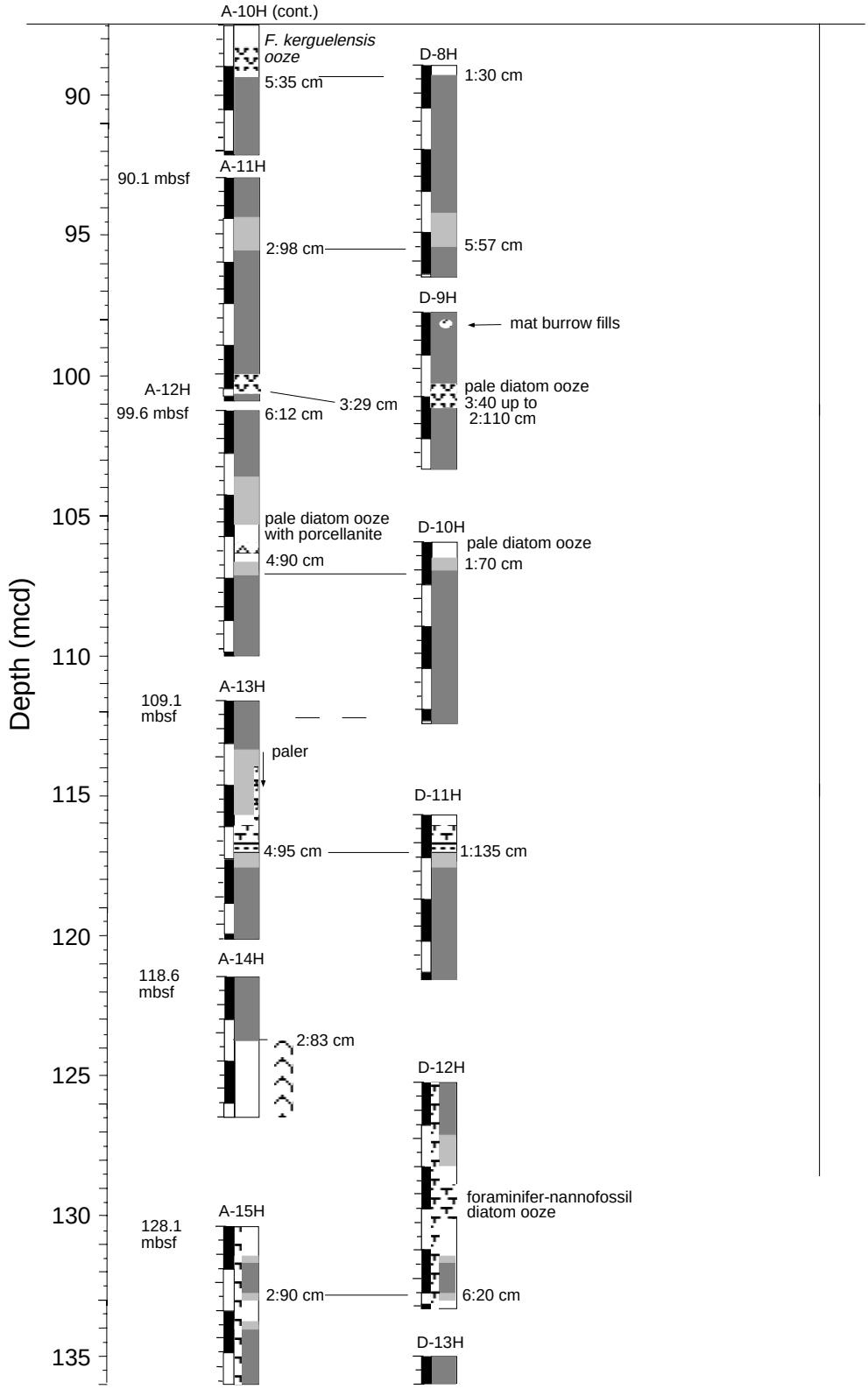

Figure F6 (continued).

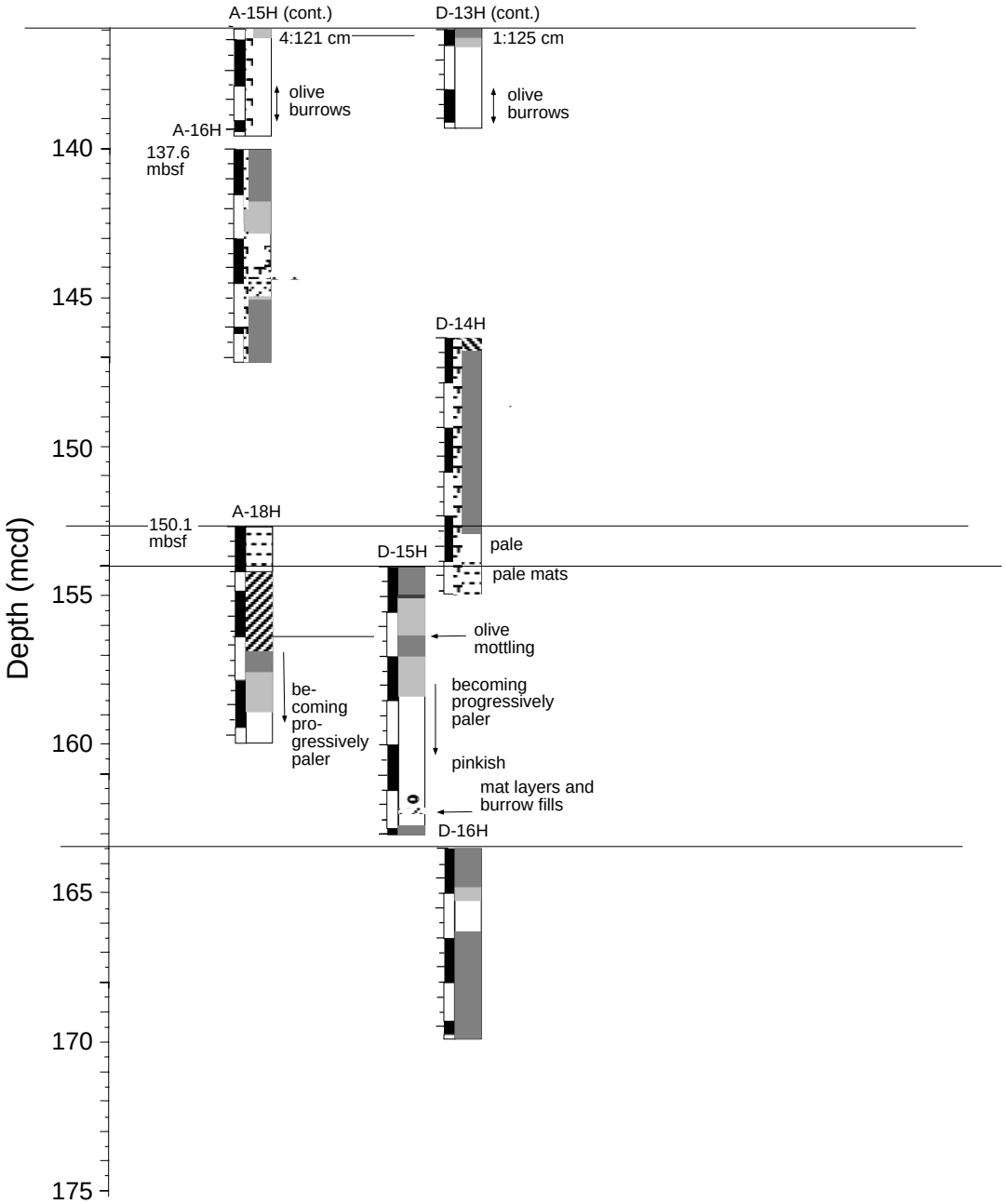

Figure F7. Comparison of carbonate, opal, and siliciclastic contents determined by coulometry, XRD, and smear-slide analyses.

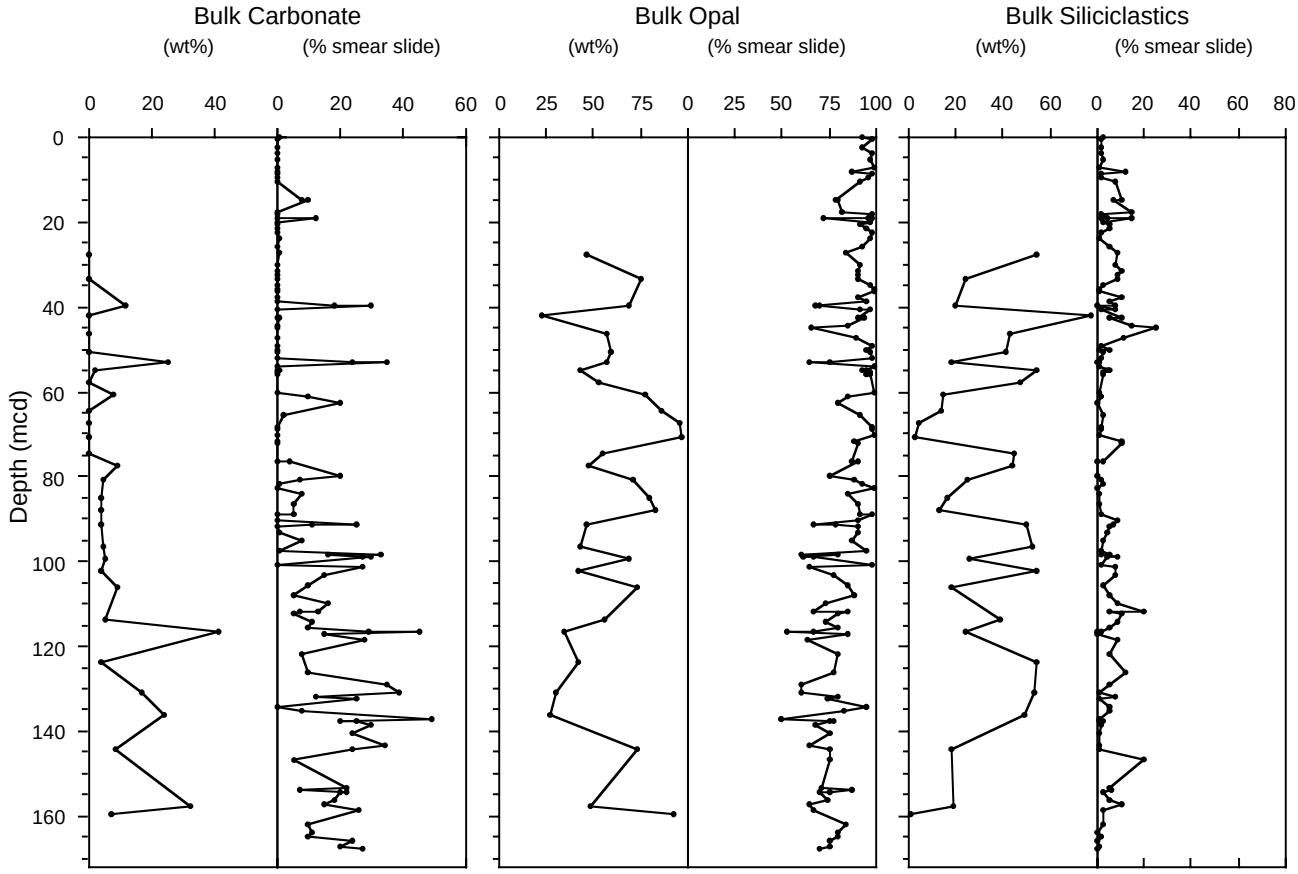

Figure F8. Loaf-shaped porcellanite concretion with concentric growth bands at 141.9 mbsf (144.22 mcd) (interval 177-1094A-16H-3, 130–150 cm).

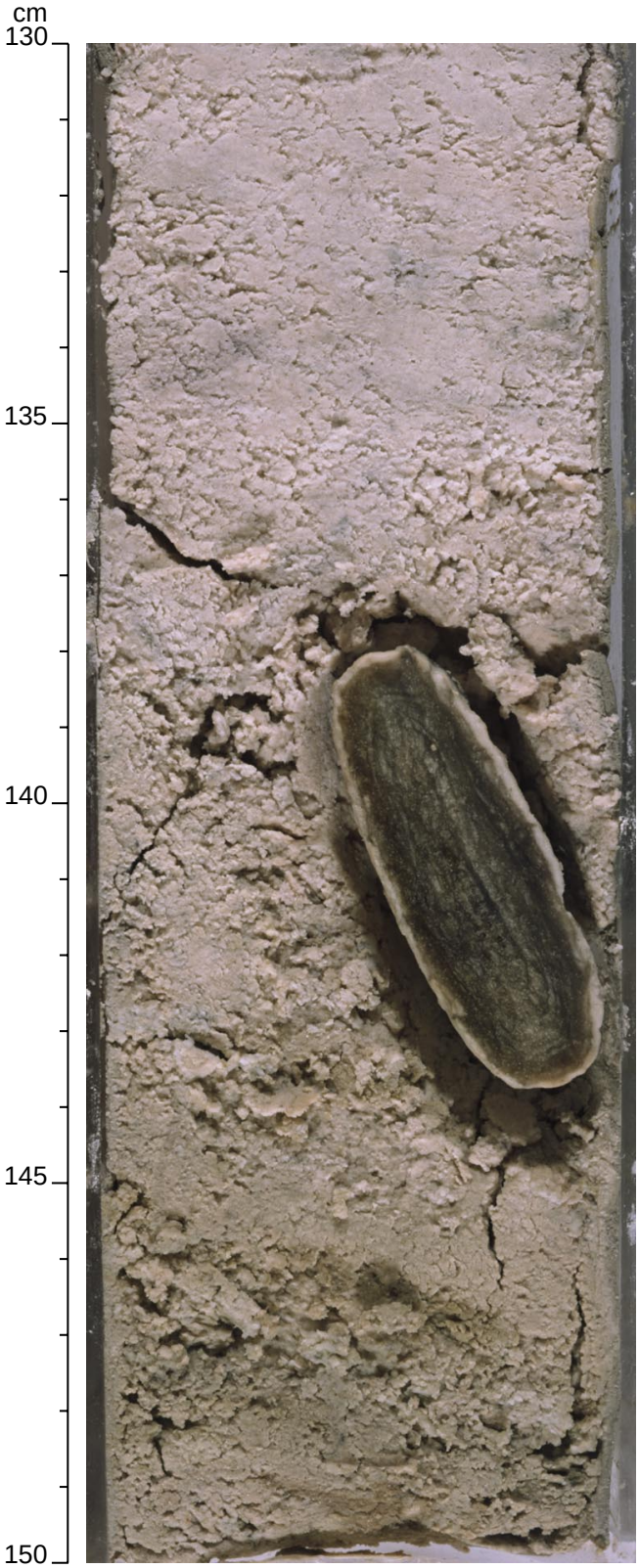

Figure F9. X-ray diffractogram of porcellanite showing a strong peak of opal-CT (interval 177-1094D-16H-2, 110–111 cm; 164.2 mbsf; 166.09 mcd).

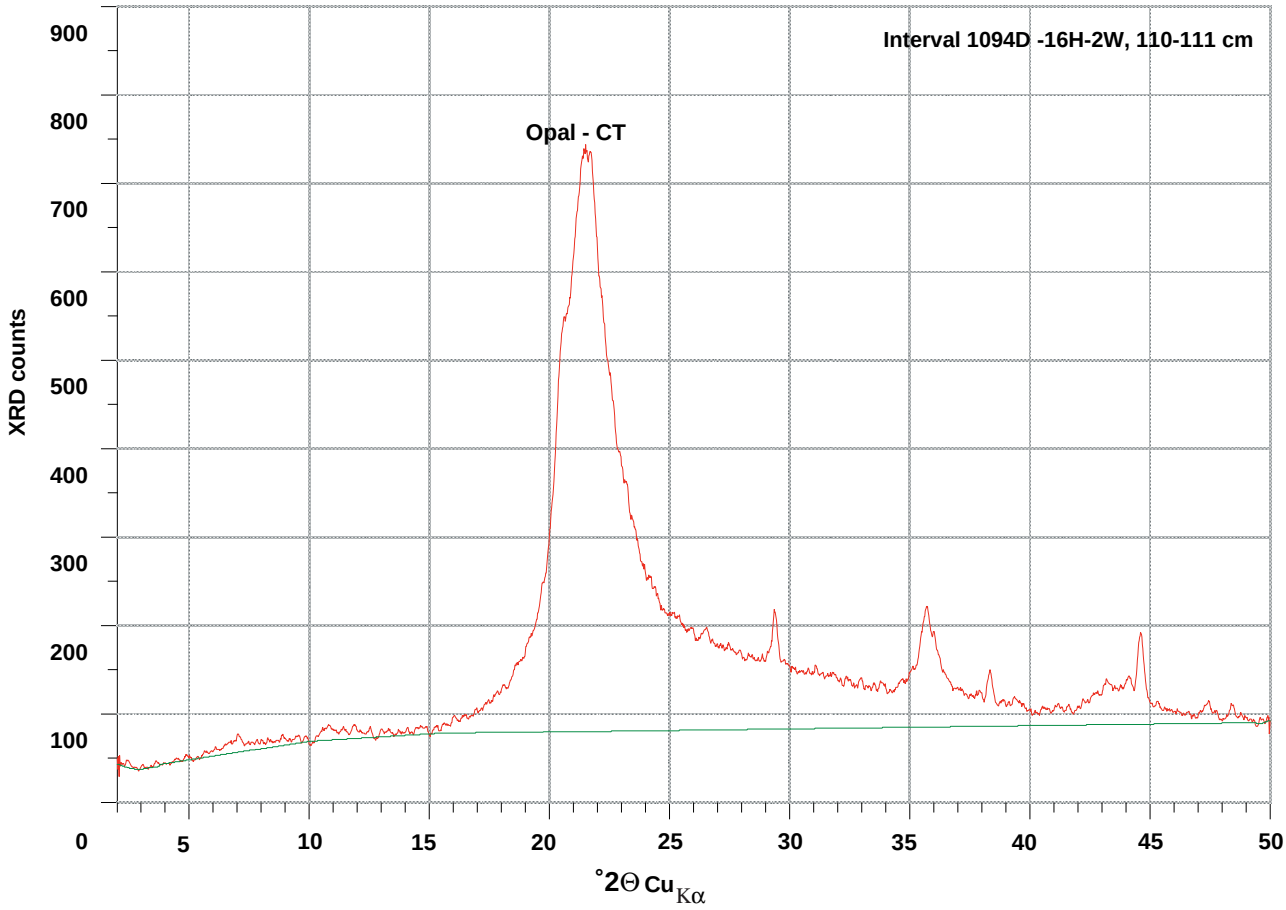

Figure F10. Volcanic ash layer in interval 177-1094A-8H-4, 65–90 cm (66.8 mbsf; 68.85 mcd).

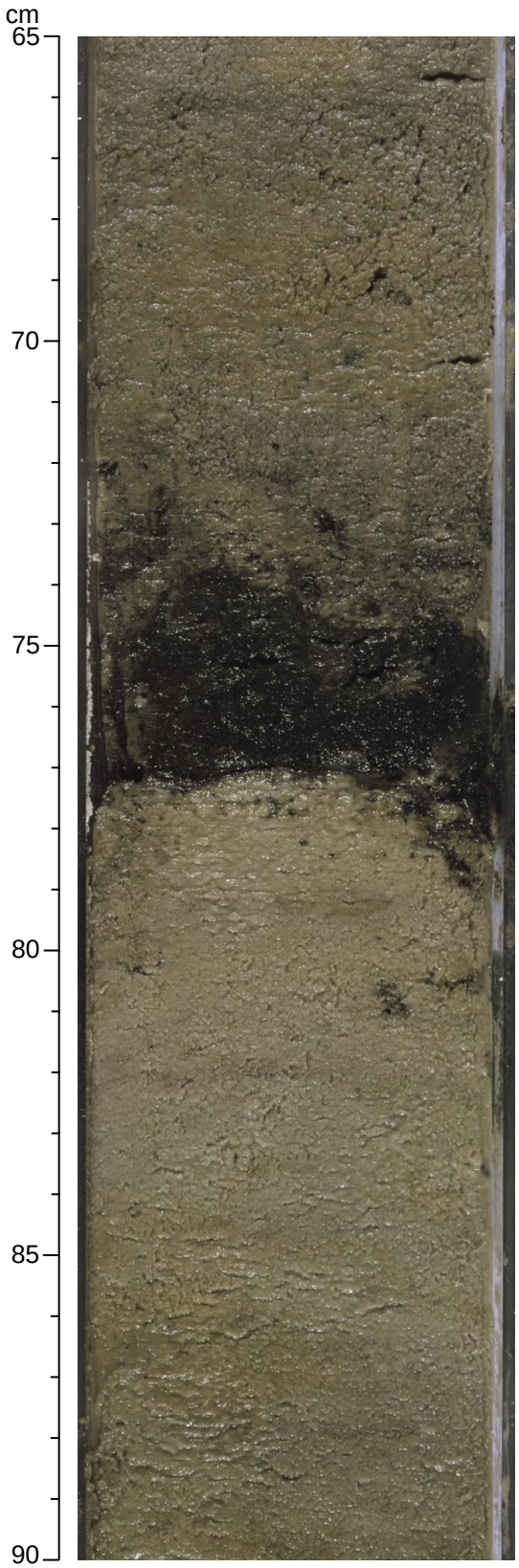

Figure F11. Fragments of a porcellanite layer (interval 177-1094A-8H-5, 22–68 cm) (67.8 mbsf; 69.92 mcd).

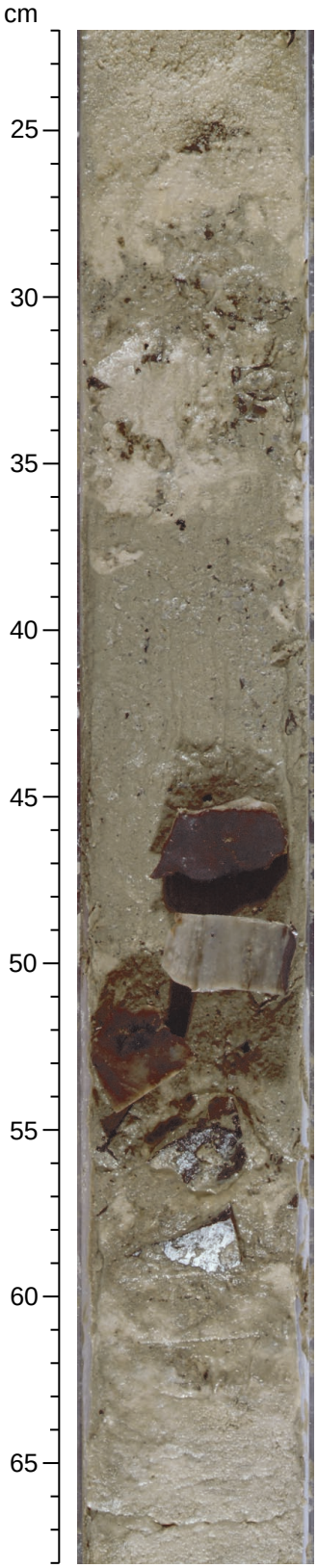

Figure F12. Part of an extremely large Echiurid-type burrow (>40 cm long), frequently encountered in Subunit IA (interval 177-1094A-2H-6, 5–50 cm) (12.15 mbsf; 13.69 mcd).

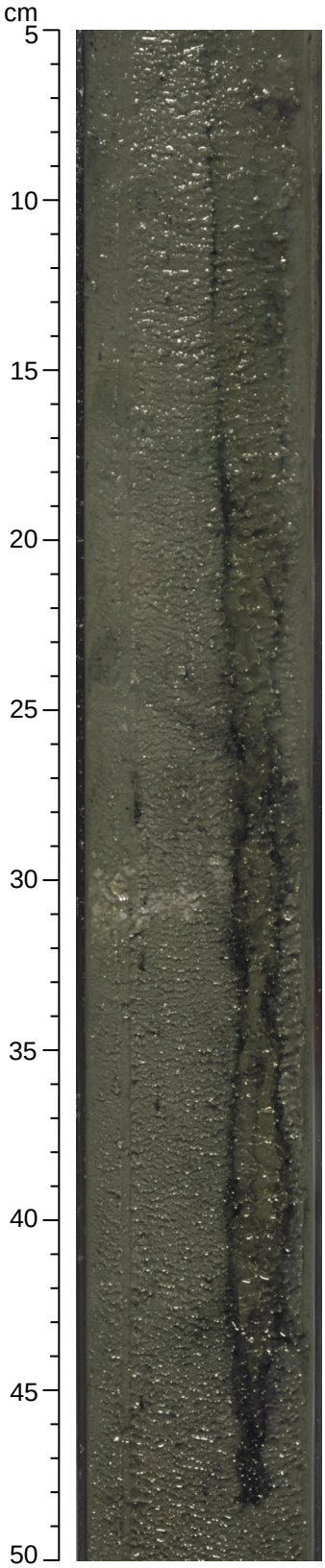

Figure F13. Smoothed (5-point average) color reflectance data (650–750 nm) for Site 1094. Holes 1094A (left curve), 1094B (second from left curve), 1094C (second from right curve), and 1094D (right curve) are horizontally offset from each other by a constant (10%). Data from the top 50 cm of these cores have been removed. Note the change in depth scale for the 100- to 170-mcd panel.

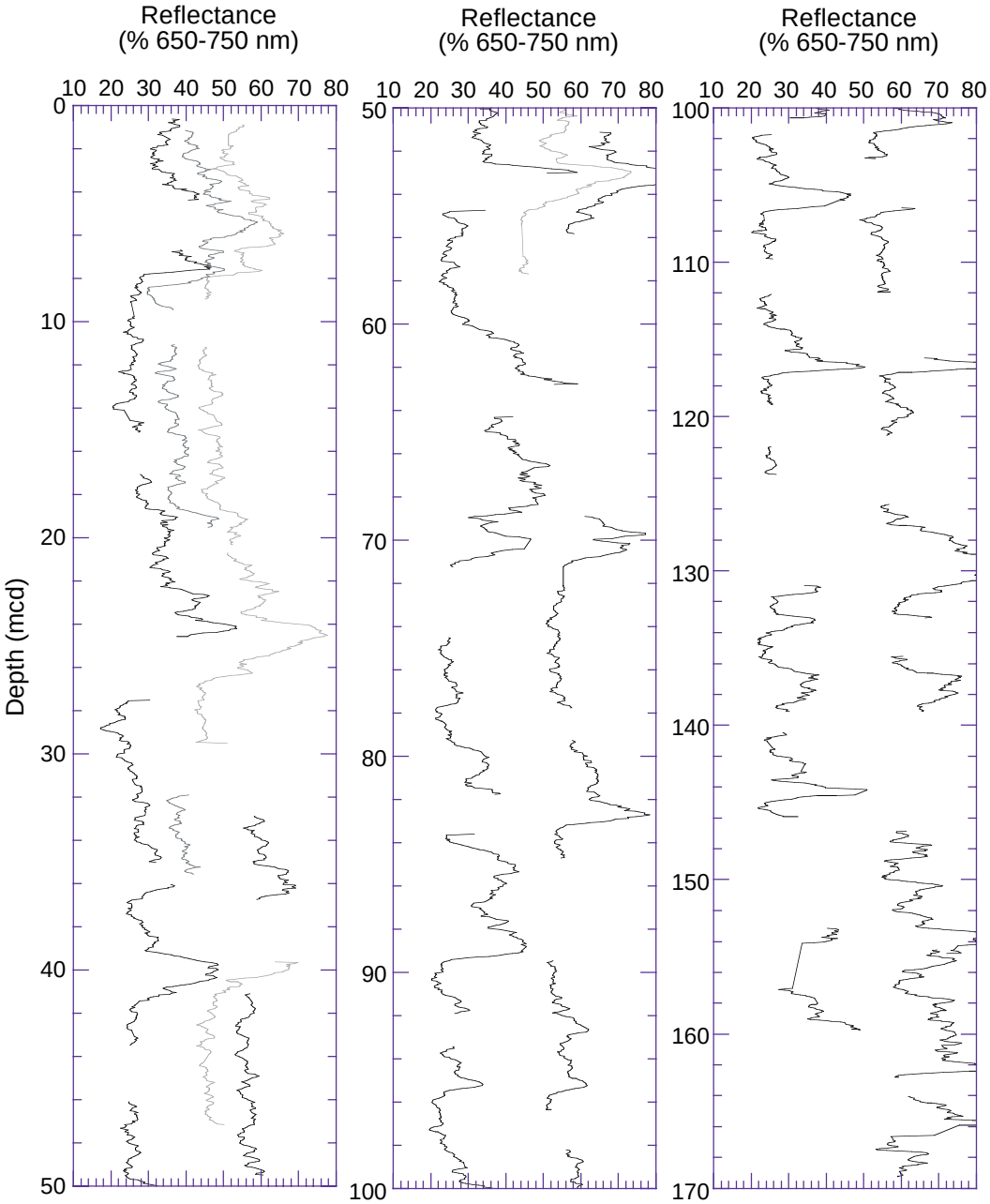

Figure F14. Smoothed (5-point average) magnetic susceptibility data (converted from instrument units to SI units) for Site 1094. Holes 1094A (left curve), 1094B (second from left curve), 1094C (second from right curve), and 1094D (right curve) are horizontally offset from each other by a constant (10×10^{-5} SI units). Data from the top 50 cm of these cores have been removed. Note the change in depth scale for the 100- to 170-mcd panel.

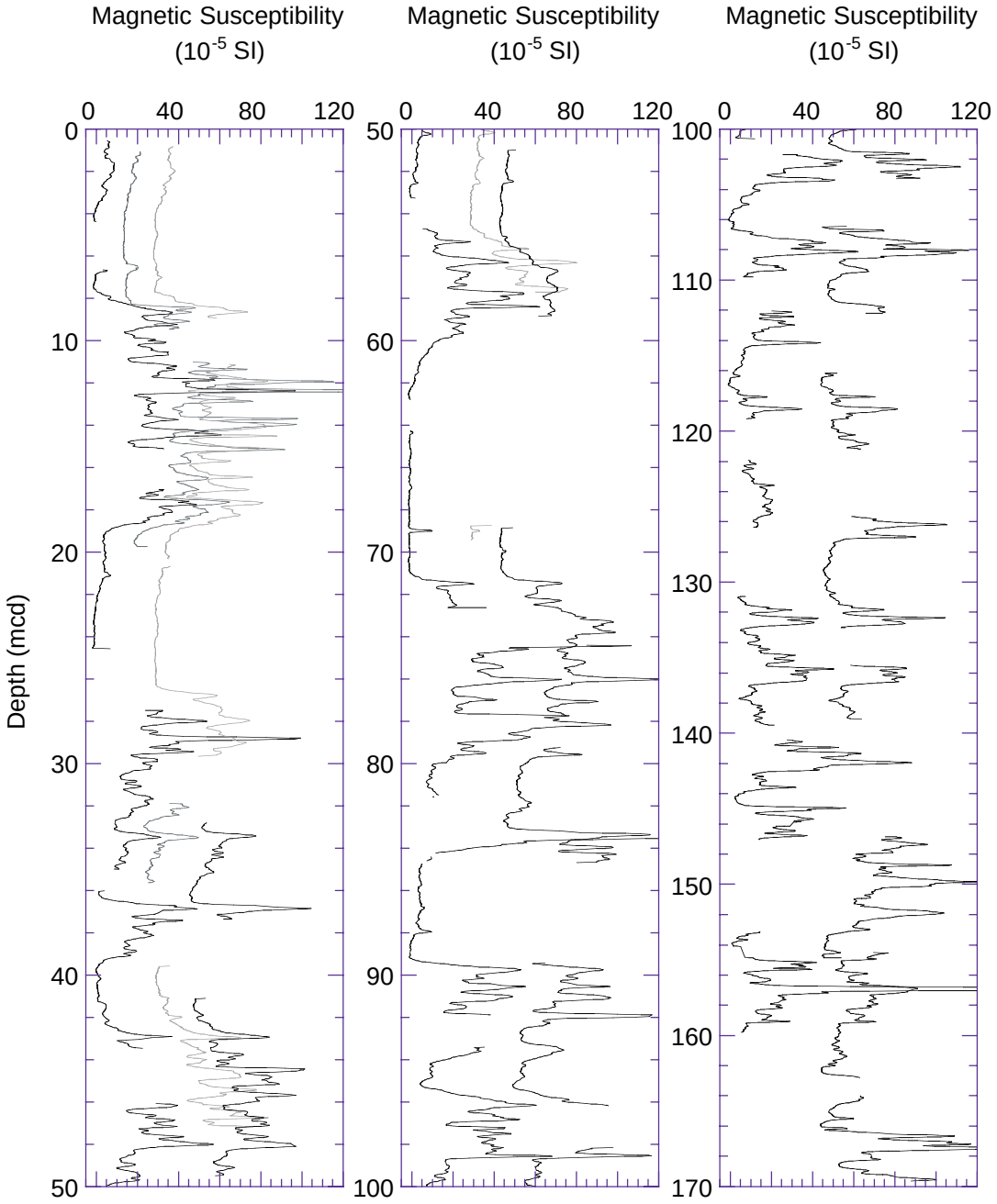

Figure F15. Smoothed (5-point average) GRA bulk density data for Site 1094. Holes 1094A (left curve), 1094B (second from left curve), 1094C (second from right curve), and 1094D (right curve) are horizontally offset from each other by a constant (0.10 g/cm³). Data from the top 50 cm of most cores have been removed. Note the change in depth scale for the 100- to 170-mcd panel.

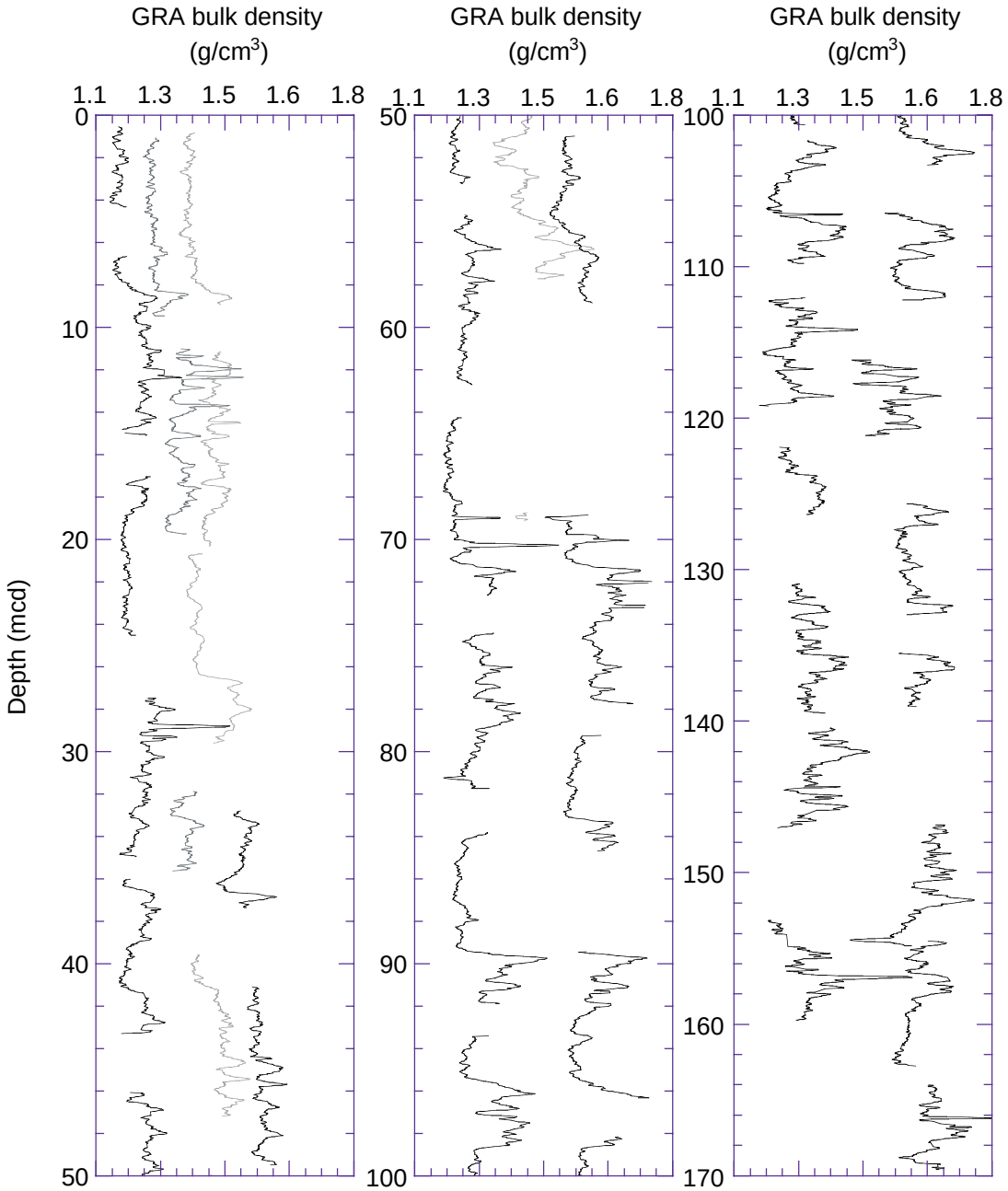

Figure F16. Spliced records of color reflectance, magnetic susceptibility, and GRA bulk density for Site 1094. Note that there is one known gap between the base of Core 177-1094A-7H and the top of Core 8H. The offset of Core 8H was arbitrarily set to the cumulative offset of Core 7H (Table T5, p. 53). All data sets are smoothed with a 5-point Gaussian filter. The horizontal lines in each plot identify the splice tie points (Table T6, p. 54).

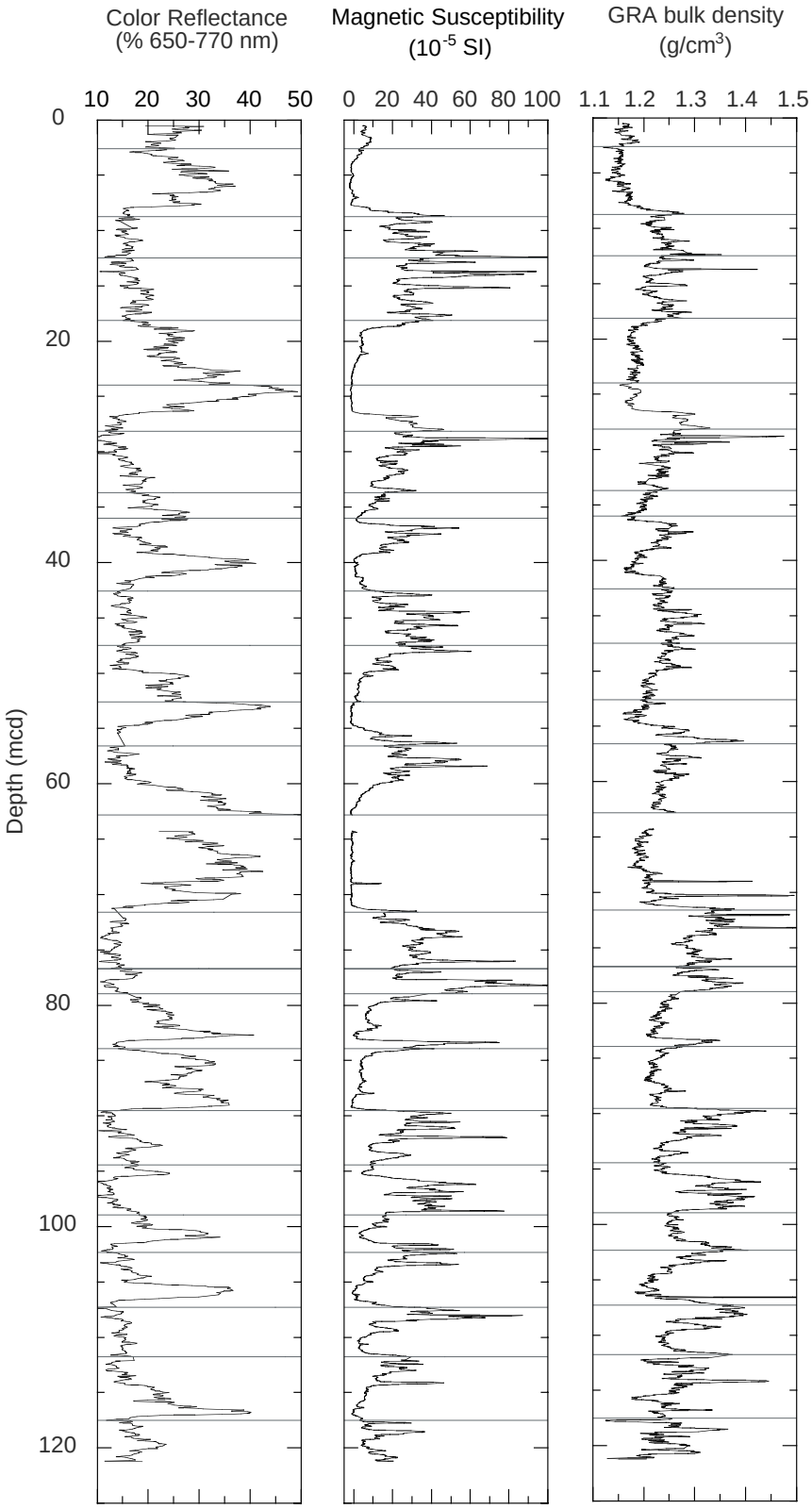

Figure F17. Biostratigraphic and magnetostratigraphic correlation chart for Site 1094, and selected absolute age designations.

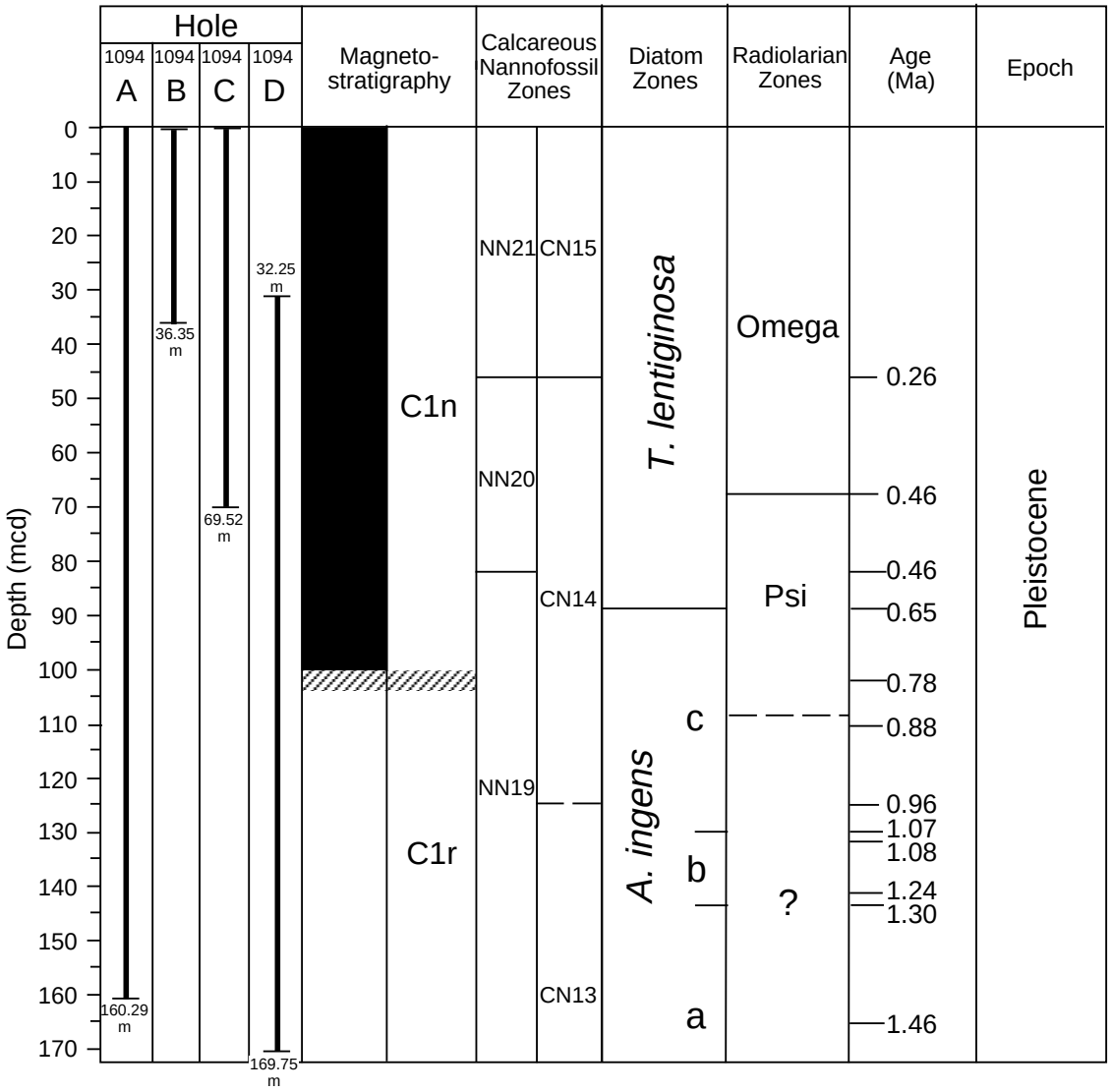

Figure F18. Age-depth plot of biostratigraphic and paleomagnetic events at Site 1094. For age-depth assignments see Table T8, p. 58. The solid lines indicate a visual best fit through the age-depth control points. Corresponding sedimentation rate averages are given in parentheses.

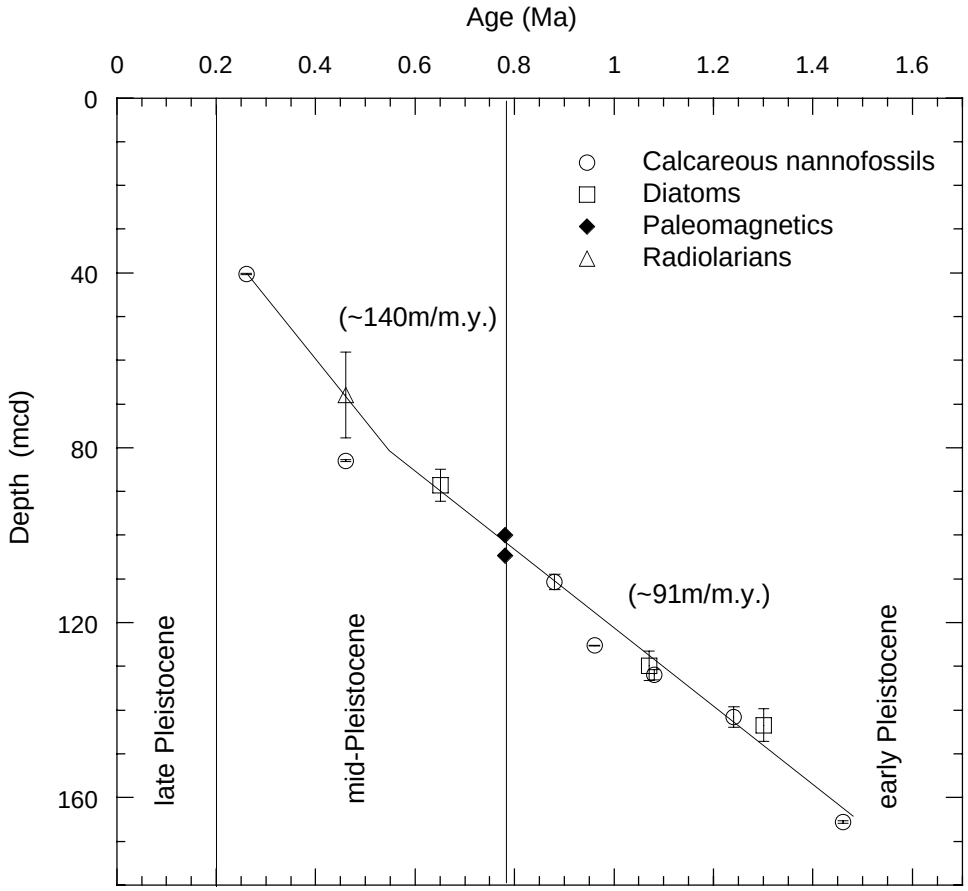

Figure F19. Inclination of the remanent magnetization after alternating-field demagnetization at peak fields of 25 mT for Holes 1094A and 1094D. The Brunhes and Matuyama Chrons are identified. Magnetic polarity shading: black = normal, white = reversed, hatched = transitional zone.

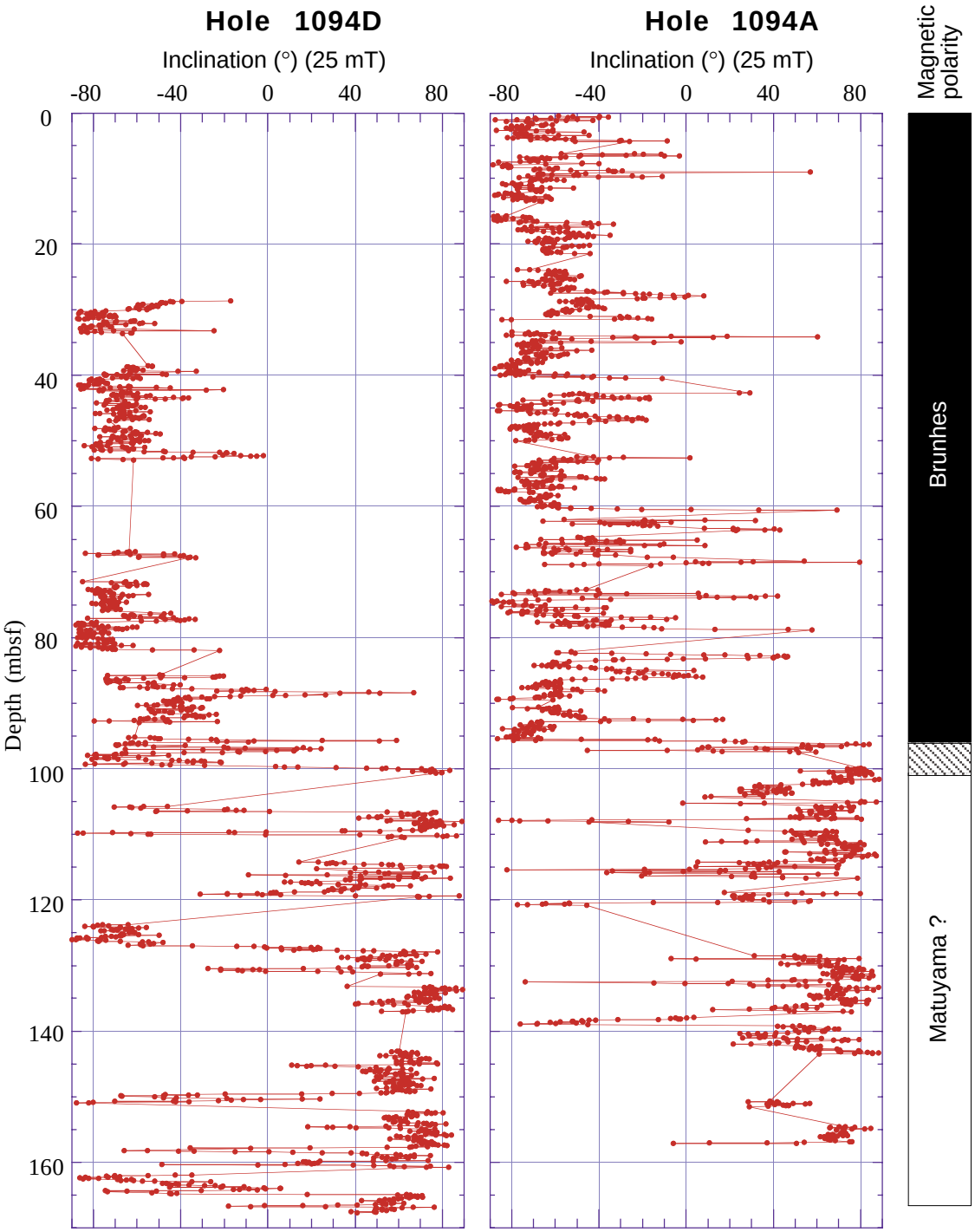

Figure F20. Concentration of methane vs. depth at Site 1094. Data are reported in Table T14, p. 66.

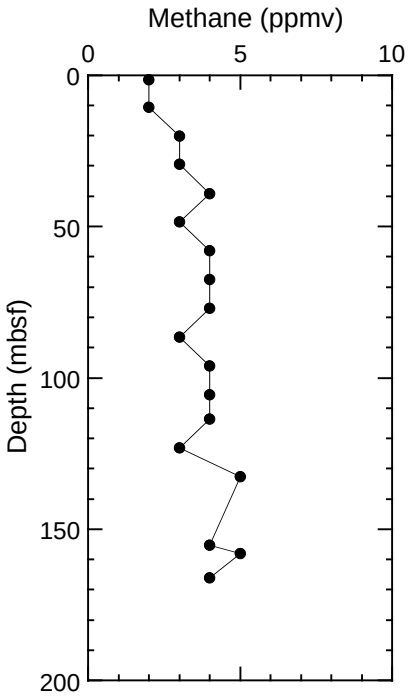

Figure F21. Interstitial water chemistry profiles vs. depth for chlorinity, alkalinity, pH, sodium, sulfate, calcium, magnesium, potassium, strontium, lithium, ammonium, phosphate, silica, manganese, and iron at Holes 1094A (open circles) and 1094D (solid circles). Data are reported in Table T15, p. 67. The horizontal line in the Cl plot indicates the approximate location of the porcellanite layer at 68 mbsf.

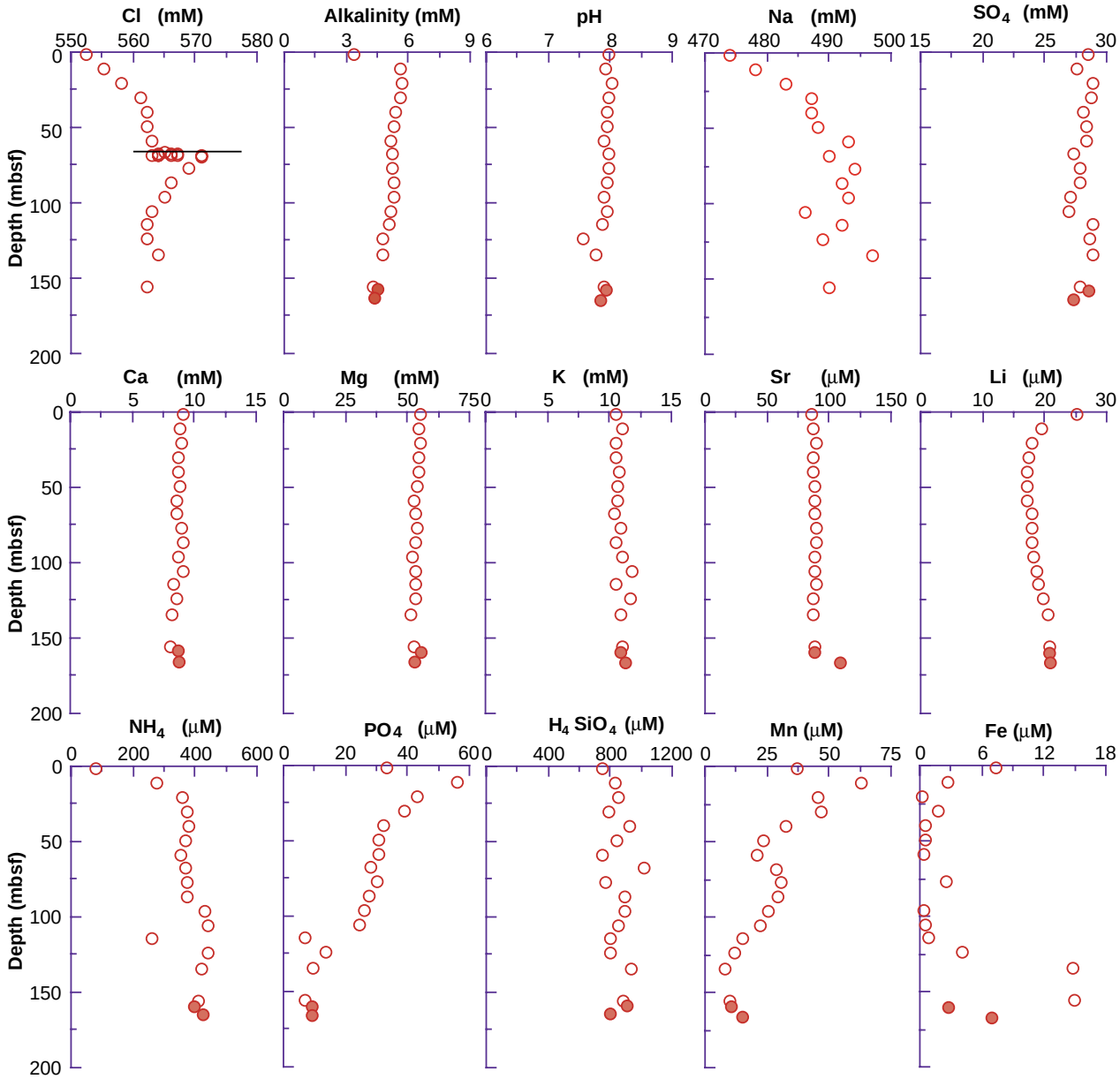

Figure F22. Concentration of calcium carbonate ($CaCO_3$), total organic carbon (TOC), total nitrogen (TN), total sulfur (TS), and TOC/TN vs. depth in sediments at Site 1094. Data are reported in Table T16, p. 69.

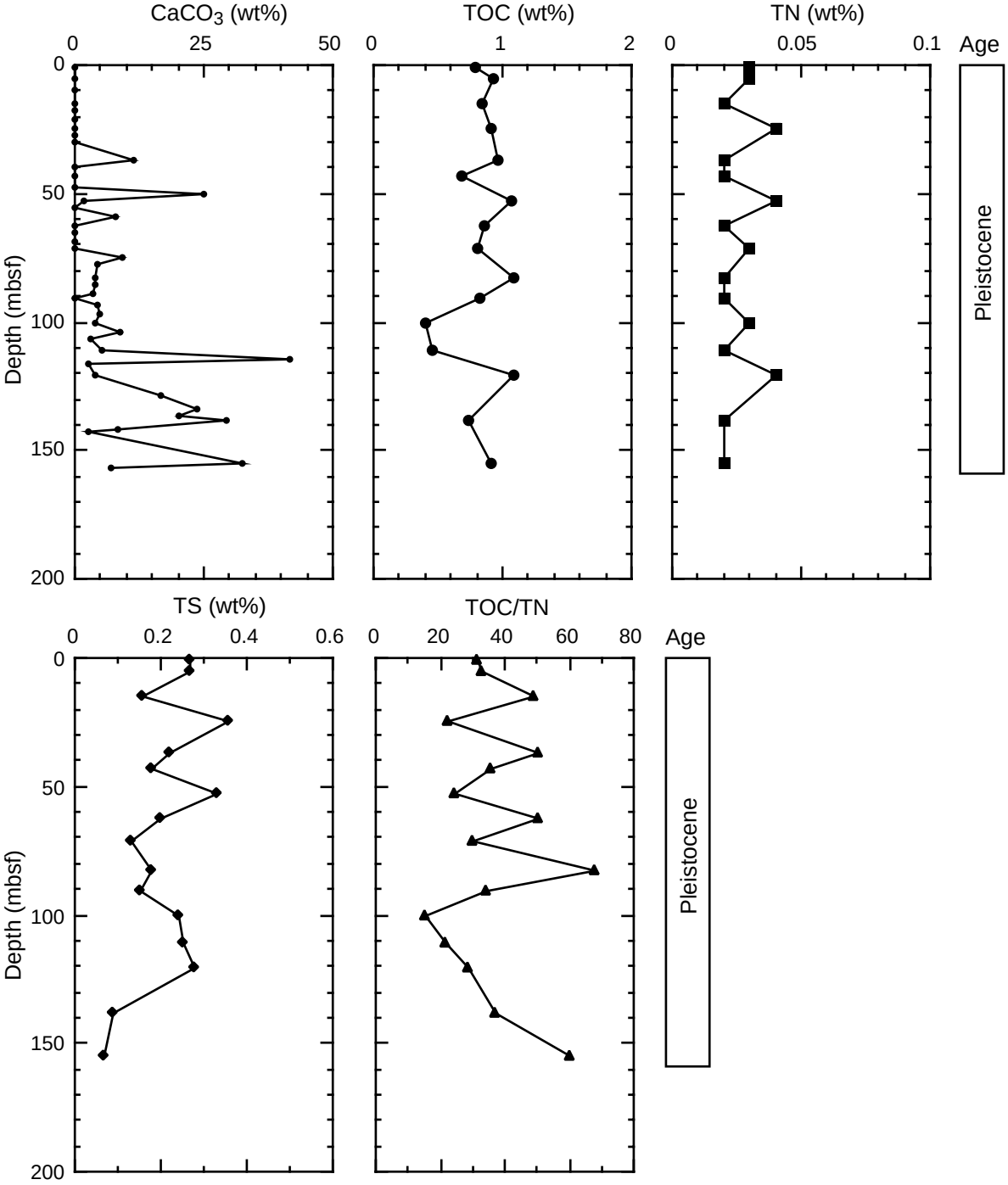

Figure F23. Site 1094 downhole variations of *P*-wave velocity (solid line = PWL, solid circles = PWS3), porosity (open circles = MAD method) and OSU-SCAT resistivity (solid line), GRA bulk density (line = smoothed data) and MAD bulk density (open circles), OSU-SCAT red/blue reflectance ratio, OSU-SCAT blue reflectance, volume-specific magnetic susceptibility, and NGR (smoothed data). Multiple lines in fourth, fifth, and seventh panels are for data from multiple holes.

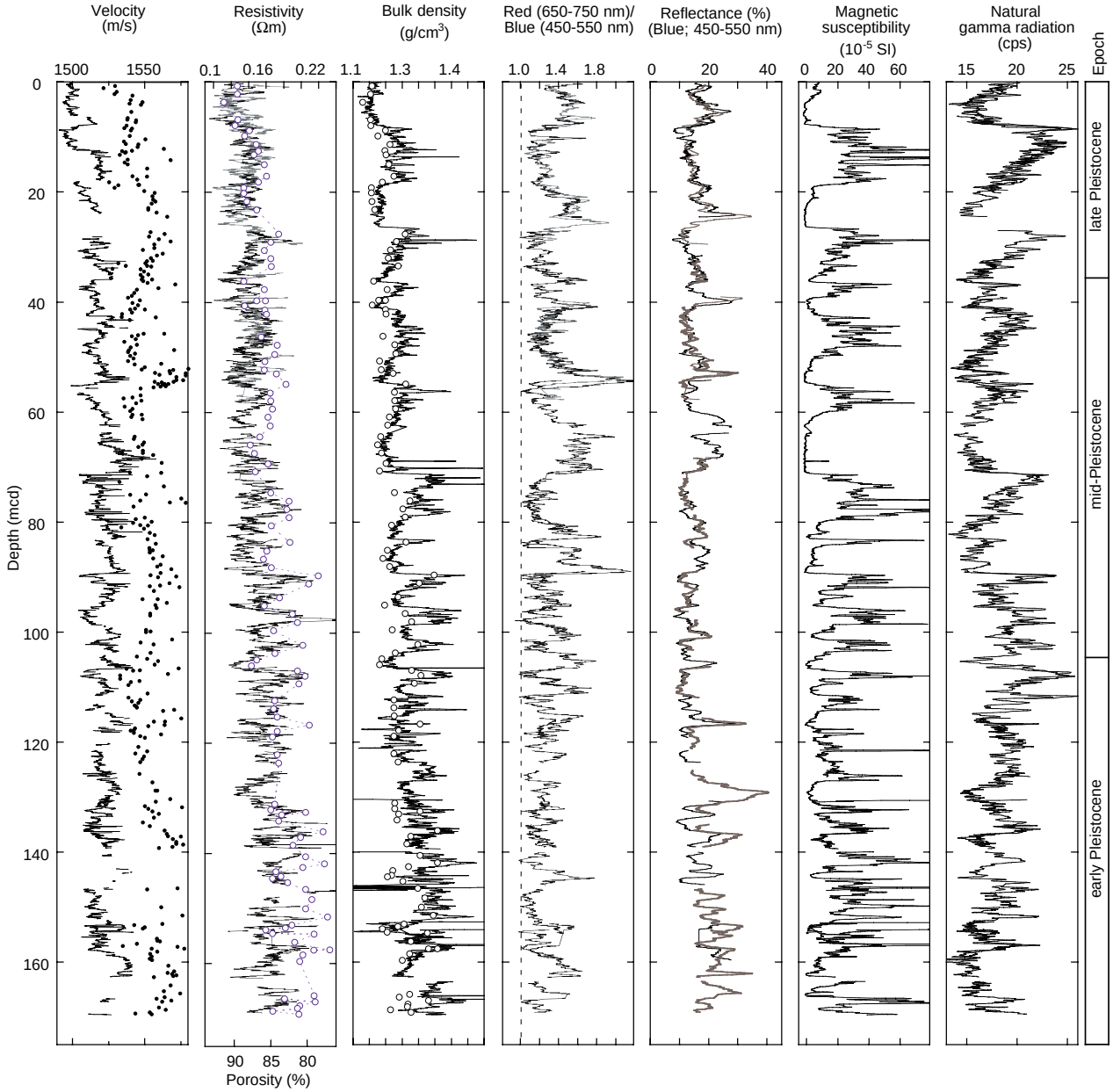

Figure F24. Relationship between GRA bulk density and gravimetric (MAD) bulk density at Site 1094.

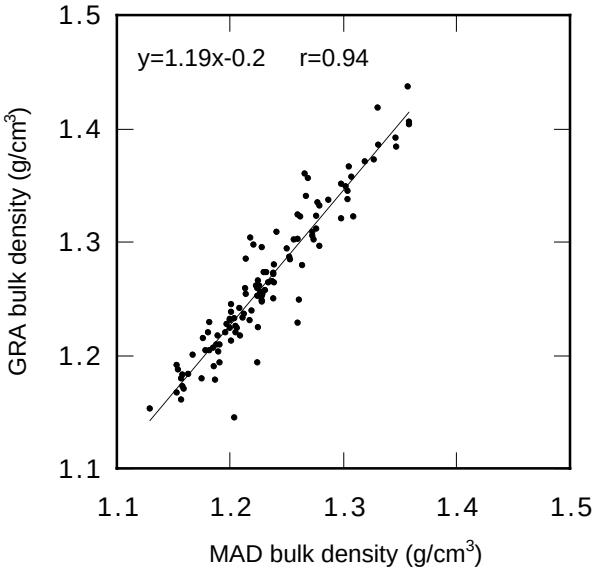

Figure F25. Thermal conductivity measurements of sediment cores at Site 1094. **A.** Frequency distribution of measured values. **B.** Correlation of measured values with interpolated GRA bulk density values. **C.** Thermal conductivity (solid circles) compared to interpolated GRA bulk density (open squares).

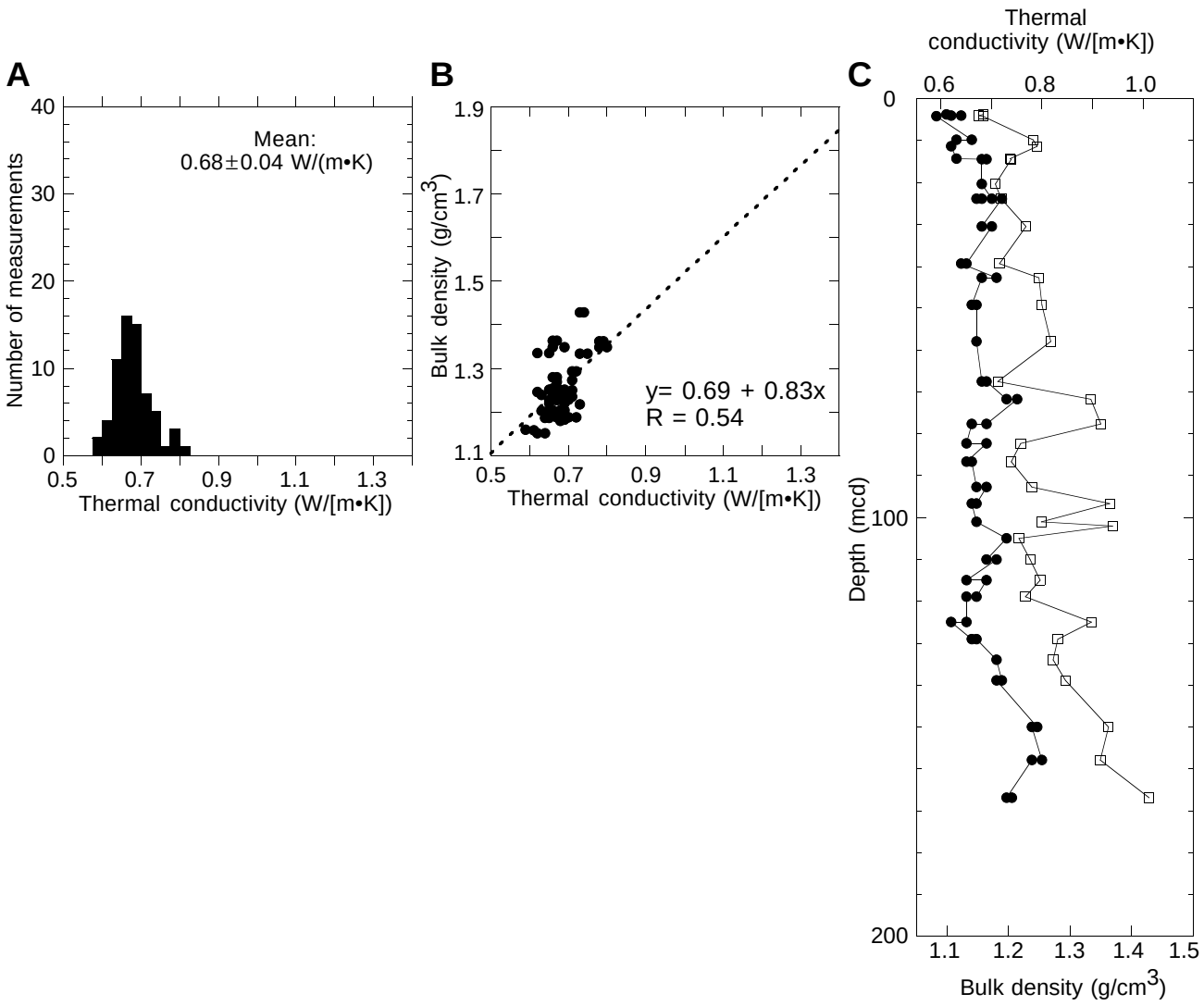

Figure F26. Downhole temperature measurements at Site 1094. Two plots are shown for each tool deployment: almost the entire time-temperature records (~1 hr) are shown on the left, and close-ups of the equilibration curves (~10 min) are shown on the right. The last deployment (158.6 mbsf) was done with the DVTP, all other deployments were done with the APCT shoe. Circles represent the model curve (APCT) or data points (DVTP) used to calculate the equilibration temperature (horizontal solid line). Uncertainties (horizontal dashed lines) were estimated visually from the condition of the equilibration curves and from multiple calculations using different curve segments. A bottom-water measurement was taken with the barrel of Core 177-1088A-1H before the core was shot. Sediment measurements were taken after the corresponding cores were shot. (Continued on next page.)

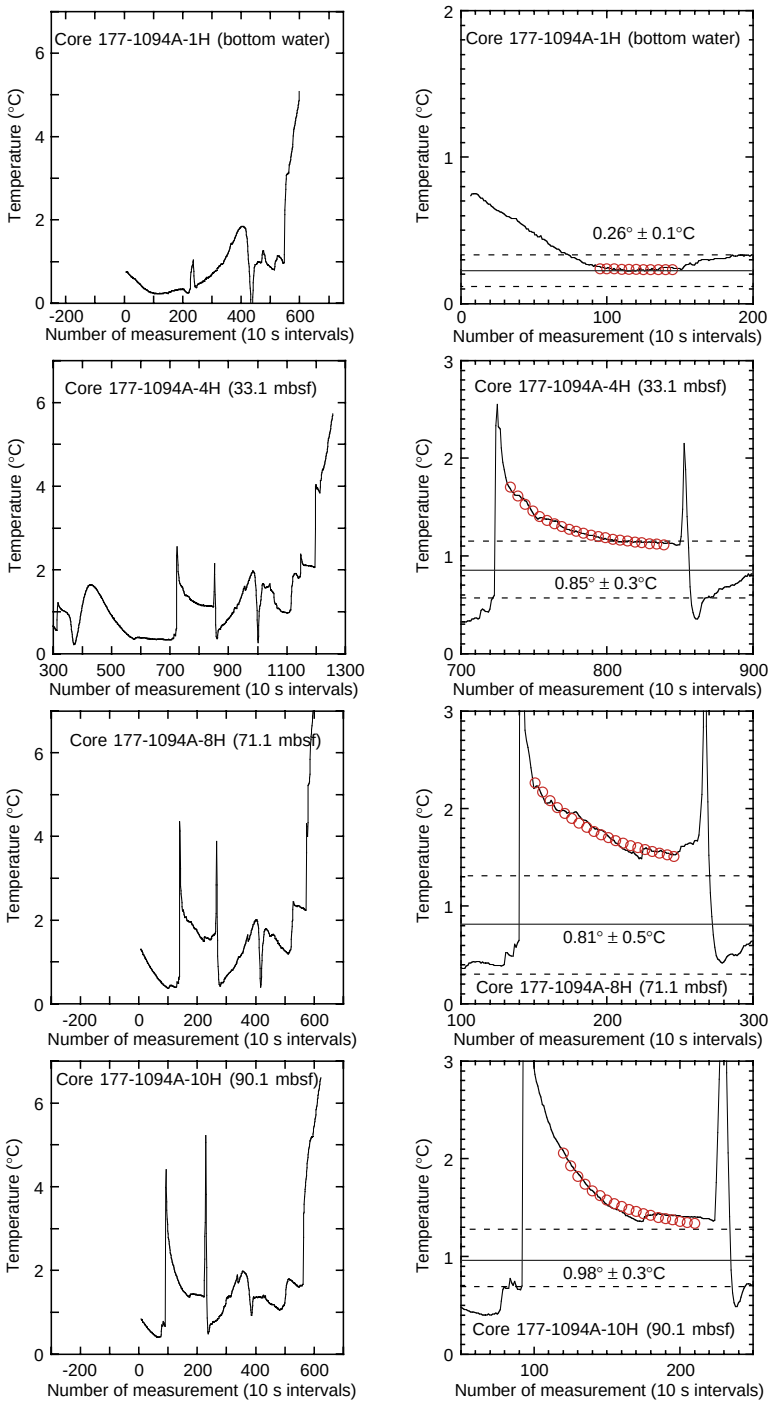

Figure F26 (continued).

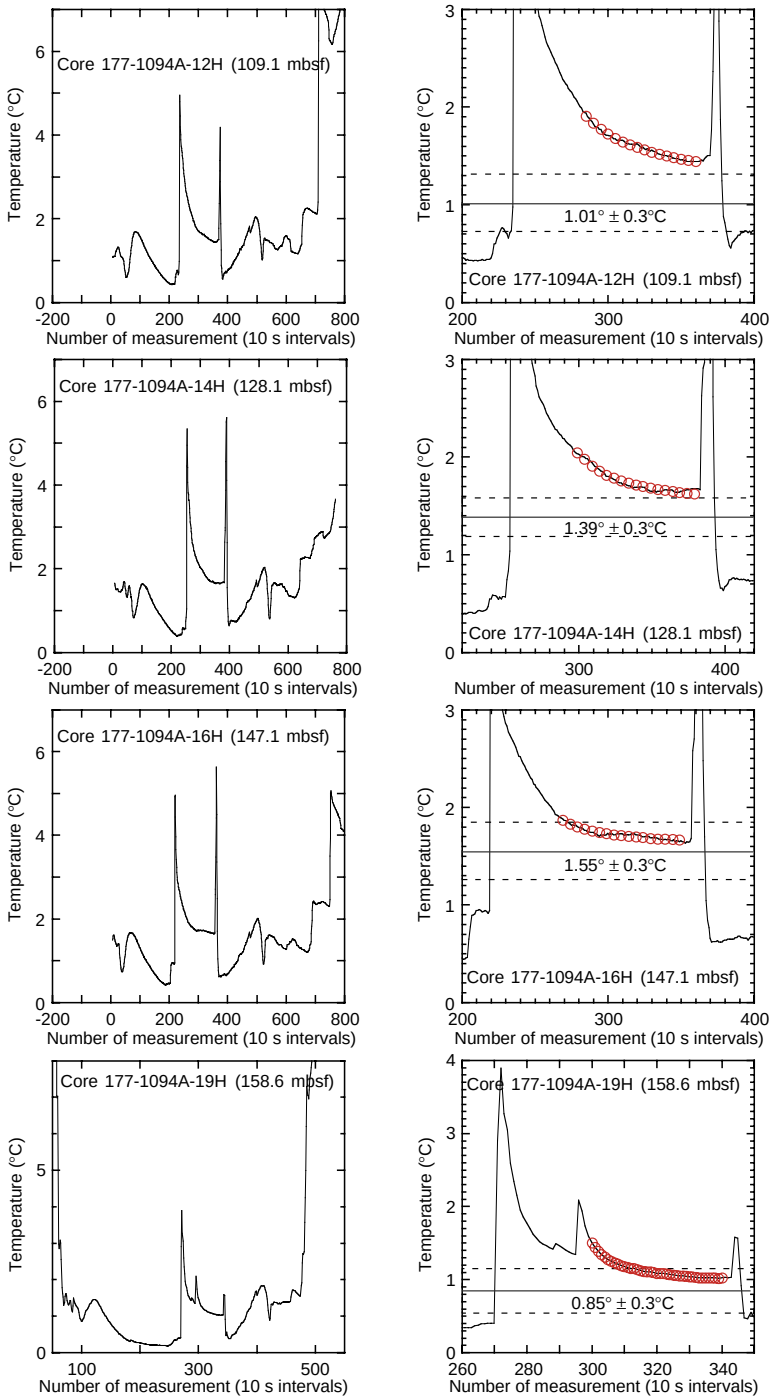

Figure F27. Depth-temperature curve for Site 1094.

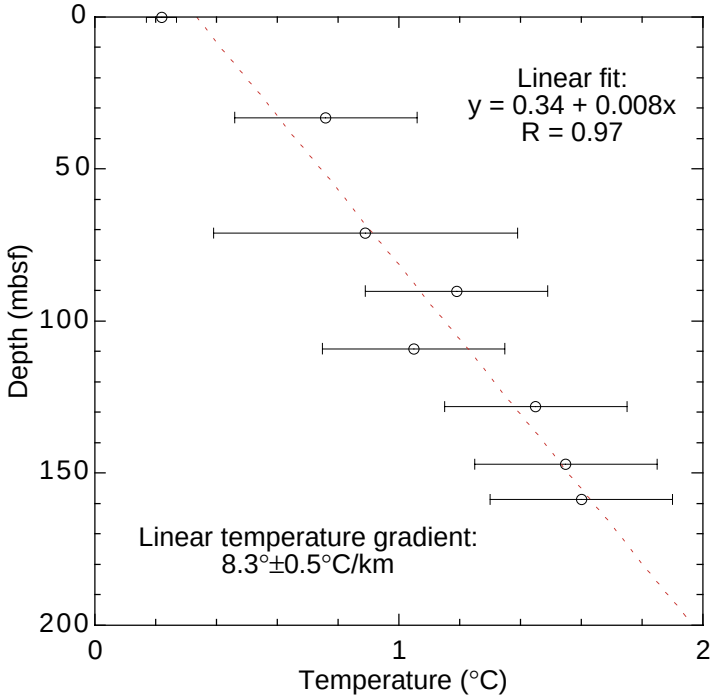

Table T1. Root-mean-square and interval velocities used for stacking of multichannel seismic data.

Time (s)	RMS velocity (m/s)	Interval velocity (m/s)	Depth from sea surface (m)
3820	1510.3	1510.3	2884.7
4002	1540.0	2067.1	3072.8
4365	1620.5	2330.4	3495.8
4644	1705.2	2704.6	3873.0
4754	1745.3	2981.2	4037.0
4900	1810.4	3288.6	4277.1
5779	2395.2	4409.9	6215.2
7115	3279.1	5696.3	10020.3
7940	3843.9	7033.6	12921.7

Notes: The data were collected at shotpoint 499 on Line AWI-94080 (Seismic streamer: 96 channels, 600 m active length, 770 m maximum offset). RMS = root mean square.

Table T2. X-ray diffraction data for Site 1094.

Core, section, interval (cm)	Depth (mbsf)	Depth (mcd)	Bulk carbonate (wt%; coulometry)	Bulk opal (wt%; XRD peak area)	Bulk siliciclastics (wt%)
177-1094A-					
4H-1, 63-64	24.24	27.60	0.0	46.1	53.9
4H-5, 66-67	30.10	33.46	0.0	75.8	24.2
5H-3, 120-122	37.31	39.72	11.4	68.9	19.7
5H-5, 70-72	39.81	42.22	0.0	22.7	77.3
6H-1, 68-69	43.29	46.25	0.0	57.0	43.0
6H-4, 67-68	47.78	50.74	0.0	59.0	41.0
6H-5, 141-142	50.02	52.98	24.9	57.0	18.1
7H-1, 71-72	52.82	54.92	1.8	43.6	54.6
7H-3, 71-72	55.82	57.92	0.0	53.0	47.0
7H-5, 71-72	58.82	60.92	7.9	77.8	14.3
8H-1, 67-68	62.28	64.42	0.0	86.3	13.7
8H-3, 67-68	65.28	67.42	0.0	95.7	4.3
8H-5, 104-105	68.65	70.79	0.0	97.2	2.8
9H-1, 71-72	71.82	74.62	0.0	55.0	45.0
9H-3, 71-72	74.82	77.62	9.1	47.0	43.9
9H-5, 71-72	77.82	80.62	4.3	70.9	24.8
10H-2, 71-72	82.82	85.16	3.9	79.8	16.3
10H-4, 71-72	85.82	88.16	3.9	82.8	13.3
10H-6, 71-72	88.82	91.16	3.6	46.1	50.3
11H-1, 71-72	90.82	93.62	0.0	55.5	44.5
11H-3, 71-72	93.82	96.62	4.3	43.1	52.6
11H-5, 71-72	96.82	99.62	5.0	69.4	25.6
12H-1, 111-112	100.70	102.30	3.8	42.1	54.1
12H-4, 27-28	104.40	106.00	8.8	72.9	18.3
13H-2, 70-71	111.30	113.80	5.4	55.5	39.1
13H-4, 70-71	114.30	116.80	41.6	34.1	24.3
14H-2, 67-68	120.80	123.60	4.0	42.1	53.9
15H-1, 66-67	128.80	131.10	16.7	30.2	53.1
15H-1, 68-69	128.80	131.10		51.5	48.5
15H-4, 122-123	133.80	136.20	23.9	26.7	49.4
16H-3, 50-51	141.10	143.40		38.1	61.9
16H-3, 88-89	141.50	143.80		53.5	46.5
16H-3, 128-129	141.90	144.20	8.5	73.4	18.1
16H-4, 70-71	142.80	145.10		68.9	31.1
18H-4, 129-130	155.10	157.60	32.4	48.5	19.1
18H-6, 39-40	157.20	159.70	7.1	92.2	0.7

Notes: XRD = X-ray diffraction. This table is also available in ASCII format in the **TABLES** directory.

Table T3. Occurrences of porcellanite at Site 1094.

Core, section, interval (cm)	Depth (mbsf)	Depth (mcd)	Description	Enclosing sediment
177-				
1094A-8H-5, 32-65	67.9	70.02	Fragmented layer	Diatom ooze
1094D-6H-2, 0-22	68.1	69.85	Fragmented layer	Diatom ooze
1094A-12H-4, 27-80	104.4	105.95	Fragmented layer	Diatom ooze
1094A-16H-3, 140	141.4	143.72	Concretion	Foraminifer-bearing diatom ooze
1094D-16H-2, 100-128	164.1	165.99	Fragmented layer	Foraminifer- and nannofossil-bearing diatom ooze
*1094D-6H-3, 71-76	70.3	72.05	Single fragment	Mud-bearing diatom ooze
*1094A-9H-3, 78-83	74.9	77.68	Single fragment	Diatom ooze
*1094A-13H-1, 16	109.3	111.70	Single fragment	Diatom ooze
*1094A-14H-1, 9-13	118.7	121.50	Fragments	Diatom ooze
*1094D-14H-1, 0-30 and 130	142.6, 143.9	146.32, 147.62	Fragments	Mud-bearing diatom ooze
*1094D-16H-3, 28-31	164.9	166.77	Single fragment	Foraminifer-bearing diatom ooze

Note: * = fragments suspected not to be in original stratigraphic position.

Table T4. Occurrences of Echiurid-type burrows at Site 1094.

Core, section interval (cm)	Depth (mbsf)	Depth (mcd)	Length (cm)	Cross-section (cm)	Notes
177-1094A-					
2H-3, 0-65	8.2	9.79	61	1.4-2	
2H-5, 7-47	11.1	12.61	ND	~2	
2H-5, 100, to 2H-6, 90	13.0	14.54	?140	1-2.5	
4H-2, 55-110	26.0	29.41	ND	1-2.5	Includes large oblique burrows
5H-2, 45	35.1	37.46	ND	1.5-2	
5H-5, 126, to 5H-6, 50	42.6	45.01	75	2	Partly open
6H-1, 45	43.1	46.01	ND		
6H-2, 0-55	44.7	47.61	53	Not observed	
177-1094B-					
2H-2, 30-150	12.5	13.52	70+	2.5+	Partly open
2H-3, 10-20	12.7	13.72	ND	2.5+	
177-1094C-					
2H-2, 60-105	11.5	12.47	45	Halos observed	
2H-3, 70-95	12.8	13.17	ND	2-2.5	
3H-5, 70-150	26.1	27.86	80	1.5	
3H-6, 100-140	27.3	29.06	40		
5H-4, 30-65	42.6	44.27	1	Includes halo	
177-1094D-					
2H-4, 0-34	33.4	37.09	1+	Open	

Note: ND = not determined.

Table T5. Composite depths for Site 1094.

Core	Depth (mbsf)	Offset (m)	Depth (mcd)
177-1094A-			
1H	0	0.00	0.00
2H	4.6	1.54	6.14
3H	14.1	2.42	16.52
4H	23.6	3.36	26.96
5H	33.1	2.41	35.51
6H	42.6	2.96	45.56
7H	52.1	2.10	54.20
8H	61.6	2.14	63.70
9H	71.1	2.80	73.90
10H	80.6	2.34	82.94
11H	90.1	2.80	92.90
12H	99.6	1.58	101.18
13H	109.1	2.44	111.54
14H	118.6	2.81	121.41
15H	128.1	2.32	130.42
16H	137.6	2.32	139.92
18H	150.1	2.52	152.62
177-1094B-			
1H	0	0.52	0.52
2H	9.5	1.02	10.52
3H	19	1.02	20.02*
4H	28.5	2.87	31.37
177-1094C-			
1H	0	0.28	0.28
2H	8.9	1.72	10.62
3H	18.4	1.76	20.16
5H	37.4	1.67	39.07
6H	46.9	2.56	49.46
8H	65.9	2.34	68.24
177-1094D-			
2H	28.6	3.65	32.25
3H	38.1	2.49	40.59
4H	47.6	2.89	50.49
5H	57.1	2.89	59.99*
6H	66.6	1.75	68.35
7H	76.1	2.62	78.72
8H	85.6	3.32	88.92
9H	95.1	2.56	97.66
10H	104.6	1.34	105.94
11H	114.1	1.54	115.64
12H	123.6	1.54	125.14
13H	133.1	1.88	134.98
14H	142.6	3.72	146.32
15H	152.1	1.89	153.99
16H	161.6	1.89	163.49

Notes: * = cores that are part of the JANUS database but were not analyzed on the multisensor track because sufficient material was not available for analysis (e.g., core catchers). The mcd offset was arbitrarily chosen to be the same as the offset of the overlying core. This table is also available in ASCII format in the **TABLES** directory.

Table T6. Site 1094 splice tie points.

Core, section, interval (cm)	Depth (mbsf)	Depth (mcd)		Core, section, interval (cm)	Depth (mbsf)	Depth (mcd)
177-				177-		
1094A-1H-2, 106	2.56	2.56	tie to	1094C-1H-2, 78	2.28	2.56
1094C-1H-6, 96	8.46	8.74	tie to	1094A-2H-2, 110	7.20	8.74
1094A-2H-5, 30	10.90	12.44	tie to	1094B-2H-2, 42	11.42	12.44*
1094B-2H-6, 6	17.06	18.08	tie to	1094A-3H-2, 6	15.66	18.08
1094A-3H-5, 141	21.52	23.94	tie to	1094C-3H-3, 77	22.18	23.94*
1094C-3H-6, 48	26.38	28.14	tie to	1094A-4H-1, 118	24.78	28.14
1094A-4H-5, 90	30.33	33.69	tie to	1094D-2H-1, 144	30.04	33.69
1094D-2H-3, 72	32.32	35.97	tie to	1094A-5H-1, 46	33.56	35.97
1094A-5H-5, 104	40.14	42.55	tie to	1094D-3H-2, 46	40.06	42.55*
1094D-3H-5, 94	44.97	47.46	tie to	1094A-6H-2, 40	44.50	47.46
1094A-6H-5, 102	49.62	52.58	tie to	1094C-6H-3, 12	50.02	52.58
1094C-6H-6, 72	53.98	56.54	tie to	1094A-7H-2, 84	54.44	56.54
1094A-7H-6, 109	60.70	62.80	append to	1094A-8H-1, 0	61.60	63.74
1094A-8H-6, 32	69.42	71.56	tie to	1094D-6H-3, 32	69.81	71.56
1094D-6H-6, 94	74.93	76.68	tie to	1094A-9H-2, 128	73.88	76.68
1094A-9H-4, 52	76.12	78.92	tie to	1094D-7H-1, 20	76.30	78.92
1094D-7H-4, 66	81.26	83.88	tie to	1094A-10H-1, 94	81.54	83.88*
1094A-10H-5, 58	87.18	89.52	tie to	1094D-8H-1, 60	86.20	89.52
1094D-8H-4, 101	91.12	94.44	tie to	1094A-11H-2, 2	91.64	94.44
1094A-11H-5, 4	96.14	98.94	tie to	1094D-9H-1, 128	96.38	98.94*
1094D-9H-4, 13	99.74	102.30	tie to	1094A-12H-1, 110	100.72	102.30*
1094A-12H-5, 8	105.68	107.26	tie to	1094D-10H-1, 132	105.92	107.26
1094D-10H-4, 130	110.40	111.74	tie to	1094A-13H-1, 20	109.30	111.74*
1094A-13H-5, 32	115.06	117.50	tie to	1094D-11H-2, 36	115.96	117.50
1094D-11H-4, 106	119.66	121.20				

Notes: * = problematic tie points (see text for discussion). This table is also available in ASCII format in the **TABLES** directory.

Table T7. Distribution of main calcareous nannofossil species at Site 1094. (**See table note.** Continued on next two pages.)

Core, section, interval (cm)	Depth (mbsf)	Depth (mcd)	Abundance	Preservation	*Reticulofenestra minuta*	*Reticulofenestra minutula*	*Coccolithus pelagicus*	*Pseudoemiliania lacunosa*	*Calcidiscus leptoporus*	*Helicosphaera carteri*	*Gephyrocapsa* small	*Gephyrocapsa caribbeanica*	*Gephyrocapsa* medium (4-5.5 µm)	*Gephyrocapsa* large (> 5.5 µm)	*Gephyrocapsa* sp. 3	*Reticulofenestra asanoi*	*Emiliania huxleyi*	Comments
177-1094A-																		
1H-2, 120-120	2.70	2.70	B															
1H-3, 80-80	3.80	3.80	B															
1H-CC, 15-20	4.57	4.57	B															
2H-1, 30-30	4.90	6.44	B															
2H-6, 95-95	13.05	14.59	B															
2H-6, 136-136	13.46	15.00	R	P					F		F		F		F			
2H-CC, 14-19	13.75	15.29	B															
3H-1, 50-50	14.60	17.02	B															
3H-3, 30-30	17.40	19.82	B															
3H-5, 130-130	21.40	23.82	B															
3H-6, 20-20	21.80	24.22	C	P					C		F				F		A	
3H-6, 50-50	22.10	24.52	F	P					F		F		F		R		R	
3H-CC, 13-18	22.31	24.73	R	P					A		A		R				F	
4H-CC, 14-19	31.81	35.17	B															
5H-3, 110-110	37.20	39.61	C	M					C		A	D	F		F		A	
5H-3, 146-146	37.56	39.97	A	M					C			A	F				D	
5H-4, 30-30	37.90	40.31	C	P			R		C			C	F		F			
5H-CC, 12-17	41.20	43.61	R	P					F	R	C	C						
6H-5, 122-122	49.82	52.78	A	M			R		R	R	D							
6H-5, 147-147	50.07	53.03	A	M						R	D	F	R					Very small placoliths D
6H-6, 15-15	50.25	53.21	A	M						R	D	C						
7H-5, 110-110	59.20	61.30	C	M					F		D	F	F					
7H-6, 40-40	60.00	62.10	F	M							D	F	R					
7H-6, 90-90	60.50	62.60	C	M							D	R	F					
7H-CC, 9-16	60.82	62.92	C	P							D		F					
8H-3, 140-140	66.00	68.14	R	M							D	F	C					
8H-CC, 8-13	70.59	72.73	B															
9H-2, 17-17	72.77	75.57	R	P				A	C									
9H-CC, 14-19	79.12	81.92	B															
10H-CC, 0-10	89.74	92.08	B															
11H-5, 120-120	97.30	100.10	F	M				F	A		D							
11H-CC, 12-17	97.98	100.78	C	P			R		F		D							
12H-3, 127-127	103.87	105.45	R	M				A	F		C		C					
12H-4, 119-119	105.29	106.87	R	M				F	A		A							
12H-CC, 0-10	108.25	109.83	B															
13H-2, 132-132	111.92	114.36	F	P		F	A	C	C							F		
13H-3, 42-42	112.52	114.96	F	P		R	A	F	C							F		
13H-3, 140-140	113.50	115.94	F	P		F	A	F							F	R		
13H-4, 65-65	114.25	116.69	A	M		F	D	F	C		C				F	R		
13H-CC, 0-10	116.82	119.26	F	P			F	F					R			R		
14H-1,137-137	119.97	122.78	B															
14H-3, 3-3	121.63	124.44	F	P			C	R	F						R	R		
14H-3, 25-25	121.85	124.66	R	P			C		R						F	R		
14H-3, 66-66	122.26	125.07	C	P			D	R	F		C				F	R		
14H-3, 88-88	122.48	125.29	F	R		R	D	F	F						cf.	R		
14H-4, 30-30	123.40	126.21	C	P		F	A	F								R		
14H-CC, 0-10	123.57	126.38	A	P		F	D	C	R	R	F					R		
15H-1, 30-30	128.40	130.72	C	P		F	D	C	R	R						R		
15H-2, 112-112	130.72	133.04	F	P		F		C	F	R								
15H-3, 24-24	131.34	133.66	C	P		F	F	A	F	R								
15H-CC, 15-20	137.32	139.64	F	P	F		R	C	C									
16H-1, 40-40	138.00	140.32	F	M	C	F	R	A	F	R								
16H-3, 98-98	141.58	143.90	R	M	C			R	C		R			C				

Table T7 (continued).

Core, section, interval (cm)	Depth (mbsf)	Depth (mcd)	Abundance	Preservation	*Reticulofenestra minuta*	*Reticulofenestra minutula*	*Coccolithus pelagicus*	*Pseudoemiliania lacunosa*	*Calcidiscus leptoporus*	*Helicosphaera carteri*	*Gephyrocapsa* small	*Gephyrocapsa caribbeanica*	*Gephyrocapsa* medium (4-5.5 µm)	*Gephyrocapsa* large (> 5.5 µm)	*Gephyrocapsa* sp. 3	*Reticulofenestra asanoi*	*Emiliania huxleyi*	Comments
16H-3, 130-130	141.90	144.22	R	M			D	R	C		R			C				
16H-4, 12-12	142.22	144.54	F	M	F	R	A	F						F				
16H-6, 92-92	144.68	147.00	R	M		F			F					C				
16H-CC, 0-10	144.75	147.07	C	P			D	F					R	C				
18H-CC, 18-23	157.54	160.06	F	P				R	F				C					
177-1094B-																		
1H-CC, 7-12	9.24	9.76	B															
2H-CC, 10-15	18.87	19.89	B															
4H-CC, 30-35	33.13	36.00	B															
177-1094C-																		
1H-CC, 19-24	8.89	9.17	B															
2H-CC, 13-18	18.80	20.52	B															
3H-CC, 6-13	27.97	29.73	B															
5H-CC, 13-18	45.70	47.37	B															
8H-CC, 0-2	67.16	69.50	B															
177-1094D-																		
2H-1, 40-40	29.00	32.65	B															
2H-3, 116-116	32.76	36.41	B															
2H-CC, 9-14	33.83	37.48	C	M					C			F	F		F		F	Very small placoliths A
3H-CC, 0-10	47.03	49.52	B															
4H-2, 90-90	50.00	52.89	A	M			R		R	R	D	A	R		R			
4H-2, 139-139	50.49	53.38	A	M					R	R	A	A	R					Very small placoliths A
4H-CC, 0-10	55.99	58.88	B															
5H-CC, 0-5	57.10	59.99	A	M	A							A						Very small placoliths A
6H-1, 5-5	66.65	68.40	B															
6H-2, 90-90	69.00	70.75	B															
6H-CC, 0-10	76.03	77.78	F	P	C				R			C						
7H-2, 30-30	77.90	80.52	F	M			F		C		D							
7H-2, 87-87	78.47	81.09	R	M					F				F					
7H-4, 149-149	82.09	84.71	R	M				A		R			C					
7H-5, 5-5	82.15	84.77	R	P			F	A	C									
7H-CC, 0-10	82.22	84.84	R	P	R	F		A	C									
8H-CC, 13-18	93.18	96.50	R	P		R		F				R						
9H-3, 24-24	98.34	100.90	F	M				F	C		D		F					
9H-4, 80-80	100.40	102.96	R	M			C	A			C							
9H-CC, 12-17	100.88	103.44	B															
10H-1, 10-10	104.70	106.04	R	M				C			R		C					
10H-2, 120-120	107.30	108.64	R	M				F			F							Almost barren
10H-CC, 13-18	111.02	112.36	B															
11H-1, 30-30	114.40	115.94	R	M			D	F					F			F		Almost barren
11H-1, 116-116	115.26	116.80	F	M			D	F			C		F			F		
11H-CC, 22-27	119.92	121.46	B															
12H-2, 117-117	126.27	127.81	F	M			D	R					R			F		
12H-3, 126-126	127.86	129.40	F	P		F	D	R		R								
12H-4, 120-120	129.30	130.84	C	P	F		D	F	R	R	F							
12H-CC, 11-16	131.63	133.17	F	P		C	F	C	F									
13H-3, 102-102	137.12	139.00	A	M		F		C	R	R	C		R					
13H-CC, 14-19	137.35	139.23	C	P	F	F		A	F	R								
14H-3, 110-110	146.70	150.42	C	P			C	F					C	C				
14H-4, 10-10	147.20	150.92	C	P			F	R					C	R				
14H-5, 20-20	148.80	152.52	F	P	R			R	R				F	R				
14H-5, 120-120	149.80	153.52	F	P				R	F		F		C	R				
14H-6, 17-17	150.27	153.99	R	P					F	R			R	C				
15H-2, 30-30	153.90	155.79	P	P	R		C	F	F	R	R		F	F				
15H-3, 50-50	155.60	157.49	C	P	R		C	C					F	R				

Table T7 (continued).

Core, section, interval (cm)	Depth (mbsf)	Depth (mcd)	Abundance	Preservation	*Reticulofenestra minuta*	*Reticulofenestra minutula*	*Coccolithus pelagicus*	*Pseudoemiliania lacunosa*	*Calcidiscus leptoporus*	*Helicosphaera carteri*	*Gephyrocapsa* small	*Gephyrocapsa caribbeanica*	*Gephyrocapsa* medium (4-5.5 µm)	*Gephyrocapsa* large (> 5.5 µm)	*Gephyrocapsa* sp. 3	*Reticulofenestra asanoi*	*Emiliania huxleyi*	Comments
15H-4, 117-117	157.77	159.66	F	P				F	F	R			C	R				
15H-6, 80-80	160.40	162.29	F	P				R	F				C	F				
15H-CC, 10-15	161.00	162.89	B															
16H-1, 34-34	161.94	163.83	F	P		R		R	R				F	F				
16H-1, 140-140	163.00	164.89	C	P			C	F	F				F	C				
16H-2, 87-87	163.97	165.86	C	P			A	F	R				C					
16H-3, 50-50	165.10	166.99	F	P				C	C	R			R					
16H-3, 100-100	165.60	167.49	F	P			C	F	F				F					
16H-3, 140-140	166.00	167.89	F	P			C	F	F				F					
16H-4, 24-24	166.34	168.23	R	P				F	R				F					
16H-CC, 0-5	167.81	169.70	R	M			F	F			F		A					

Notes: Abundance abbreviations: D = dominant, A = abundant, C = common, F = few, R = rare, B = barren. Preservation abbreviations: M = moderate, P = poor. For more specific definitions, refer to the **"Explanatory Notes"** chapter. The distributions of the species are mainly described in stratigraphic intervals where events are identified. This table is also available in ASCII format in the **TABLES** directory.

Table T8. Summary of biostratigraphic age assignments for Site 1094. (**See table note.** Continued on next page.)

Core, section, interval (cm)	Depth (mbsf)	Depth (mcd)	Calcareous nannofossil zone	Calcareous nannofossil age (Ma)	Diatom zone	Diatom age (Ma)	Diatom comment	Radiolaria zone	Radiolaria age (Ma)	Radiolaria comments	Comment
177-1094A-											
1H-CC, 15-20	4.57	4.57			*T. lentiginosa*	0-0.65		Omega	0-0.46		Barren CN
2H-6, 68-68	12.78	14.32			*T. lentiginosa*	0-0.65	Cold-water assemblage, burrow fill				
2H-6, 69-69	12.79	14.33			*T. lentiginosa*	0-0.65	Outside burrow				
2H-CC, 14-19	13.75	15.29			*T. lentiginosa*	0-0.65	Cold-water assemblage				Barren CN
3H-CC, 13-18	22.31	24.73	NN21	0-0.26	*T. lentiginosa*	0-0.65	Warm-water assemblage	Omega	0-0.46		
4H-5, 54-54	29.97	33.33			*T. lentiginosa*	0-0.65	Cold-water assemblage, burrow fill				
4H-5, 55-55	29.98	33.34			*T. lentiginosa*	0-0.65	Cold-water assemblage beneath burrow				
4H-CC, 14-19	31.81	35.17			*T. lentiginosa*	0-0.65	Warm-water assemblage				Barren CN
5H-3, 146-146	37.56	39.97	NN21	0-0.26				Omega	0-0.46		
5H-4, 30-30	37.90	40.31	NN20	0.26-0.46							
5H-CC, 12-17	41.20	43.61	NN20	0.26-0.46	*T. lentiginosa*	0-0.65	Cold-water assemblage				
6H-CC, 11-16	50.45	53.41			*T. lentiginosa*	0-0.65					
7H-CC, 9-16	60.82	62.92	NN20	0.26-0.46	*T. lentiginosa*	0-0.65		Omega	0-0.46		
8H-CC, 8-13	70.59	72.73			*T. lentiginosa*	0-0.65	Cold-water assemblage	Psi	0.46-0.83		Barren CN
9H-2, 17-17	72.77	75.57	?	?							
9H-CC, 14-19	79.12	81.92			*T. lentiginosa*	0-0.65	Cold-water assemblage				Barren CN
10H-CC, 0-10	89.74	92.08			*A. ingens* Subzone c	0.65-1.07		Psi	0.46-0.83		Barren CN
11H-CC, 12-17	97.98	100.78	NN19	?	*A. ingens* Subzone c	0.65-1.07	Cold-water assemblage				
12H-4, 119-119	11.92	106.87	NN19	0.46-0.88							
12H-CC, 0-10	108.25	109.83			*A. ingens* Subzone c	0.65-1.07	Cold-water assemblage	?	?	No index	Barren CN
13H-2, 132-132	111.92	114.36	NN19	0.88-0.96							
13H-3, 42-42	112.52	114.96	NN19	0.88-0.96							
13H-CC, 0-10	116.82	119.26	NN19	0.88-0.96	*A. ingens* Subzone c	0.65-1.07	Cold-water assemblage				
14H-3, 66-66	122.26	125.07	NN19	0.88-0.96							
14H-3, 88-88	122.48	125.29	NN19	0.96-1.08							
14H-CC, 0-10	123.57	126.38	NN19	0.96-1.08	*A. ingens* Subzone c	0.65-1.07		?	?	No index, reworked	
15H-1, 30-30	128.40	130.72	NN19	0.96-1.08							
15H-2, 112-112	130.72	133.04	NN19	1.08-1.24							
15H-CC, 15-20	137.32	139.64	NN19	1.08-1.24	*A. ingens* Subzone b	1.07-1.3					
16H-1, 40-40	138.00	140.32	NN19	1.08-1.24							
16H-3, 98-98	141.58	143.90	NN19	1.24-1.46							
16H-CC, 0-10	144.75	147.07	NN19	1.24-1.46	*A. ingens* Subzone a	1.3-1.8	Cold-water assemblage	?	?	No index, reworked	
18H-CC, 18-23	157.54	160.06	NN19	1.46-1.69	*A. ingens* Subzone a	1.3-1.8	*A. ingens* acme	?	?	No index	
177-1094B-											
1H-CC, 7-12	9.24	9.76			*T. lentiginosa*	0-0.65	Cold-water assemblage				
2H-CC, 10-15	18.87	19.89			*T. lentiginosa*	0-0.65	Warm-water assemblage	Omega	0-0.46		
3H-CC, 14-19	19.14	20.16			*T. lentiginosa*	0-0.65	Warm-water assemblage				
4H-CC, 30-35	33.13	36.00			*T. lentiginosa*	0-0.65	Cold-water assemblage	Omega	0-0.46		
177-1094C-											
1H-CC, 19-24	8.89	9.17			*T. lentiginosa*	0-0.65		Omega			
2H-CC, 13-18	18.80	20.52			*T. lentiginosa*	0-0.65					
3H-CC, 6-13	27.97	29.73			*T. lentiginosa*	0-0.65	Cold-water assemblage	Omega	0-0.46		
5H-CC, 13-18	45.70	47.37			*T. lentiginosa*	0-0.65		Omega	0-0.46		

Table T8 (continued).

Core, section, interval (cm)	Depth (mbsf)	Depth (mcd)	Calcareous nannofossil zone	Calcareous nannofossil age (Ma)	Diatom zone	Diatom age (Ma)	Diatom comment	Radiolaria zone	Radiolaria age (Ma)	Radiolaria comments	Comment
6H-CC, 13-18	55.33	57.89			*T. lentiginosa*	0-0.65					
8H-CC, 0-2	67.16	69.50			*T. lentiginosa*	0-0.65					Barren CN
177-1094D-											
2H-CC, 9-14	33.83	37.48	NN21	<0.26	*T. lentiginosa*	0-0.65		Omega	0-0.46		
3H-CC, 0-10	47.03	49.52			*T. lentiginosa*	0-0.65					Barren CN
4H-CC, 0-10	55.99	58.88			*T. lentiginosa*	0-0.65		Omega	0-0.46		Barren CN
5H-CC, 0-5	57.10	59.99		<0.46	*T. lentiginosa*	0-0.65					
6H-CC, 0-10	76.03	77.78			*T. lentiginosa*	0-0.65		Psi	0.46-0.83		
7H-2, 87-87	78.47	81.09	NN20	<0.46							
7H-4, 149-149	82.09	84.71	NN19	0.46-0.88							
7H-CC, 0-10	82.22	84.84	NN19	0.46-0.88	*T. lentiginosa*	0-0.65					
8H-CC, 13-18	93.18	96.50	NN19	0.46-0.88	*A. ingens* Subzone c	0.65-1.07		Psi	0.46-0.83		
9H-CC, 12-17	100.88	103.44			*A. ingens* Subzone c	0.65-1.07					Barren CN
10H-CC, 13-18	111.02	112.36			*A. ingens* Subzone c	0.65-1.07	Cold-water assemblage	Psi	0.46-0.83		Barren CN
11H-1, 30-30	114.40	115.94	NN19	0.88-0.96							
11H-CC, 22-27	119.92	121.46			*A. ingens* Subzone c	0.65-1.07	Cold-water assemblage				Barren CN
12H-CC, 11-16	131.63	133.17	NN19	>1.08	*A. ingens* Subzone b	1.07-1.3		?	?	No index	
13H-CC, 14-19	137.35	139.23	NN19	1.08-1.24	*A. ingens* Subzone b	1.07-1.3					
14H-3, 110-110	146.70	150.42	NN19	1.24-1.46							
14H-CC, 14-19	151.32	155.04			*A. ingens* Subzone a	1.3-1.8		?	?	No index	
15H-CC, 10-15	161.00	162.89			*A. ingens* Subzone a	1.3-1.8					Barren CN
16H-2, 30-30	163.40	165.29	NN19	1.24-1.46							
16H-2, 87-87	163.97	165.86	NN19	1.46-1.69							
16H-CC, 0-5	167.81	169.70	NN19	<1.69	*A. ingens* Subzone a	1.3-1.8		?	?	No index	

Notes: CN = calcareous nannofossil. This table is also available in ASCII format in the **TABLES** directory.

Table T9. Control points used to calculate sedimentation rates at Site 1094.

Code	Event/Zone/Chron	Depth range of stratigraphic datums: Top Core, section, interval (cm)	Top Depth (mbsf)	Top Depth (mcd)	Base Core, section, interval (cm)	Base Depth (mbsf)	Base Depth (mcd)	Mean Depth (mbsf)	Mean Depth (mcd)	Age (Ma)	Sedimentation rate (m/m.y.)
		177-			177-						
CN	FO *E. huxleyi*	1094A-5H-3, 146-146	37.56	39.97	1094A-5H-4, 30-30	37.90	40.31	37.73	40.14	0.26	
RAD	BOT Omega Zone	1094A-7H-CC, 9-16	60.82	62.92	1094A-8H-CC, 8-13	70.59	72.73	65.71	67.83	0.46	~140
CN	LO *P. lacunosa*	1094D-7H-2, 87-87	78.47	81.09	1094D-7H-4, 149-149	82.09	84.71	80.28	82.90	0.46	
DIAT	TOP *A. ingens* Subzone c	1094D-7H-CC, 0-10	82.22	84.84	1094A-10H-CC, 0-10	89.74	92.08	85.98	88.46	0.65	
PMAG	BOT C1n (Brunhes)	1094A-11H-4, 80-80	95.40	98.20	1094A-12H-1, 40-40	100.00	101.58	97.70	99.89	0.78	
CN	LO *R. asanoi*	1094A-12H-4, 119-119	105.29	106.87	1094A-13H-2, 132-132	111.92	114.36	108.60	110.62	0.88	
CN	RE *Gephyrocapsa* medium (4-5.5 µm)	1094A-14H-3, 66-66	122.26	125.07	1094A-14H-3, 88-88	122.48	125.29	122.37	125.18	0.96	
DIAT	TOP *A. ingens* Subzone b	1094A-14H-CC, 0-10	123.57	126.38	1094D-12H-CC, 11-16	131.63	133.17	127.60	129.77	1.07	~91
CN	FO *R. asanoi*	1094A-15H-1, 30-30	128.40	130.72	1094A-15H-2, 112-112	130.72	133.04	129.56	131.88	1.08	
CN	LO *Gephyrocapsa* large (>5.5 µm)	1094D-13H-CC, 14-19	137.35	139.23	1094A-16H-3, 98-98	141.58	143.90	139.46	141.56	1.24	
DIAT	TOP *A. ingens* Subzone a	1094A-15H-CC, 15-20	137.32	139.64	1094A-16H-CC, 0-10	144.75	147.07	141.04	143.35	1.30	
CN	FO *Gephyrocapsa* large (>5.5 µm)	1094D-16H-2, 30-30	163.40	165.29	1094D-16H-2, 87-87	163.97	165.86	163.68	165.58	1.46	

Notes: Code abbreviations: CN = calcareous nannofossil, DIAT = diatom, RAD = radiolaria, PMAG = magnetic polarity. Event abbreviations: FO = first occurrence, LO = last occurrence, RE = reentrance, TOP = top of zone, BOT = bottom of zone. This table is also available in ASCII format in the **TABLES** directory.

Table T10. Distribution of major planktic foraminifer species at Site 1094.

Core, section, interval (cm)	Depth (mbsf)	Depth (mcd)	Abundance	Preservation	*Globigerina bulloides*	*Globigerina quinqueloba*	*Globigerinita glutinata*	*Globorotalia inflata*	*Globorotalia puncticuloides*	*Neogloboquadrina pachyderma* (sinistral)
177-1094A-										
1H-CC, 15-20	4.57	4.57	C	G		R				D
2H-CC, 14-19	13.75	15.29	R	G						D
3H-CC, 13-18	22.31	24.73	R	G	A	F	F			D
4H-CC, 14-19	31.81	35.17	T							
5H-CC, 12-17	41.20	43.61	F	M						D
6H-CC, 11-16	50.45	53.41	R	M	F					D
7H-CC, 9-16	60.82	62.92	A	M	F					D
8H-CC, 8-13	70.59	72.73	R	G						D
9H-CC, 14-19	79.12	81.92	F	G		F				D
10H-CC, 0-10	89.74	92.08	C	M		R				D
12H-CC, 0-10	108.25	109.83	A	G						D
13H-CC, 0-10	116.82	119.26	A	M						D
14H-CC, 0-10	123.57	126.38	A	G		F			P	D
15H-CC, 15-20	137.32	139.64	A	G						D
16H-CC, 0-10	144.75	147.07	A	G					P	D
18H-CC, 18-23	157.54	160.06	A	G						D
177-1094B-										
1H-CC, 7-12	9.24	9.76	C	G						D
2H-CC, 10-15	18.87	19.89	R							D
3H-CC, 14-19	19.14	20.16	F	G	D	F		P		D
4H-CC, 30-35	33.13	36.00	R	G						D
177-1094C-										
1H-CC, 19-24	8.89	9.17	F	G						D
2H-CC, 13-18	18.80	20.52	F	G						D
3H-CC, 6-13	27.97	29.73	F	M						D
5H-CC, 13-18	45.70	47.37	B							
6H-CC, 13-18	55.33	57.89	R	G	R					D
7H-CC										
8H-CC, 0-2	67.16	69.50	C	M						D
177-1094D-										
2H-CC, 9-14	33.83	37.48	F	G	R					D
3H-CC, 0-10	47.03	49.52	R	G						D
4H-CC, 0-10	55.99	58.88	R	M						D
5H-CC, 0-5	57.10	59.99	C	M		R				D
6H-CC, 0-10	76.03	77.78	F	M						D
7H-CC, 0-10	82.22	84.84	A	M						D
8H-CC, 13-18	93.18	96.50	C	M						D
9H-CC, 12-17	100.88	103.44	C	M						D
10H-CC, 13-18	111.02	112.36	A	G						D
11H-CC, 22-27	119.92	121.46	R	G						D
12H-CC, 11-16	131.63	133.17	A	M						D
13H-CC, 14-19	137.35	139.23	A	M						D
14H-CC, 14-19	151.32	155.04	A	G		F				D
15H-CC, 10-15	161.00	162.89	R	M						D
16H-CC, 0-5	167.81	169.70	A	M						D
18H-CC										

Notes: Abundance abbreviations: D = dominant, A = abundant, C = common, F = few, R = rare, T = trace, P = present. Preservation abbreviations: G = good, M = moderate. For more specific definitions, refer to the **"Explanatory Notes"** chapter. This table is also available in ASCII format in the **TABLES** directory.

Table T11. Distribution of benthic foraminifers in Hole 1094A.

Core, section, interval (cm)	Depth (mbsf)	Depth (mcd)	Abundance	Preservation	Anomalinoides sp.	Astrononion pusillum	Bolivina spp.	Bulimina aculeata	Cancris sp.	Cassidulina reniforme	Cassidulina teretis	Cibicidoides spp.	Cibicidoides wuellerstorfi	Cribrostomoides sp.	Cyclammina sp.	Dentalina sp.	Eggerella bradyi	Ehrenbergina sp.	Epistominella exigua	Fissurina spp.	Francesita sp.	Globobulimina sp.	Globocassidulina subglobosa	Gyroidinoides soldanii	Gyroidinoides spp.	Indeterminates (agg.)	Indeterminates (calc.)	Karreriella bradyi	Lagena spp.	Laticarinina pauperata	Lenticulina sp.	Martinotiella sp.	Melonis barleeanum	Melonis pompilioides	Melonis sp.	Miliolinella sp.	Nonionella sp.	Nuttallides umbonifera	Oolina spp.	Oridorsalis umbonatus	Parafissurina sp.	Polymorphinid spp.	Pullenia bulloides	Pullenia sp.	Pullenia quinqueloba	Pullenia subcarinata	Pyrgo murrhina	Pyrgo spp.	Quinqueloculina sp.	Reophax sp.	Siphotextularia sp.	Sphaeroidina bulloides	Stainforthia sp.	Triloculina trigona	Triloculina trihedra	Uvigerina hispidicostata	Sample sum	Number of species	Abundance (specimens/cm^3)
177-1094A-																																																											
1H-CC, 15-20	4.57	4.57	R	M													1							2	1																					1			1								6	5	0.3
2H-CC, 14-19	13.75	15.29	R	M										1			3									2						7																									13	4	0.65
3H-CC, 13-18	22.31	24.73	C	G	1		3	14			2	1	7				8	3	3	3			10	25			1		1				10	24					1	15		3	40		5	3	4		1		8						196	27	9.8
4H-CC, 14-19	31.81	35.17	R	M																												6																									6	1	0.3
5H-CC, 12-17	41.2	43.61	F	M									6				2			1									1			7	7	3			3			1						4				3				1			39	12	1.95
6H-CC, 11-16	50.45	53.41	F	M	1				5											2			1								1															2	1										13	8	0.65
7H-CC, 9-16	60.82	62.92	C	M	4		1		3				12			1	20	1	4	3			6	3	8	1	2				2		10	12		11		1		23	1		26			5	5	2				4					171	29	8.55
8H-CC, 8-13	70.59	72.73	F	M									1										11									14		1																1				1			29	6	1.45
9H-CC, 14-19	79.12	81.92	R	M									2						1					3																			2										1				9	5	0.45
10H-CC, 0-10	89.74	92.08	F	P									2	2			1			4						3	1					3		1		1				3		4			2						1	1					29	16	1.45
11H-CC, 12-17	97.98	100.78	C	P									10				13	1		4		4	56	6	1	1	2		1		2	1		12	1		1			11	1		26		5	12					1		3	1	1		177	25	8.85
12H-CC, 0-10	108.25	109.83	F	M		2											1		2	1			2	3		1							10	1			3			2			4		4	8					1						45	15	2.25
13H-CC, 0-10	116.82	119.26	C	M						2		2	3				4		1	1									2			6	39	3					1	4	1	2	9		7	13					1		3				104	22	5.2
14H-CC, 0-10	123.57	126.38	C	M								1	8			1	19	1	27	6	1		14	5	12	3			5	1		5	24	18			2			21			28		14	9	1	3		1	7	1		1			239	33	11.95
15H-CC, 15-20	137.32	139.64	C	M								2	6				3						3		1	8						1					1		2	9			14		1	3					1						55	16	13.75
16H-CC, 0-10	144.75	147.07	C	M								2	19				5		20	3			3		2	8		1			2		23	8					5	17	1		9		4	12	1				4		1				150	28	22.5
18H-CC, 18-23	157.54	160.06	C	M								2	7		1		10		38	7			11	2	4					7	1	6		14					3	52			55													1	221	19	11.05

Notes: Abundance abbreviations: C = common, F = few, R = rare. Preservation abbreviations: G = good, M = moderate, P = poor. For more specific definitions, refer to the **"Explanatory Notes"** chapter. This table is also available in ASCII format in the **TABLES** directory.

Table T12. Diatom, silicoflagellate, ebridian, *Actiniscus*, sponge spicule, and opaline phytolith occurrence in smear slides investigated from Site 1094. (**See table note.** Continued on next page.)

Core, section, interval (cm)	Depth (mbsf)	Depth (mcd)	Diatom abundance (uncleaned)	Diatom preservation	Silicoflagellate occurrence	Ebridian occurrence	*Actiniscus* occurrence	Sponge spicule occurrence	Opaline phytolith occurrence	*Actinocyclus actinochilus*	*Actinocyclus ingens*	*Actinocyclus karstenii*	*Asteromphalus hookeri*	*Asteromphalus parvulus*	*Azpeitia tabularis*	*Chaetoceros* spp.	*Ethmodiscus rex*	*Eucampia antarctica*	*Fragilariopsis angulata*	*Fragilariopsis barronii*	*Transition F. barronii/F.kerguelensis*	*Fragilariopsis curta*	*Fragilariopsis cylindrus*	*Fragilariopsis interfrigidaria*	*Fragilariopsis kerguelensis*	*Fragilariopsis obliquecostata*	*Fragilariopsis ritscheri*	*Fragilariopsis separanda*	*Fragilariopsis sublinearis*	*Fragilariopsis* sp. A (Gersonde, 1991)	*Hemidiscus karstenii*	*Rhizosolenia antennata* fo. *semispina*	*Rouxia isopolica*	*Thalassionema nitzschioides*	*Thalassiosira elliptipora*	*Thalassiosira fasciculata*	*Thalassiosira gracilis*	*Thalassiosira lentiginosa*	*Thalassiosira oestrupii*	*Thalassiosira oliverana*	*Thalassiosira tetraoestrupii* var. *reimeri*	*Thallassiothrix antarctica-longissima* gr.	Diatom zone	Diatom age (Ma)
177-1094A-																																									
1H-CC,15-20	4.57	4.57	A	G	T	B	B	B	B						R										D											F	C			R	*T. lentiginosa*	0-0.65
2H-6, 68-68	12.78	14.32	A	G-M	T	B	B	B	B	F						F		F				F			F-C	R	F		R							C			R	*T. lentiginosa*	0-0.65
2H-6, 69-69	12.79	14.33	A	G	R	X	B	B	B	R					R			R				R			A			R							R	C		R	R	*T. lentiginosa*	0-0.65
2H-CC, 14-19	13.75	15.29	A-C	M	T	B	B	B	B	R								F				F			C											R	F			R	*T. lentiginosa*	0-0.65
3H-CC, 13-18	22.31	24.73	A	G	T	B	B	B	B						R-F	R		R							A											R	C	R		F	*T. lentiginosa*	0-0.65
4H-5, 54-54	29.97	33.33	A	G	R	B	B	B	B	R				R				F	R						C	R	F	R									C		R	R	*T. lentiginosa*	0-0.65
4H-5, 55-55	29.98	33.34	A	G	R	B	B	B	B	R					T	R		R				T			C	R		R									C		R	R	*T. lentiginosa*	0-0.65
4H-CC, 14-19	31.81	35.17	A	G	T	B	B	B	B						F	R									A											R	F	R		F	*T. lentiginosa*	0-0.65
5H-CC, 12-17	41.20	43.61	A	G	B	B	B	B	B									R				R			A		R							R			C			F	*T. lentiginosa*	0-0.65
6H-CC, 11-16	50.45	53.41	A	G	B	B	B	B	B					T	F			F							A			R								R	F		R	F	*T. lentiginosa*	0-0.65
7H-CC, 9-16	60.82	62.92	A	G	B	B	B	B	B						R			R							D												F	R		R	*T. lentiginosa*	0-0.65
8H-CC, 8-13	70.59	72.73	A	G	R	B	B	B	B	R								F				R			F												F		R	R	*T. lentiginosa*	0-0.65
9H-CC, 14-19	79.12	81.92	A	G	T	B	B	B	B		R				R			F							D												F			R	*T. lentiginosa*	0-0.65
10H-CC, 0-10	89.74	92.08	A	G	R	B	B	B	B		F							R				T			C		T	R						R			C-A		R	R	*A. ingens* Subzone c	0.65-1.07
11H-CC, 12-17	97.98	100.78	A	G	B	B	B	B	B		C							R				R					F	R						R-F	R		F			F	*A. ingens* Subzone c	0.65-1.07
12H-CC, 0-10	108.25	109.83	A	G	B	B	B	B	B		F					R	X	R							C		F	R			T				R		F			F	*A. ingens* Subzone c	0.65-1.07
13H-CC, 0-10	116.82	119.26	A	G	T	B	B	B	B		F		T			F			R			R			F		R				R				R	T		C	R	F	*A. ingens* Subzone c	0.65-1.07
14H-CC, 0-10	123.57	126.38	A	G	R	B	B	B	B	T	C				T		X	R							F		R						R		T	T		C	R	F	*A. ingens* Subzone c	0.65-1.07
15H-CC, 15-20	137.32	139.64	A	G-M	T	B	B	B	B		F						X	R			R	R		T*	F		F							R	T		R	C	R	F	*A. ingens* Subzone b	1.07-1.3
16H-CC, 0-10	144.75	147.07	A	M	B	B	B	B	B	T	R							F		F		F			F		C		R					R		R	C	R	F	*A. ingens* Subzone a	1.3-1.8
18H-CC, 18-23	157.54	160.06	A	G	R	B	B	B	B		D									F	F				F					R				R					F	R	R	*A. ingens* Subzone a	1.3-1.8
177-1094B-																																										
1H-CC, 7-12	9.24	9.76	A	G-M	B	B	B	B	B	R					T	R		F	R			R			C	R												F		R	R	*T. lentiginosa*	0-0.65
2H-CC, 10-15	18.87	19.89	A	G	R	B	B	B	B					R	F			R				R			D			R									C		R	R	*T. lentiginosa*	0-0.65
3H-CC, 14-19	19.14	20.16	A	G	R	B	B	B	B						F										D-A			R								R	F		R	R	*T. lentiginosa*	0-0.65
4H-CC, 30-35	33.13	36.00	A	G	B	B	B	B	B	T					T	R		R	R			R			A			R									F		R	R	*T. lentiginosa*	0-0.65
177-1094C-																																										
1H-CC, 19-24	8.89	9.17	A	G-M	B	B	B	B	B	T						R		R				R			C	R												C		R	R	*T. lentiginosa*	0-0.65
2H-CC, 13-18	18.80	20.52	A	G	B	B	B	B	B					T	F										A											R	C		R	R	*T. lentiginosa*	0-0.65
3H-CC, 6-13	27.97	29.73	A	G-M	B	B	B	B	B	R								F				F			C	R		R									C			R	*T. lentiginosa*	0-0.65
5H-CC, 13-18	45.70	47.37	C	M	B	B	B	B	B									R				R			A			R									C			R	*T. lentiginosa*	0-0.65
6H-CC, 13-18	55.33	57.89	A	G	T	B	B	B	B	R					R			R				R			A		R				T		R			R	C			R	*T. lentiginosa*	0-0.65
8H-CC, 0-2	67.16	69.50	A	G	T	B	B	B	B						R	R		R				T			D			R									C		R	R	*T. lentiginosa*	0-0.65

Table T12 (continued).

Core, section, interval (cm)	Depth (mbsf)	Depth (mcd)	Diatom abundance (uncleaned)	Diatom preservation	Silicoflagellate occurrence	Ebridian occurrence	*Actiniscus* occurrence	Sponge spicule occurrence	Opaline phytolith occurrence	*Actinocyclus actinochilus*	*Actinocyclus ingens*	*Actinocyclus karstenii*	*Asteromphalus hookeri*	*Asteromphalus parvulus*	*Azpeitia tabularis*	*Chaetoceros* spp.	*Ethmodiscus rex*	*Eucampia antarctica*	*Fragilariopsis angulata*	*Fragilariopsis barronii*	*Transition F. barronii/F.kerguelensis*	*Fragilariopsis curta*	*Fragilariopsis cylindrus*	*Fragilariopsis interfrigidaria*	*Fragilariopsis kerguelensis*	*Fragilariopsis obliquecostata*	*Fragilariopsis ritscheri*	*Fragilariopsis separanda*	*Fragilariopsis sublinearis*	*Fragilariopsis* sp. A (Gersonde, 1991)	*Hemidiscus karstenii*	*Rhizosolenia antennata* fo. *semispina*	*Rouxia isopolica*	*Thalassionema nitzschioides*	*Thalassiosira elliptipora*	*Thalassiosira fasciculata*	*Thalassiosira gracilis*	*Thalassiosira lentiginosa*	*Thalassiosira oestrupii*	*Thalassiosira oliverana*	*Thalassiosira tetraoestrupii* var. *reimeri*	*Thallassiothrix antarctica-longissima* gr.	Diatom zone	Diatom age (Ma)
177-1094D-																																									
2H-CC, 9-14	33.83	37.48	A	G	R	B	B	B	B	T					R	R		R	R			F			A	R		R		T					C			R		T. *lentiginosa*	0-0.65
3H-CC, 0-10	47.03	49.52	A	G-M	B	B	B	B	B	R					R			R				R			A		T	R					T			R	C	R	R		T. *lentiginosa*	0-0.65
4H-CC, 0-10	55.99	58.88	A	G-M	B	B	B	X	B													R			A			R									C			R		T. *lentiginosa*	0-0.65
5H-CC, 0-5	57.10	59.99	A	G	R	B	B	B	B	R				T	R			R							A		F										C		F		F		T. *lentiginosa*	0-0.65
6H-CC, 0-10	76.03	77.78	A	G-M	B	B	B	X	B	T					R			R							C-A		R	R					T				F		F		R		T. *lentiginosa*	0-0.65
7H-CC, 0-10	82.22	84.84	A	G	R	B	B	B	B	T	R							R							D			R									C		R		R		T. *lentiginosa*	0-0.65
8H-CC, 13-18	93.18	96.50	A	G-M	B	B	B	B	B		F					R	X								C		F						T				F		R		R		*A. ingens* Subzone c	0.65-1.07
9H-CC, 12-17	100.88	103.44	A	G-M	B	B	B	B	B		C							R				T			F										R		F-C		R		R		*A. ingens* Subzone c	0.65-1.07
10H-CC, 13-18	111.02	112.36	A	G	R	B	B	B	B	T	F							R				R			C		C		R				R		R		F		R		F		*A. ingens* Subzone c	0.65-1.07
11H-CC, 22-27	119.92	121.46	A	M	B	B	B	B	B		F	T						R			R	F-R			F		F	R						T	R	R	C		R		R		*A. ingens* Subzone c	0.65-1.07
12H-CC, 11-16	131.63	133.17	A	G-M	B	B	B	B	B		A			T				R							F		R						R			R	C		R		F		*A. ingens* Subzone b	1.07-1.3
13H-CC, 14-19	137.35	139.23	A	G-M	B	B	B	B	B		C		T		R			R							F		R-F						R			R	C		R		F		*A. ingens* Subzone b	1.07-1.3
14H-CC, 14-19	151.32	155.04	A	G-M	R	B	B	B	B		C	T								R	F				F		F									R	C	C		R		*A. ingens* Subzone a	1.3-1.8
15H-CC, 10-15	161.00	162.89	A	M	R	B	B	B	B		A							R		R	R				R												F		R		R		*A. ingens* Subzone a	1.3-1.8
16H-CC, 0-5	167.81	169.70	A	G	B	B	B	B	B		A							R		C																	F			T	R		*A. ingens* Subzone a	1.3-1.8

Notes: Abundance abbreviations: D = dominant, A = abundant, C = common, F = few, R = rare, T = trace, X = present, B = barren, * = reworking. Preservation abbreviations: G = good, M = moderate. For more specific definitions, refer to the "**Explanatory Notes**" chapter. This table is also available in ASCII format in the **TABLES** directory.

Table T13. Distribution of the main components of the radiolarian assemblages at Site 1094.

Core, section, interval (cm)	Depth (mbsf)	Depth (mcd)	Abundance	Preservation	*Antarctissa denticulata*	*Antarctissa longa*	*Botryostrobus aquilonlis*	*Cycladophora davisiana*	*Cycladophora pliocenica*	*Cycladophora davisiana cornutoides*	*Desmospyris spongiosa*	*Eucyrtidium carvertense*	*Helotholus vema*	*Lamprocyrtis heteroporos*	*Lithelius nautiloides*	*Phormacantha* sp.	*Prunopyle antarctica*	*Prunopyle tetrapila*	*Pterocanium trilobum*	*Pterocorys* spp.	*Saccospyris antarctica*	*Saturnalis circularis*	*Siphocampe lineata*	*Spogodiscus osculosus*	*Spongoplegma antarctica*	*Spongotrochus glacialis*	*Spongurus pylomaticus*	*Stylatractus universus*	*Triceraspyris antarctica*
177-1094A-																													
1H-CC, 15-20	4.57	4.57	C	E	A	A		C	R	F											F		F						
2H-CC, 14-19	13.75	15.29																											
3H-CC, 13-18	22.31	24.73	C	E	A	A		C	R	F										F	F		F						
4H-CC, 14-19	31.81	35.17																											
5H-CC, 12-17	41.2	43.61	C	E	A	A	R	C	R						F		F	F			F					F			F
6H-CC, 11-16	50.45	53.41																											
7H-CC, 9-16	60.82	62.92	C	E	A	A		F							F		F								F	F	F		F
8H-CC, 8-13	70.59	72.73	C	E	A	A		F							F		F										F	R	F
9H-CC, 14-19	79.12	81.92																											
10H-CC, 0-10	89.74	92.08	C	E	A	A		F							F		F										F	R	F
11H-CC, 12-17	97.98	100.78																											
12H-CC, 0-10	108.25	109.83	R	E	A	A		F	R						F		F										F		F
13H-CC, 0-10	116.82	119.26																											
14H-CC, 0-10	123.57	126.38	R	E	A	A		C			R			R												F			
15H-CC, 15-20	137.32	139.64																											
16H-CC, 0-10	144.75	147.07	R	E	C		F	F			R	R	R		F							F				F	F		
18H-CC, 18-23	157.54	160.06	R	E	C	C	F		R												F	F	F					R	
177-1094B-																													
1H-CC, 7-12	9.24	9.76																											
2H-CC, 10-15	18.87	19.89	A	E	A	A		C	R	F										R	F			F		F	F		
4H-CC, 30-35	33.13	36	C	E	A	A		C	R	F					F					R	F			F		F	F		
177-1094C-																													
1H-CC, 19-24	8.89	9.17	C	E	A			C							F		F												F
2H-CC, 13-18	18.8	20.52																											
3H-CC, 6-13	27.97	29.73	A	E	A	A		C							F		F			F			F			F	F		
5H-CC, 13-18	45.7	47.37	C	E	A			C	R	F													F		F				
8H-CC, 0-2	67.16	69.5																											
177-1094D-																													
2H-CC, 9-14	33.83	37.48	C	E	A	A			R						F					R	F		F		F	F			
3H-CC, 0-10	47.03	49.52																											
4H-CC, 0-10	55.99	58.88	C	E	A	A		F	R	F							F	F			F						F		R
5H-CC, 0-5	57.1	59.99																											
6H-CC, 0-10	76.03	77.78	F	E	C			C							F		F	F			F					F	F		
7H-CC, 0-10	82.22	84.84																											
8H-CC, 13-18	93.18	96.5	R	E	C												C	C								C	C	R	
9H-CC, 12-17	100.88	103.44																											
10H-CC, 13-18	111.02	112.36	C	E	A	A		F							F						F		F			F	F	F	
11H-CC, 22-27	119.92	121.46																											
12H-CC, 11-16	131.63	133.17	C	E	A	A		C								F	F	F					F	F		F	F	F	
13H-CC, 14-19	137.35	139.23																											
15H-CC, 10-15	161	162.89																											
16H-CC, 0-5	167.81	169.7	C	E	A	A		C							F						F	F	F			F	F		

Notes: Abundance abbreviations: A = abundant, C = common, F = few, R = rare. Preservation abbreviations: E = excellent. For more specific definitions, refer to the **"Explanatory Notes"** chapter. This table is also available in ASCII format in the **TABLES** directory.

Table T14. Concentrations of methane obtained by the headspace technique at Site 1094.

Core, section, interval (cm)	Depth (mbsf)	C_1 (ppmv)
177-1094A-		
1H-2, 0-5	1.52	2
2H-5, 0-5	10.62	2
3H-5, 0-5	20.12	3
4H-5, 0-5	29.46	3
5H-5, 0-5	39.12	4
6H-5, 0-5	48.62	3
7H-5, 0-5	58.12	4
8H-5, 0-5	67.62	4
9H-5, 0-5	77.12	4
10H-5, 0-5	86.62	3
11H-5, 0-5	96.12	4
12H-5, 0-5	105.62	4
13H-4, 0-5	113.62	4
14H-4, 0-5	123.12	3
15H-5, 0-5	132.62	5
18H-5, 0-5	155.28	4
177-1094D-		
15H-5, 0-5	158.12	5
16H-4, 0-5	166.12	4

Note: C_1 = methane.

Table T15. Interstitial water chemistry from shipboard measurements at Site 1094. (Continued on next page.)

Core, section, interval (cm)	Depth (mbsf)	pH	Method	Alkalinity (mM)	Method	Salinity	Method	Cl (mM)	Method	SO_4 (mM)	Method	Na (mM)	Method	Mg (mM)	Method	Ca (mM)	Method
177-1094A-																	
1H-1, 145-150	1.48	7.97	ISE	3.357	T	34.5	R	552	T	28.4	I	474	CB	55.0	I	9.0	I
2H-4, 145-150	10.58	7.92	ISE	5.597	T	34.5	R	555	T	27.5	I	478	CB	54.5	I	8.8	I
3H-4, 145-150	20.08	8.01	ISE	5.671	T	35.0	R	558	T	28.8	I	483	CB	54.8	I	8.9	I
4H-4, 140-145	29.40	7.97	ISE	5.611	T	35.0	R	561	T	28.7	I	487	CB	54.6	I	8.7	I
5H-4, 145-150	39.08	7.93	ISE	5.385	T	35.0	R	562	T	28.0	I	487	CB	54.3	I	8.7	I
6H-4, 145-150	48.58	7.94	ISE	5.286	T	36.0	R	562	T	28.3	I	488	CB	53.8	I	8.8	I
7H-4, 145-150	58.08	7.90	ISE	5.118	T	35.5	R	563	T	28.3	I	493	CB	52.2	I	8.6	I
8H-4, 145-150	67.58	7.97	ISE	5.166	T	35.5	R	564	T	27.2	I	490	CB	53.1	I	8.6	I
9H-4, 145-150	77.08	7.96	ISE	5.173	T	35.5	R	569	T	27.9	I	494	CB	53.6	I	8.9	I
10H-4, 145-150	86.58	7.94	ISE	5.292	T	35.5	R	566	T	27.8	I	492	CB	53.0	I	9.1	I
11H-4, 145-150	96.08	7.89	ISE	5.297	T	35.5	R	565	T	27.1	I	493	CB	51.6	I	8.7	I
12H-4, 145-150	105.60	7.95	ISE	5.125	T	35.5	R	563	T	26.8	I	486	CB	53.1	I	9.0	I
13H-3, 145-150	113.60	7.85	ISE	5.009	T	35.5	R	562	T	28.9	I	492	CB	52.7	I	8.3	I
14H-3, 145-150	123.10	7.55	ISE	4.715	T	35.5	R	562	T	28.6	I	489	CB	52.9	I	8.6	I
15H-4, 145-150	134.10	7.75	ISE	4.703	T	35.5	R	564	T	28.8	I	497	CB	51.2	I	8.1	I
18H-4, 145-150	155.20	7.90	ISE	4.296	T	35.5	R	562	T	27.8	I	490	CB	52.3	I	8.1	I
177-1094D-																	
15H-4, 145-150	158.10	7.96	ISE	4.595	T	35.0	R		T	28.2	I		CB	54.4	I	8.4	I
16H-3, 145-150	166.10	7.80	ISE	4.388	T	35.0	R		T	27.0	I		CB	52.5	I	8.5	I

Note: Method abbreviations: ISE = ion selective electrode, T = titration, R = refractometer, I = ion chromatography, CB = charge balance calculation, S = spectrophotometry, AAS = atomic absorption spectrometry, AES = atomic emission spectrometry.

Table T15 (continued).

Core, section, interval (cm)	Depth (mbsf)	K (mM)	Method	H_4SiO_4 (µM)	Method	NH_4 (µM)	Method	HPO_4 (µM)	Method	Sr (µM)	Method	Fe (µM)	Method	Mn (µM)	Method	Li (µM)	Method
177-1094A-																	
1H-1, 145-150	1.48	10.5	I	744	S	79	S	33	S	85	AAS	7.3	AAS	36.6	AAS	25.0	AES
2H-4, 145-150	10.58	11.0	I	823	S	274	S	56	S	86	AAS	2.6	AAS	62.4	AAS	19.5	AES
3H-4, 145-150	20.08	10.5	I	853	S	356	S	43	S	89	AAS	0.2	AAS	45.4	AAS	17.9	AES
4H-4, 140-145	29.40	10.5	I	788	S	375	S	39	S	87	AAS	1.6	AAS	46.3	AAS	17.3	AES
5H-4, 145-150	39.08	10.8	I	916	S	380	S	32	S	86	AAS	0.4	AAS	32.3	AAS	17.0	AES
6H-4, 145-150	48.58	10.7	I	836	S	368	S	31	S	88	AAS	0.5	AAS	23.0	AAS	17.2	AES
7H-4, 145-150	58.08	10.6	I	749	S	352	S	31	S	88	AAS	0.3	AAS	20.4	AAS	17.2	AES
8H-4, 145-150	67.58	10.4	I	1017	S	368	S	28	S	88	AAS	-0.3	AAS	28.4	AAS	17.8	AES
9H-4, 145-150	77.08	10.9	I	766	S	371	S	30	S	89	AAS	2.5	AAS	30.6	AAS	17.8	AES
10H-4, 145-150	86.58	10.5	I	890	S	375	S	28	S	89	AAS	-0.0	AAS	29.3	AAS	17.9	AES
11H-4, 145-150	96.08	11.0	I	886	S	427	S	26	S	88	AAS	0.4	AAS	25.4	AAS	18.1	AES
12H-4, 145-150	105.60	11.8	I	844	S	438	S	24	S	88	AAS	0.5	AAS	21.7	AAS	18.7	AES
13H-3, 145-150	113.60	10.5	I	792	S	260	S	7	S	89	AAS	0.8	AAS	14.7	AAS	18.9	AES
14H-3, 145-150	123.10	11.7	I	801	S	438	S	13	S	86	AAS	4.1	AAS	11.5	AAS	19.7	AES
15H-4, 145-150	134.10	10.8	I	929	S	419	S	9	S	87	AAS	14.7	AAS	7.5	AAS	20.4	AES
18H-4, 145-150	155.20	11.0	I	875	S	410	S	7	S	88	AAS	15.0	AAS	9.7	AAS	20.8	AES
177-1094D-																	
15H-4, 145-150	158.10	10.8	I	897	S	401	S	9	S	88	AAS	2.9	AAS	10.4	AAS	20.6	AES
16H-3, 145-150	166.10	11.3	I	790	S	421	S	9	S	108	AAS	6.7	AAS	15.3	AAS	20.9	AES

Table T16. Interstitial water chemistry from shipboard measurements of small-volume samples taken across selected porcellanite intervals in Holes 1094A and 1094D.

Core, section, interval (cm)	Depth (mbsf)	pH	Alkalinity (mM)	Cl (mM)	SO_4 (mM)	Mg (mM)	Ca (mM)	K (mM)
177-1094A-								
8H-4, 10-15	66.22	8.09	5.225	565	30.2	52.82	9.0	10.96
8H-4, 60-65	66.72	8.04	5.356	566	30.0	52.39	8.9	11.40
8H-4, 87-92	67.00	8.05	5.376	567	28.6	52.65	9.1	11.45
8H-5, 0-5	67.62	8.05	5.061	564	28.7	52.37	9.2	10.91
8H-5, 22-27	67.84	8.00	5.338	563	29.7	52.55	9.5	10.45
8H-5, 52-57	68.14	8.03	4.961	564	31.2	52.57	9.4	10.33
8H-5, 57-62	68.20	8.13	5.237	564	29.5	52.27	9.7	10.75
8H-5, 62-67	68.24	7.91	5.225	566	29.9	52.35	9.3	10.73
8H-5, 73-78	68.36	7.92	5.370	567	30.9	53.12	9.8	10.76
8H-5, 88-93	68.50	8.16	5.249	571	28.8	52.71	9.6	10.87
8H-5, 113-118	68.76	8.15	5.345	571	28.4	52.12	10.1	11.16
8H-5, 134-139	68.96	8.05	5.296	—	29.4	52.07	10.1	12.34
8H-6, 10-15	69.23	8.08	5.246	—	28.8	51.23	9.6	13.14
12H-3, 55-60	103.18	7.82	5.080	—	29.1	53.34	9.6	11.65
12H-4, 19-24	104.32	8.00	5.080	—	27.1	53.94	9.4	10.63
12H-4, 43-48	104.56	7.90	4.926	—	27.5	52.72	9.0	10.61
12H-4, 55-60	104.68	8.15	5.333	—	29.5	54.62	9.1	11.09
12H-4, 68-73	104.80	7.94	4.691	—	27.6	53.75	9.1	11.10
12H-4, 82-87	104.94	7.82	5.166	—	30.8	52.59	8.3	11.58
12H-4, 105-110	105.18	7.62	5.324	—	27.1	51.07	8.5	13.01
12H-5, 55-60	106.18	7.99	5.320	—	27.1	50.20	8.0	13.50
177-1094D-								
6H-1, 5-10	66.68	—	—	564	29.3	51.98	9.3	11.06
6H-1, 40-45	67.03	—	—	571	29.6	52.82	9.7	11.33
6H-1, 95-100	67.58	—	—	564	28.5	52.30	9.8	11.28
6H-1, 125-130	67.88	—	—	564	27.6	54.10	9.9	11.17
6H-1, 144-149	68.06	—	—	562	27.8	53.87	10.2	10.43
6H-2, 3-8	68.16	—	—	564	28.3	52.13	9.6	10.82
6H-2, 11-16	68.24	—	—	564	27.8	53.17	10.1	10.80
6H-2, 21-26	68.34	—	—	570	27.8	52.59	9.7	11.01
6H-2, 48-53	68.60	—	—	568	27.8	51.80	9.8	10.97
6H-2, 80-85	68.92	—	—	566	27.3	52.06	10.2	11.13
6H-2, 130-135	69.42	—	—	566	28.0	51.21	10.3	12.62
6H-3, 40-45	69.92	—	—	566	27.9	50.73	9.9	13.93
6H-3, 140-145	70.92	—	—	569	27.3	50.75	9.7	14.47
6H-4, 120-125	72.22	—	—	568	27.3	50.67	9.7	14.26
6H-5, 140-145	73.92	—	—	569	28.5	52.36	9.8	13.40

Note: Methods are identical to those used for standard interstitial water samples (see Table **T15,** p. 67).

Table T17. Analytical results of inorganic carbon, calculated calcium carbonate, total carbon, total organic carbon, total nitrogen, total sulfur, and TOC/TN at Site 1094.

Core, section, interval (cm)	Depth (mbsf)	IC (wt%)	$CaCO_3$ (wt%)	TC (wt%)	TOC (wt%)	TN (wt%)	TS (wt%)	TOC/TN
177-1094A-								
1H-1, 68-69	0.68	0.00	0.0	0.79	0.79	0.02	0.27	31.6
2H-1, 69-70	5.30	0.00	0.0	0.93	0.93	0.03	0.27	33.3
2H-4, 69-70	9.80	0.00	0.0					
3H-1, 58-59	14.68	0.00	0.0	0.84	0.84	0.02	0.16	49.3
3H-3, 67-68	17.78	0.00	0.0					
3H-5, 67-68	20.78	0.00	0.0					
4H-1, 63-64	24.24	0.00	0.0	0.91	0.91	0.04	0.36	22.3
4H-3, 67-68	27.16	0.00	0.0					
4H-5, 66-67	30.10	0.00	0.0					
5H-3, 119-120	37.30	1.37	11.4	2.33	0.96	0.02	0.22	50.4
5H-5, 69-70	39.80	0.00	0.0					
6H-1, 67-68	43.28	0.00	0.0	0.68	0.68	0.02	0.18	35.7
6H-4, 68-69	47.78	0.00	0.0					
6H-5, 140-141	50.00	2.99	24.9					
7H-1, 69-70	52.80	0.21	1.8	1.28	1.07	0.04	0.33	24.8
7H-3, 69-70	55.80	0.00	0.0					
7H-5, 69-70	58.80	0.95	7.9					
8H-1, 68-69	62.28	0.00	0.0	0.86	0.86	0.02	0.20	50.7
8H-3, 68-69	65.28	0.00	0.0					
8H-5, 103-104	68.64	0.00	0.0					
9H-1, 69-70	71.80	0.00	0.0	0.80	0.80	0.03	0.13	29.9
9H-3, 69-70	74.80	1.09	9.1					
9H-5, 69-70	77.80	0.52	4.3					
10H-2, 69-70	82.80	0.46	3.9	1.55	1.09	0.02	0.18	67.9
10H-4, 69-70	85.80	0.46	3.9					
10H-6, 69-70	88.80	0.43	3.6					
11H-1, 69-70	90.80	0.00	0.0	0.82	0.82	0.02	0.15	34.2
11H-3, 69-70	93.80	0.52	4.3					
11H-5, 69-70	96.80	0.60	5.0					
12H-1, 111-112	100.72	0.45	3.8	0.86	0.41	0.03	0.24	15.7
12H-4, 27-28	104.38	1.05	8.8					
12H-5, 69-70	106.30	0.36	3.0					
13H-2, 69-70	111.30	0.64	5.4	1.11	0.46	0.02	0.25	22.1
13H-4, 69-70	114.30	4.99	41.6					
13H-6, 23-24	116.48	0.32	2.6					
14H-2, 67-68	120.78	0.48	4.0	1.55	1.08	0.04	0.28	29.1
15H-1, 68-69	128.78	2.00	16.7					
15H-4, 122-123	133.82	2.87	23.9					
15H-6, 59-60	136.20	2.42	20.2					
16H-1, 70-71	138.30	3.55	29.6	4.29	0.74	0.02	0.09	37.2
16H-3, 130-131	141.90	1.02	8.5					
16H-4, 88-89	142.99	0.32	2.7					
18H-4, 128-129	155.04	3.89	32.4	4.80	0.91	0.02	0.07	60.5
18H-6, 39-40	157.15	0.85	7.0					

Note: IC = inorganic carbon, $CaCO_3$ = calcium carbonate, TC = total carbon, TOC = total organic carbon, TN = total nitrogen, TS = total sulfur.

Table T18. Summary of physical properties measurements conducted at Site 1094.

Measurement	Core 177-1094A-	Core 177-1094B-	Core 177-1094C-	Core 177-1094D-
GRA sample spacing	1H-18H: 2 cm	1H-4H: 2 cm	1H-3H1, 5H-8H: 2 cm, 3H2-3H7: 4 cm	2H-16H: 2 cm
MS sample spacing	1H-18H: 2 cm	1H-4H: 2 cm	1H-3H1, 5H-8H: 2 cm, 3H2-3H7: 4 cm	2H-16H: 2 cm
NGR sample spacing	1H-18H: 4 cm	1H-4H: 4 cm	1H-2H, 5H-8H: 4 cm	2H-10H: 4 cm, 11H-16H: 2 cm
PWL sample spacing	1H-18H: 2 cm	1H-4H: 2 cm	1H-2H, 5H-8H: 2 cm	2H-16H: 2 cm
OSU-SCAT sample spacing	1H-18H: 4 cm	1H-4H: 4 cm	1H-8H: 4 cm	1H-16H: 4 cm
PWS3	*N* = 244	*N* = 9	*N* = 39	*N* = 103
MAD	*N* = 97	—	—	*N* = 17
TC	*N* = 15	*N* = 2	*N* = 7	*N* = 11

Notes: GRA = gamma-ray attenuation, MS = magnetic susceptibility, NGR = natural gamma radiation, PWL = *P*-wave logger, OSU-SCAT = Oregon State University Split Core Analysis Track, PWS3 = *P*-wave velocity sensor 3 for split cores, MAD = moisture and density, TC = thermal conductivity.

Table T19. Thermal conductivity measurements at Site 1094. (**See table note.** Continued on next page.)

Core, section, interval (cm)	Depth (mbsf)	Depth (mcd)	TC (W/[m·K])	Start (s)	Length (s)	End (s)
177-1094A-						
1H-3, 75	3.75	3.75	0.61	75.0	25.0	100.0
2H-3, 75	8.35	9.89	0.66	43.0	28.0	71.0
2H-3, 75	8.35	9.89	0.63	113.0	25.0	138.0
3H-3, 75	17.90	20.30	0.68	36.5	25.5	62.0
4H-3, 75	27.20	30.60	0.70	82.0	25.0	107.0
4H-3, 75	27.20	30.60	0.68	111.0	25.5	136.0
5H-3, 75	36.90	39.30	0.64	89.0	25.5	115.0
5H-3, 75	36.90	39.30	0.65	37.5	25.5	63.0
6H-3, 75	46.40	49.30	0.67	73.0	25.0	98.0
6H-3, 75	46.40	49.30	0.66	91.5	25.0	117.0
7H-3, 75	55.90	58.00	0.67	105.0	25.0	130.0
7H-3, 75	55.90	58.00	0.67	77.0	25.0	102.0
8H-3, 75	65.40	67.50	0.68	66.0	25.0	91.0
8H-3, 75	65.40	67.50	0.69	36.0	26.5	62.5
9H-3, 75	74.90	77.70	0.69	61.5	25.0	86.5
9H-3, 75	74.90	77.70	0.66	124.0	25.0	149.0
10H-3, 75	84.40	86.70	0.66	83.5	25.0	109.0
10H-3, 75	84.40	86.70	0.65	111.0	25.0	136.0
11H-3, 75	93.90	96.70	0.67	91.5	26.0	118.0
11H-3, 75	93.90	96.70	0.66	106.0	31.0	137.0
12H-3, 75	103.00	105.00	0.73	107.0	26.0	133.0
12H-3, 75	103.00	105.00	0.73	73.5	25.0	98.5
13H-3, 75	113.00	115.00	0.69	72.0	25.0	97.0
13H-3, 75	113.00	115.00	0.65	117.0	25.5	142.0
14H-3, 75	122.00	125.00	0.62	124.0	25.0	149.0
14H-3, 75	122.00	125.00	0.65	58.0	25.0	83.0
15H-3, 75	132.00	134.00	0.71	118.0	25.0	143.0
15H-3, 75	132.00	134.00	0.71	96.5	25.0	122.0
177-1094B-						
1H-3, 75	3.75	4.27	0.59	121.0	25.0	146.0
1H-3, 75	3.75	4.27	0.59	120.0	25.5	146.0
2H-3, 75	13.30	14.30	0.63	106.0	25.5	131.0
2H-3, 75	13.30	14.30	0.63	98.5	25.0	124.0
177-1094C-						
1H-3, 75	3.75	4.03	0.64	39.5	25.0	64.5
1H-3, 75	3.75	4.03	0.62	75.0	25.0	100.0
2H-3, 75	12.70	14.40	0.68	106.0	25.5	132.0
2H-3, 75	12.70	14.40	0.69	66.0	25.0	91.0
3H-3, 75	22.20	23.90	0.70	79.5	25.5	105.0
3H-3, 75	22.20	23.90	0.72	30.5	25.0	55.5
5H-3, 75	41.20	42.80	0.71	47.0	25.0	72.0
5H-3, 75	41.20	42.80	0.68	87.5	27.0	115.0
2H-1, 75	9.65	11.40	0.62	57.0	25.5	82.5
3H-3, 75	22.20	23.90	0.67	103.0	25.5	129.0
3H-3, 75	22.20	23.90	0.68	94.5	26.0	121.0
177-1094D-						
6H-3, 60	70.10	71.80	0.73	97.0	27.0	124.0
6H-3, 60	70.10	71.80	0.75	64.5	25.0	89.5
7H-3, 60	79.70	82.30	0.69	53.5	28.5	82.0
7H-3, 60	79.70	82.30	0.65	120.0	30.0	150.0
8H-3, 75	89.40	92.70	0.67	95.0	25.0	120.0
8H-3, 75	89.40	92.70	0.69	50.5	30.0	80.5
9H-3, 75	98.90	101.00	0.67	84.5	29.5	114.0
9H-3, 75	98.90	101.00	0.67	84.0	25.0	109.0
10H-3, 75	108.00	110.00	0.71	108.0	25.0	133.0
10H-3, 75	108.00	110.00	0.69	110.0	25.0	135.0
11H-3, 75	118.00	119.00	0.67	74.5	25.0	99.5
11H-3, 75	118.00	119.00	0.65	89.5	25.0	115.0
12H-3, 75	127.00	129.00	0.67	93.0	25.0	118.0
12H-3, 75	127.00	129.00	0.66	76.5	28.0	105.0
13H-3, 75	137.00	139.00	0.71	121.0	25.0	146.0
13H-3, 75	137.00	139.00	0.72	73.5	25.0	98.5
14H-3, 75	146.00	150.00	0.78	94.5	29.5	124.0
14H-3, 75	146.00	150.00	0.79	62.0	26.0	88.0

Table T19 (continued).

Core, section, interval (cm)	Depth (mbsf)	Depth (mcd)	TC (W/[m·K])	Start (s)	Length (s)	End (s)
15H-3, 75	156.00	158.00	0.78	120.0	27.5	148.0
15H-3, 75	156.00	158.00	0.80	75.5	25.0	101.0
16H-3, 75	165.00	167.00	0.74	61.0	25.0	86.0
16H-3, 75	165.00	167.00	0.73	63.0	31.0	94.0

Notes: TC = thermal conductivity. Start, Length, and End refer to the interval of the time-temperature series used for the determination of thermal conductivity. This table is also available in ASCII format in the **TABLES** directory.